FUNCTIONAL ANALYSIS OF MICRORNA-181A: IDENTIFICATION OF TARGET PROTEINS AND APPLICATION IN HCC THERAPY

TAN YI LIN JANE

School of Chemical and Biomedical Engineering and

School of Bioengineering

A thesis submitted to the Nanyang Technological University and

Imperial College London in partial fulfilment of the requirement for the degree of Doctor of Philosophy

2013

Declaration of Originality

I declare that the above-mentioned thesis is my own original work. I confirm that this work has been produced by me without assistance and I have properly referenced all sources used.

Copyright Declaration

Acknowledgement

I would like to express my deepest appreciation to all who have provided me the support and invaluable guidance through the four years of this PhD program. A special gratitude I give particularly to my primary supervisor, Professor CHEN Wei Ning William, for all the advice and constant financial support in my scientific work, without which I would not have been able to complete half of what I have. He has been a very good advisor who brings out the optimism in us—a very important trait required in research!

My most sincere thanks also to my co-supervisors, Professor HABIB Nagy and Dr. DICKINSON Robert, for their friendly support and guidance while carrying out my work in London. It was a wonderful experience that made me aware of the various ways of research of the different cultures in different parts of the world. They have shown me how research can be applied to the real life, and have made me realize the value of the work I do. I thank you both so much for that.

A great shout out also to my fellow work mates and post-doctorates who have been so patient with me all this time. Dr. ZHANG Jian Hua, thank you so much for being such a good advisor and friend. To Dr. MINTZ Paul and Dr. REEBYE Vikash, thank you so much for your valuable help while I was working in London. To my fellow work mates: Dr. FENG Huixing, Ms. SADROLODABAEE Laleh, Mr. TAN Kee Yang, Ms. SHI Jiahua, Ms. TANG Xiao Ling, Ms. CHEN Liwei, Ms. LI Xiang, Ms. LEE Jie Lin Jaslyn and Mr. THWAITES John, thank you so much for your friendship.

Last, but definitely not the least, a big thank you to my family and friends for being there for me all this while. Half the battle was won with all your love and encouragement!

Table of Contents

Contents

List of Figures

List of Tables

List of Abbreviations

AGO	Argonaute
AMOs	Anti-miRNA oligonucleotides
AP-1	Activator protein 1
APCI	Atmospheric pressure chemical ionisation
APPI	Atmospheric pressure photo-ionisation
ATCC	American type culture collection
BMPs	Bone morphogenetic proteins
BMPR2	Bone morphogenetic protein receptor type II
β-ME	β-Mercaptoethanol
CDKs	Cyclin-dependent kinases
CDKN1β	Cyclin-dependent kinase inhibitor 1B
CSCs	Cancer stem cells
C_t	Threshold cycle number
DGCR8	DiGeorge syndrome critical region gene 8
DNA	Deoxyribonucleic acid
DTT	Dithiothreitol
E2F7	Transcriptional factor E2F7
EDC	N-ethyl-N'-[3-(diethylamino)propyl]carbodiimide
eIF	Eukaryotic translation initiation factor
FBS	Fetal bovine serum
ESI	Electrospray ionisation
Exp-5	Exportin-5
GC-MS	Gas chromatography to mass spectrometry

GRPs	Glucose-regulated proteins
HIF	Hypoxia-inducible factors
HBV	Hepatitis B virus
HCC	Hepatocellular carcinoma
HCV	Hepatitis C virus
HIF	Hypoxia-inducible factors
HIF	Hypoxia-inducible factors
HBV	Hepatitis B virus
HCV	Hepatitis C virus
HepG2	Human hepatoma cell line
HpSC-HCC	Hepatic Stem Cell-like HCC
HPLC	High performance liquid chromatography
HSPs	Heat shock proteins
Hsp-90β	Heat shock protein 90β
ICAT	Isotope-coded affinity tags
iTRAQ	Isobaric tag for relative and absolute quantification
LC	Liquid chromatography
LIMK	LIM domain kinase 1
MDR-1	Multi-drug resistant gene
MEM	Minimal essential medium
MiRNA	MicroRNA
mRNA	Messenger RNA
MS	Mass spectrometry
m/z	Mass to charge ratio
NHS	N-hydroxysuccinimide

NPM1	Nucleophosmin
PAZ	Piwi/Argonaute/Zwille
PCR	Polymerase chain reaction
PI	Propidium iodide
PVDF	Polyvinylidene Fluoride
RISC	RNA-induced silencing complex
RNA	Ribonucleic acid
RNases	Ribonucleases
RT-PCR	Real-time reverse transcription polymerase chain reaction
saRNAs	Small activating RNAs
SDS PAGE	Sodium dodecyl sulfate polyacrylamide gel electrophoresis
SILAC	Stable isotope labelling with amino acids in cell culture
SPR	Surface plasmon resonance
SRC	v-src sarcoma viral oncogene homolog
TACE	Transarterial chemoembolization
TCTEX	Tctex-type 1
TEMED	N, N, N', N'-tetramethylethylenediamine
THF	Tetrahydrofuran
TMT	Tandem mass tags
TOF	Time of flight
WST-1	Water soluble Tetrazolium
UTR	Untranslated region

Publications

1. **Y. Lin Jane Tan**, N. A. Habib, W. Ning Chen, A Quantitative Proteomics Approach in the Study of MicroRNA 181a in HepG2 Cells, *Current Proteomics, 9* (2012) 262-271.
2. **Y. Lin Jane Tan**, N. A. Habib, Y. W. Chuah, Y. H. Yau, S. Geifman-Shochat, W. Ning Chen, Identification of Cellular Targets of MicroRNA-181a in HepG2 Cells: A New Approach for Functional Analysis of MicroRNAs (Submitted)
3. **Y. Lin Jane Tan**, W. Ning Chen, microRNAs as Therapeutic Strategy for HBV-associated HCC: Current Status and Future Prospects, *World Journal of Gastroenterology* (Accepted for publication)
4. Feng HX, Zhang JH, **Tan J**, Sadrolodabaee L and Chen W*. (2012). Proteomics-related Biomarkers for Hepatitis B Virus-Associated Hepatocellular Carcinoma: Current Status and Future Prospects. *Future Virology, 7,* 161-71.
5. Zhang, J., J. Shi, B. J. Lee, L. Chen, K. Y. Tan, X. Tang**, J. Y. Tan**, X. Li, H. Feng and W. N. Chen, 2013. Proteomic analysis of vascular smooth muscle cells with S- and R-enantiomers of atenolol by iTRAQ and LC-MS/MS. *Methods Mol Biol. 1000*, 45-52.

Summary

Hepatocellular carcinoma (HCC), or the cancer of the liver, is of great concern due to its poor patient outcome despite the various treatments available. It is imperative, therefore, that a novel, viable treatment method is developed such that patient survival rates may be improved from current statistics of less than 50%. The role of miRNAs in the regulation of gene expression and cellular development makes it an important player in cancer development process, as it is found that the aberrant expression of miRNAs is a typical feature of cancer cells or even pre-disposed cancer cells. MiR-181a has been shown to be an important miRNA involved in HCC. In this study, we investigated the potential effects of miR-181a in HepG2 cells and the mechanisms in which it works in controlling cell fate. As chemotherapy is widely used in liver cancer treatment, we also study the use of miR-181a along with chemotherapy (i.e. *Cisplatin*). Using iTRAQ-coupled 2D LC-MS/MS analysis, we report here the study of protein profile of HepG2 cells transfected with miR-181a and its inhibitor respectively. Three main types of cellular proteins including metabolic enzymes, protein binding and stress proteins displayed changes. The changes in the level of proteins (14-3-3σ, Hsp-90β and NPM1) involved in important cancer processes like cell growth were further supported by a Western blot analysis. MiR-181a was subsequently found to significantly increase HepG2 cell viability while inhibiting it displayed the opposite effect. Inhibiting miR-181a also sensitized HepG2 cells to *cisplatin* treatment and retards cell cycle progression by decreasing the proportion of cells in S and G2/M phases.

We next investigated the reasons behind these observations at a molecular level. As miRNAs are known to regulate genes by binding to and targeting mRNAs, we first used

bioinformatics to screen out potential cellular targets. Two important genes identified, cyclin-dependent kinase inhibitor 1B (CDKN1β) and transcriptional factor E2F7 (E2F7), which are involved in cell cycle and cell proliferation, were chosen to be further experimentally studied. *In vitro* validation via surface plasmon resonance (SPR) technique showed a positive binding between miR-181a and the seed regions of the 3'UTRs of the two putative mRNA targets, with dissociation constants being 272.5 ± 0.008 nM and 1.186 ± 0.009 uM for CDKN1β and E2F7 respectively. *In vivo* luciferase assay studies further validated the miR-181a:mRNA bindings, in both cases displaying significant decrease in luciferase activity when HepG2 cells were co-transfected with the 3'UTR-containing reporter plasmids and miR-181a. A positive binding, however, may not necessarily lead to a lowered expression of protein levels. A Western blot study on the expression levels of the two proteins, however, showed a decrease in the levels of CDKN1β and E2F7.

Lastly, to gain an insight into the overall effects miR-181a has in HepG2 cells, a microarray analysis was performed. Cellular pathways important in cancer were studied and results show that miR-181a significantly activated the MAPK/JNK pathway by increasing the expression levels or activity of transcription factor activator protein 1 (AP-1). Inhibiting miR-181a, on the other hand, abolished this observation and significantly decreased expression levels or activity of hypoxia-inducible factors (HIF) and also significantly upregulated the expression levels or activity of SMAD2/3/4 proteins, possibly inducing a cancer-suppressing effect. Overall, miR-181a appears to activate mainly cancer-promoting pathways, and may act as an oncogene in HepG2 cells. Inhibiting it, on the other hand, activates mainly the tumour-suppressing pathways,

making it a possible option for therapy. A separate microarray analysis on gene expression showed that one way in which miR-181a could have activated the SMAD, NFκB and MAPK pathways is via the significant increase in gene expression of bone morphogenetic protein receptor type II (BMPR2), a cellular receptor that mediates the signal transduction of these pathways.

Our findings provide a new platform of identifying miRNA targets, in the process offering molecular evidence on the mechanism of action of miR-181a, including the beneficial effects of inhibiting miR-181a in HCC therapy.

1. Introduction

1.1. Hepatocellular Carcinoma

Hepatocellular carcinoma (HCC) is a primary malignancy of the liver and is known to be the fifth most common cancer worldwide today. It is also the third leading cause of cancer-related deaths, claiming more than 500,000 lives and affecting another 500,000 new patients yearly [1]. HCC usually develops with liver cirrhosis, which may be caused by Hepatitis B virus (HBV) or Hepatitis C virus (HCV) infection, excessive consumption of alcohol or hemochromatosis. HCC comes with poor prognosis despite the many treatments available nowadays like chemotherapy, liver transplantation, surgical resection, transarterial chemoembolization (TACE) and hormonal therapy [2]. Most of these treatment options have relatively low survival rates of less than 50%, and patients do develop recurrences or second primary tumours. The reason as to why the effectiveness of these treatments is low may be attributed to the complicated nature of the disease. HCC is a disease of heterogeneous etiology and takes on various disease progression pathways after the onset of liver cirrhosis. Liver cirrhosis may lead to portal hypertension with hyper-splenism, platelet sequestration, varices and gastrointestinal bleeding, hepatic encephalopathy, hypoalbuminemia, differential drug binding and distribution, and altered pharmacokinetics. These complications restrict the use of many cytotoxic compounds available for targeting the cancerous cells [3]. In addition, HCC tumours express the multi-drug resistant gene *MDR-1* [4], rendering drug-related treatments to be ineffective.

However, a general consensus of cancer is that it may originate from a genetic mutation or from an epigenetic cause like DNA methylation or histone covalent modification [5]. In either case, the result would be an abnormality in the expression of both coding and non-coding genes. More specifically, cancers result from the alterations in oncogenes, tumour-suppressor genes and microRNA (miRNA) genes [6]. Usually more than one such gene alteration would be required to transform a normal cell into a cancer cell, which would mean that cancer cells contain aberrant genetic and proteomic profiles, deviating from its normal, healthy cell counterpart. Therefore, in order to effectively target cancer cells, the use of therapy that controls the level of aberrant genes, preferably to a level on par with that of normal cells, could possibly restore the state of the cancer cells to that of normal cells. This brings us to the study of miRNAs as a possible, potential target in cancer therapy. Figure 1 illustrates the transformation of a healthy mice liver into malignancy.

As aforementioned, due to its heterogeneous nature, HCC is a complicated type of cancer that could, and perhaps should, be represented by many types of *in vitro* cell line models. In this project, we have chosen the HepG2 human liver carcinoma cell line to be used to exemplify HCC. HepG2 is a perpetual cell line of well-differentiated HCC, and is a type of epithelial cell that is able to secrete many plasma proteins, not unlike the liver itself. One reason why we have chosen to use this particular cell line is because it has been shown to be very comparable to primary hepatocytes, and therefore is a suitable candidate in our studies [7]. Furthermore, as we are mainly interested in the characterizing and understanding of the potential effects of miRNAs in HCC, we will simplify our studies in this case to focus on a single cell line in an attempt to minimize complications arising from this type of cancer. This way, we are able to get a more in depth understanding of

the potential mechanisms of our chosen miRNA in our study. Notwithstanding this simplification, similar work in the future on other HCC-derived cell lines could be done such that a more comprehensive study on the effects of miRNAs in HCC may be elucidated.

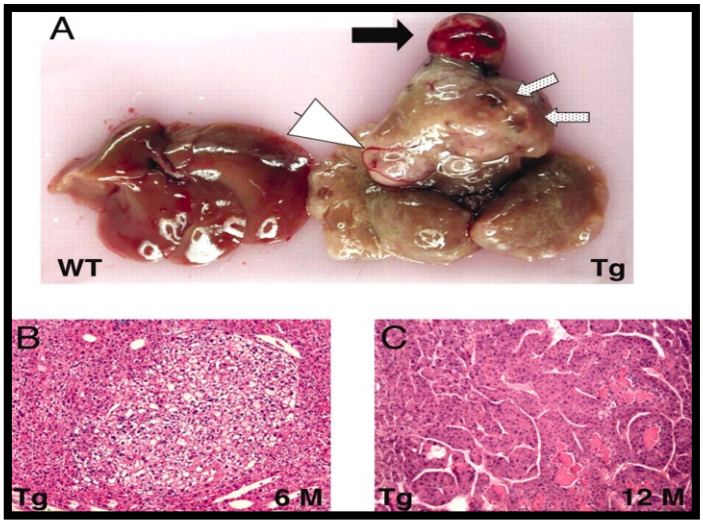

Figure 1. PDGF-C Tg mice develop HCC. As PDGF-C Tg mice age, their livers become enlarged (A) and show a variety of pathologies, including HCC (black arrow), angiogenesis (white arrow head), and multilocular pseudocysts (speckled arrows). A liver from a WT littermate is shown (Left). Tg mice develop dysplastic foci or foci of altered hepatocytes by 6 months (B), and carcinomas are seen in 12-month-old mice (C). Note the loss of sinusoidal spaces and pseudogland formation in C. Original magnification in B and C is ×100 [8]. Copyright (2013) National Academy of Sciences, U.S.A. (Permission from ref.7 was obtained from publisher to use this figure).

1.2 MiRNA Biogenesis

Figure 2 illustrates the biogenesis of miRNAs and their regulatory function in cells.

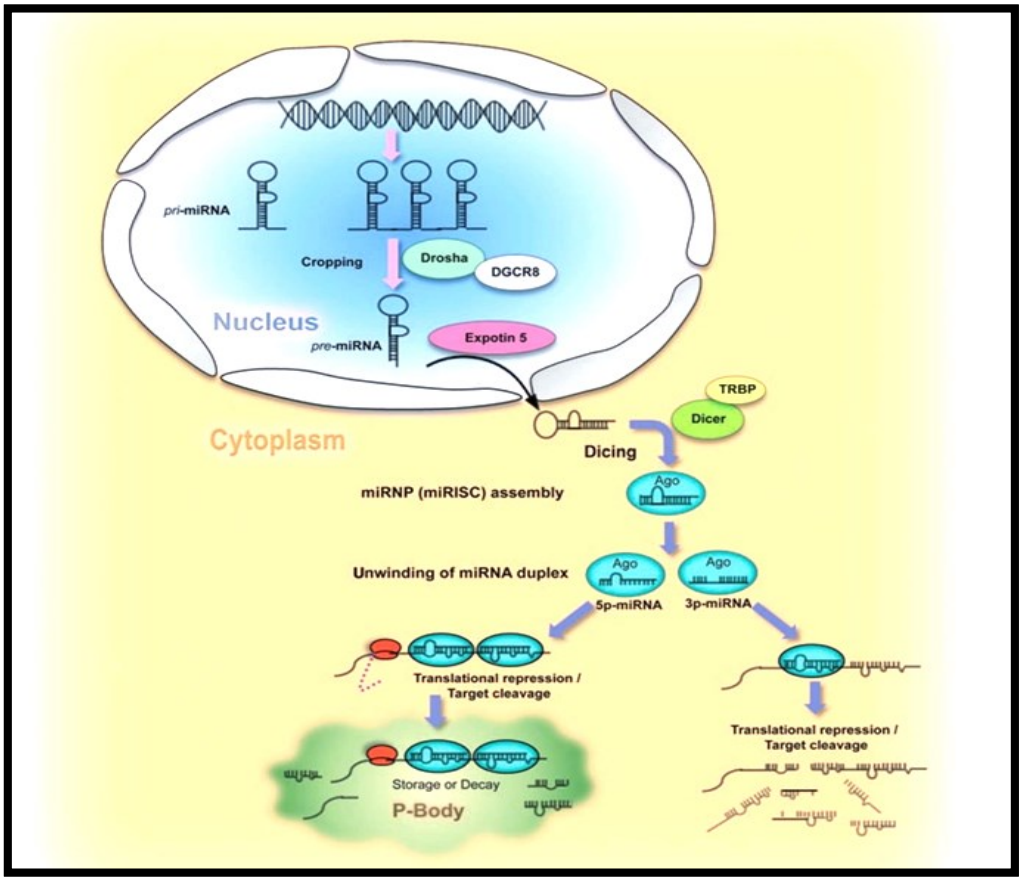

Figure 2. MicroRNA biogenesis and function. RNA polymerase II transcribes the miRNA gene into a pri-miRNA in the nucleus. The pri-miRNA is processed into pre-miRNA by Drosha, which is then exported into the cytoplasm by Ran-GTP cofactor and Exp-5. Dicer and TRBP cleave the miRNA duplex from the pre-miRNA, while helicase unwinds the mature miRNA duplex. One of the strands of the mature miRNA is subsequently incorporated into the miRISC, mediating the degradation or translational inhibition of the target mRNAs [9]. (Permission from ref.8 was obtained from publisher to use this figure).

Pri-miRNA

Most miRNA genes are located in the intergenic regions of the DNA [10] while some others are found in the introns or even in exons of DNA. MiRNA biogenesis begins with the transcription of the miRNA genes by RNA polymerase II (Pol II) at the promoter

regions [11, 12] in the nucleus, resulting in the formation of a long primary miRNA (pri-miRNA) transcript that contains a fold-back structure with a stem loop between flanking segments of nucleotides [13]. Similar to mRNAs, this pri-miRNA transcript possesses the 7-methylguanosine cap and a poly (A) tail [13, 14], but these are eventually removed during miRNA processing.

Pri-miRNA to pre-miRNA

After the pri-miRNA is formed, it is processed by a microprocessor complex made up of Drosha, an RNase III enzyme, and DiGeorge syndrome critical region gene 8 (DGCR8), a double-stranded RNA-binding domain protein, into 70-80 nucleotide long pre-miRNAs [15, 16] that consists of an imperfect stem-loop structure. This process is known as cropping, where the stem loop structure of pri-miRNAs is cleaved, producing a pre-miRNA hairpin with two nucleotide 3' overhangs. This cleavage by Drosha at a specific site of the pri-miRNA depends on the terminal loop size, stem structure, and the flanking sequence of the cleavage site because any change at these sites significantly decreases or entirely stops the Drosha processing of pri-miRNAs [17, 18]. The precision of this cleavage is very important in miRNA maturation. A shift in a single nucleotide on the pri-miRNA will subsequently affect Dicer cleavage, and this could result in different 5' and 3' ends in the mature miRNA. This may reverse the relative stability of the original guide strand and its associated passenger strand, thereby incorporating the wrong mature strand into the RNA-induced silencing complex (RISC) for silencing of target mRNA. Even if the correct mature miRNA strand is incorporated into the RISC, the shift in its 5'-end will change the position of the seed sequence of the target mRNA, thus targeting the wrong mRNA altogether [19].

Pre-miRNA export to cell cytoplasm

The pre-miRNA is exported out of the nucleus and into the cytoplasm by exportin-5 (Exp-5) in the presence of Ran-GTP as a cofactor [20-22]. Exp-5 belongs to the karyopherin family of nucleocytoplasmic transport factors, and its association with Ran-GTP aids in the specific binding of the pre-miRNA in the nucleus and its export to the surrounding cytoplasm [23]. It has been reported that Exp-5 is able to identify the 'minihelix motif' of pre-miRNAs. This translocation process involves the hydrolysis of GTP to GDP by the cytoplasmic Ran GTPase-activating protein [24].

Pre-miRNA to mature miRNA

In the cytoplasm, the pre-miRNA is processed into a ~22 nucleotide duplex miRNA by the RNase III enzyme, Dicer. Dicer is an ATP-dependent multidomain enzyme that cleaves both double-stranded siRNAs and miRNAs. Unlike Drosha, the mechanism of identification of its substrate pre-miRNA is not known [25]. The result of Dicer cleavage is a duplex with the mature miRNA in one of the strands of the stem loop, while the other strand contains its imperfectly paired passenger strand. Imperfectly paired, because both arms of the duplex contain G:U wobble pairs and single nucleotide insertions. These, in turn, cause one strand of the duplex to be less stable at its 5'-end [19]. Dicer binds with high affinity to the ends of dsRNAs with two nucleotide 3'-overhangs, resulting in the unwinding of the duplex. The unwinding of the duplex starts off at the end with lower thermodynamic stability, resulting in two ssRNA strands with different relative stabilities at their 5'-terminus. A general rule is that the strand with lower thermodynamic stability at this terminus is selected to be the mature strand (guide strand) while the other

(passenger strand) is degraded. In rare cases where both stands have similar 5'-end stability, each of the two strands are incorporated into the RISC at similar frequencies [26].

1.3 Mature miRNA and mRNA Targeting

Once the mature miRNA is selected, it is loaded into the RISC, which contains argonaute (AGO) proteins that form the core component of the RISC. There are eight AGO homologs reported in humans [27] and in particular, AGO2-associated RISCs have been reported to be involved in the cleavage of mRNA targets [28, 29]. AGOs contain two main domains – PAZ (Piwi/Argonaute/Zwille) and PIWI, both of which are important in miRNA processing. The PAZ domain binds to the 3'-end of the mature miRNA, probably by recognition of the 3'-overhangs. The PIWI domain is reported to possess slicer activity based on mutagenesis studies [28].

The recognition of the mRNA target by the RISC is based on the nucleotide sequence complementarity between the loaded miRNA and the target. In humans, miRNAs bind with imperfect complementarity to its target mRNAs, although nucleotides 2-8 of the miRNA (the 'seed region') do often match very closely to the mRNA target. The degree of complementarity will decide whether the mRNA undergoes endonucleolytic cleavage or translational repression. Most of the time, in humans, miRNAs target their corresponding mRNAs via translational repression rather than mRNA cleavage. MiR-196 is an example of a special case where its mRNA target *Hoxb8* is cleaved [30].

MiRNAs regulate translational activities by mediating pre-translational, co-translational or post-translational gene silencing. In eukaryotic cells, the initiation of translation begins with the recognition of the 5'-terminal cap of the mRNA by the eIF4E subunit of the

eukaryotic translation initiation factor (eIF), eIF4F and eIF4G. The association of eIF4G with eIF4E and polyadenylate-binding protein 1 starts off the translation process [31]. Where miRNA represses translation, AGO2 and related proteins may compete with the eIF4E for the 5'-terminal cap for binding, therefore preventing the translation of mRNAs [32]. MiRISCs are also reported to increase co-translational degradation of nascent proteins, reduce the elongation rate of the translation process and to increase the rate of mRNA deadenylation [33-37]. All these act to repress the translation of mRNAs into proteins.

Following translational repression, mRNAs accumulate in processing bodies (P-bodies) of the cytoplasm. P-bodies include Dcp1p/Dcp2p, the activators of decapping, Dhh1p, Pat1p, Lsm1-7p, Edc3p and the 5'-3'-exonuclease Xrn1p [38-41]. It is in P-bodies that mRNAs are degraded, firstly by the shortening of the 3'-poly(A) tail, which then becomes the substrate for the decapping complex to remove its 5'-cap structure. Lastly, the transcript is degraded by the 5'-3'-exonuclease [42, 43]. There have been studies done that show that approximately 20% of let-7-repressed reporter mRNAs and 20% of fluorescently labelled microinjected let-7 miRNA co-localized in P-bodies [33, 34]. This may mean that the RISC complex directs the translationally repressed mRNAs into P-bodies for degradation or temporary storage away from any translation machinery, and this process is miRNA-dependent [44]. Sometimes, the targeted mRNA is stored in P-bodies and later released back into the cytoplasm to be translated (ie. Delayed translation). These illustrate the importance of miRNAs in the regulation of cellular activities via the control of the translation of mRNAs.

1.4 Use of miRNAs in Cancer Therapy (RNA Interference)

RNA interference has shown to be a potential method for use in cancer therapy, where oncogenes are targeted for knockdown. The use of small interfering RNAs (siRNAs) has been successful in performing this as compared to using double-stranded RNAs (dsRNAs) due to the evoking of the interferon response by longer exogenous RNA strands. siRNAs and miRNAs are essentially very similar, and they both employ Dicer enzyme and argonaute proteins in their biogenesis and silencing, respectively. Their origins differ slightly; miRNAs are thought to be endogenously expressed for various cellular purposes while siRNAs are viewed as exogenous compounds, for example, from viruses, transposons or transgene trigger. Their pre-cursors are also slightly different, where those of miRNAs being incompletely double-stranded while those of siRNAs are fully complementary dsRNAs. Functionally, they both are involved in gene knockdown, but with a slight difference in their effects. siRNAs are thought to bind with a higher level of complementarity as compared to miRNAs to their mRNA targets, and that they are somewhat more specific than miRNAs, although both are prone to produce off-target effects [45]. The higher the level of complementarity, the higher the chances of mRNA target degradation. Therefore, siRNAs typically control gene expression by causing a cleavage of mRNA targets while miRNAs mainly act by repression the translation of mRNAs into their proteins. Either way, they both generally lead to the inhibition of gene expression. The use of miRNAs will be further discussed.

miRNAs form a subclass of small RNAs and are single-stranded, non-coding RNAs of 19-25 nucleotides in length, originating from its precursor endogenous hairpin-shaped

transcripts [46]. Up to now, 2578 mature human miRNAs have been documented in the Sanger miRBase sequence database and more are expected to be identified [47]. Other subclasses of small RNAs include siRNAs, repeat associated small interfering RNAs [48], small nuclear RNAs, small nucleolar RNAs, Piwi-interating RNAs [49] and transacting short interfering RNAs [50]. Among these, miRNAs have recently been the spotlight of cancer research ever since they have shown to possess a functional role in humans. They have a diverse set of functions and are involved in various physiologically important processes in the body such as cellular proliferation, differentiation, cell cycle regulation, angiogenesis, metabolism, regulation of immune response and apoptosis [51, 52]. The fact that miRNAs are able to affect these important processes implies their significance in maintaining the integrity of a cell. One reason why miRNAs are able to possess so many vastly different functions is because they have a "one hit, multiple targets" property. This means that a single miRNA is able to negatively regulate multiple target proteins through direct interaction with the mRNAs. Conversely, a single mRNA gene is influenced by many different types of miRNAs. Approximately 3% of the entire human genome encodes for miRNAs and they regulate up to 30% of human protein coding genes [53].

As miRNAs are able to regulate a large number of proteins, their aberrant expression disrupts the normal functioning of the cell, either by activating oncogenes or deactivating tumour suppressor networks. miRNAs, when overexpressed or upregulated in cancer cells, are considered to be oncogenes and have anti-apoptotic activity while those that are underexpressed or downregulated are considered to be tumour suppressors and have pro-apoptotic activity. These various upregulations and downregulations of different miRNAs contribute to the initiation and progression of many cancers in humans [54-57]. Currently,

many miRNAs have been identified and correlated with various cancers, and many of them are expressed exclusively in certain tissue types. Studies show that miRNA profiling in neoplasms provides an even higher accuracy for tumour diagnosis as compared to mRNA profiling [58]. Not only that, but miRNA signatures have also been shown to correlate with the extent of histological tumour differentiation in HCCs [59]. This could potentially mean that the use of miRNA profiles may help determine the degree of disease progression, the site of disease origin, and may also provide a platform for new and more effective treatment methods of cancer [60]. Table 1 shows several miRNA signatures in various types of cancers.

Table 1. Cancer-related miRNAs [52]. (Permission from ref.51 was obtained from publisher to use this figure).

Cancer	Up-regulated miRNAs	Down-regulated miRNAs
Breast cancer	miR-21, miR-155, miR-29b-2	miR-143, miR-145, miR-155, miR-200
Lung cancer	miR-21, miR-189, miR-200b, miR-17-92 cluster	let-7 family, miR-126, miR-30a, miR-143, miR-145, miR-188, miR-331, miR-34s
Colon cancer	miR-223, miR-21, miR-17, miR-106m, miR-34s	miR-143, miR-145, miR-195, miR-130a, miR-331
Prostate cancer	Let-7d, miR-195, miR-203, miR-125b, miR-20a, miR-221, miR-222	miR-143, miR-145, miR-128a, miR-146a, miR-126
Brain cancer	miR-21, miR-221	miR-181
Hepatocellular carcinoma	miR-34s, miR-224, miR-18, miR-21	miR-17-19b cluster, miR-200a, miR-125a, miR-199a, miR-195

As described above, cancer cells typically involve alterations of miRNAs or miRNA pathways. Therefore, by normalizing or correcting the miRNA expression levels to that of normal, healthy cellular levels, it could result in (i) the recovery of a normal cellular phenotype from a cancerous state; (ii) increased tumour differentiation; (iii) induction of tumour death; and/or (iv) prevention of metastasis. This correction of miRNA expression levels could either refer to an introduction of downregulated miRNAs or an inhibition of

upregulated miRNAs, both potentially resulting in restoring the miRNA levels to that of normal, healthy cells.

1.4.1 miRNA Mimic Therapy

The decreased expression of certain miRNAs in cancer cells that serve as tumour suppressors contributes to oncogene activation. mRNAs that were originally translationally repressed by these miRNAs will be more abundant and are translated into proteins that encourage growth and proliferation of cancer cells. A therapeutic approach may be to increase the expression of these repressed miRNAs using synthetic miRNA mimics. These mimics may be unstable, or only have a transient effect in cells. Hence, for sustained effect of the miRNAs in cancer cells, vector-based miRNA expression may be used to produce stably expressed miRNAs. MiRNA mimic therapy has been applied successfully by Takamizawa et al.[61], where they designed expression constructs to synthesize the mature miRNAs of two Let-7 isoforms (Let-7a and Let-7f) and introduced them separately into A549 adenocarcinoma cell line. Results from their experiments show a 78.6% reduction in the number of colonies. Another batch of similar experiments carried out on lung cancer cell lines show enhanced lung cancer cell radio-sensitivity [62], altered cell cycle progression and reduced cell division [63]. Other than this group of researchers, there have been many other groups reported to have successfully used miRNA mimics to repress cancer proliferation of various cell lines. Liang et al. [64] used a miR-155-based BLOCK-iT^{TM} Pol II miR RNAi expression vector in MDA-MB-231 breast cancer cells that silences *CXCR4*, resulting in the reduction of migration and invasion *in vitro*. They also found that mice injected with CXCR4 miRNA-expressing breast cancer cells

developed fewer lung metastases within one month than those injected with breast cancer cells without the miRNA. It has been thought that the CXCR4/SDF1/AKT pathway, which is a pathway that takes part in the invasion and metastasis of breast cancer cells, had been inhibited by the increase in miR-155 expression. These independent studies show that an artificial introduction of underexpressed miRNAs in malignant cells is a potential therapeutic method in the treatment of cancer.

1.4.2 Anti-miRNA Therapy

Contrary to the miRNA mimic therapy, the overexpression of another subgroup of miRNAs in malignant cells requires an anti-miRNA therapy. These overexpressed miRNAs act as oncogenes themselves. Therefore, an introduction of synthetic antisense oligonucleotides complementary to the overexpressed, endogenous miRNAs or their precursors may result in their pairing with the miRNAs, occupying their binding sites and leaving their target mRNA in the unbound state [65]. There are three commonly used anti-miRNA oligonucleotides (AMOs): (i) 2'-O-methyl AMOs; (ii) 2'-O-methoxyethyl AMOs and (iii) locked nucleic acid AMOs. These modified RNA oligos are known to have a greater stability and have a delayed clearance following systemic administration [66], and their most important property is their specificity and high binding affinity for RNA. Anti-miRNA therapy has been used in the knockdown of oncogene miR-21. In those studies, the use of 2'-O-methyl- and/or DNA/LNA-mixed oligonucleotides to inhibit miR-21 in glioblastoma and breast cancer cells suppressed cell growth due to the increase in pro-apoptosis caspase activity [67, 68]. Not only that, but the inhibition of miR-21 also significantly reduced invasion and lung metastasis in MDA-MB-231 metastatic breast

cancer cells [69], RKO human colon cancer cells [70], and glioblastoma cells [71]. Figure 3 illustrates the interference in the miRNA pathway by modified antisense synthetic oligonucleotides.

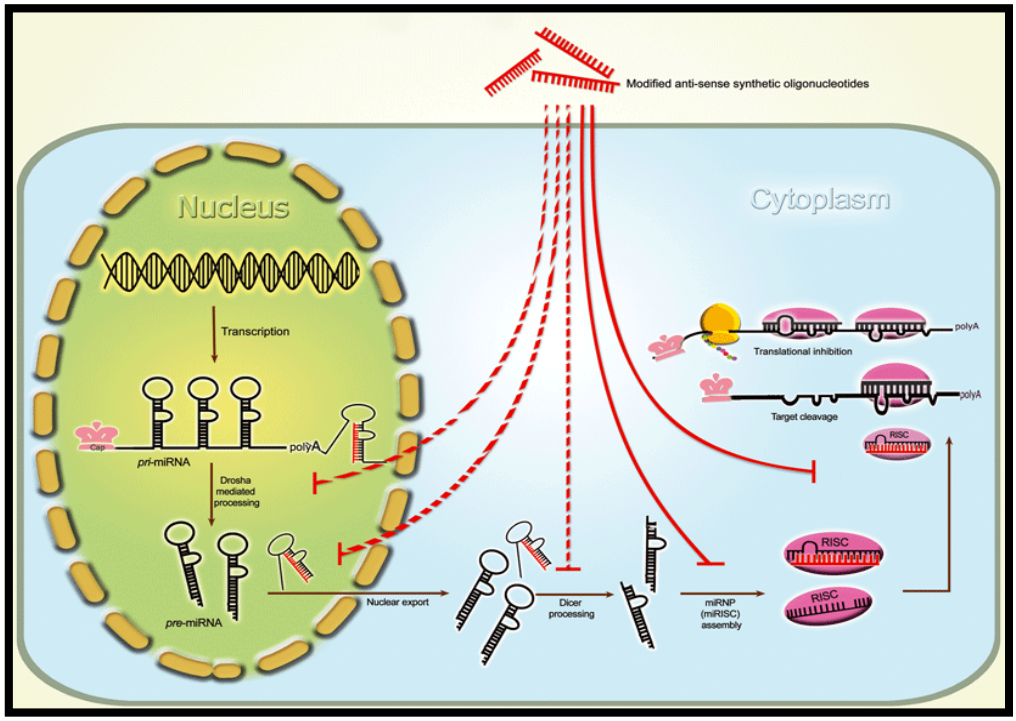

Figure 3. Interference in the miRNA pathway by modified antisense synthetic oligonucleotides. Inhibition of miRNA can be achieved by introducing antisense synthetic oligonucleotides against miRNAs in the cytoplasm (shown as continuous lines). The possible targets of antisense synthetic oligonucleotides against miRNAs in the nucleus are pri-miRNA and pre-miRNA (shown as dotted lines) [9]. (Permission from ref.8 was obtained from publisher to use this figure).

1.5 MicroRNAs in Hepatocellular Carcinoma

The development of hepatocellular tumour is known to be a multi-step process that involves several structural and genomic alterations such that many subsequent pathways are affected [60, 72]. The changes in miRNA expression levels occur early during hepatocarcinogenesis. Even before the onset of HCC (ie. During liver cirrhosis and other pre-malignant lesions [73]), these changes may already be detected and therefore, it

remains an exciting possibility that miRNAs could actually act as early warning markers for liver cancer initiation or progression. This has been demonstrated in the case of miR-145 and miR-198, where their downregulation in cirrhotic tissue has been observed, followed by their further downregulation in HCCs of increasing histological grades [74]. This has also been shown to take place in other cancer-affected organ sites like in the colons [75] and the thyroid [76].

Thus far, many studies on miRNAs and their profiles in HCC have been done by many different groups of researchers. The geographical origins of patients involved varied from the USA, Italy, Japan, France, Germany, China and Singapore. The predisposing risk factors and etiologies of HCCs in those studies were inhomogeneous, and the methods used in the studies varied. Therefore, even though many hundreds of precursor and mature miRNAs have been studied, only limited overlaps exists between the results of overexpressed and underexpressed miRNAs in HCCs. Table 2 shows the miRNAs that are found to be dysregulated by more than one group of researchers and are therefore more likely to be of significance in hepatocellular carcinogenesis.

Table 2. Frequently dysregulated microRNAs in hepatocellular carcinomas [77]. (Permission from ref.76 was obtained from publisher to use this figure).

miRNA	Location	Dysregulation	Suggested Targets
miR-122a	18q21.3	Decreased	Cyclin G1, CAT1, EDN1, VAV3, GYS1
miR-125a	19q13.3	Decreased	TIMP3, FAK,VEGF,EDN1
miR-139	7p22.1	Decreased	CTNNB1
miR-150	9p24.3	Decreased	MYB
miR-145	5q32	Decreased	MAP3K, MAP4K4, PXN
miR-199a	1q24.3	Decreased	KRAS, CASP2, TIMP3, Fibronectin
miR-200b	1p36.33	Decreased	PTPN12, ZFHX1B
miR-214	9p24.3	Decreased	BCL2L11, PTEN

miR-223		Decreased	HLF, C/EBPα
let-7a	22q13.3	Increased	RAS, NF2
miR-21	17q23.2	Increased	PTEN, RECK, TIMP3
miR-221	Xp11.3	Increased	FAT2, c-Kit
miR-222	Xq11.3	Increased	FAT2, c-Kit
miR-224	Xq28.3	Increased	API5
miR-301	17q23.2	Increased	MET

1.5.1 MicroRNA 181a

MiR-181a has been shown to be up-regulated in HCC, and is found especially to be up-regulated in Hepatic Stem Cell-like HCC (HpSC-HCC) [78]. These are HCC cells that are EpCAM and AFP positive (i.e. $EpCAM^{+}AFP^{+}$ HCC), which respectively, serves as a hepatic stem/progenitor cell-specific marker and a marker indicative for HCC [78]. MiR-181a is also involved in the activated Wnt/β-catenin signalling pathway in HpSC-HCC [78]. This pathway has been found to be over-activated in at least 60% of HCC, as the levels of β-catenin protein in the nucleus and/or cytoplasm was found to be increased in these cases. One group also found that the expression of β-catenin or Tcf4, a co-transcriptional activator of β-catenin, induces the expression of miR-181s in HuH7 and HuH1 cells. An activated Wnt/β-catenin pathway often leads to the transcription of genes that are involved in cell growth, differentiation and survival [79]. An example of a validated mRNA target of miR-181a is RalA [80], which is a protein often dysregulated in cancer. These findings may indicate the significant involvement of miR-181a in liver cancer. In this study, we propose to investigate the overall effect of miR-181a in HepG2 cells, especially on important cellular aspects like cell growth, cell cycle and changes in protein profile. We also delve into the molecular dynamics of miR-181a in HepG2 cells, particularly, identifying its potential mRNA targets as well as the various cancer-related pathways that it may affect. By performing both an overall and a molecular study of miR-

181a, we gain an insightful knowledge of its mechanisms of action and identify it as a potential target in liver cancer therapy. The following lists the mature sequence of miR-181a; its seed region in bold.

5' A**ACAUUCAA**CGCUGUCGGUGAGU 3'

1.6 Protein Profiling Using Liquid Chromatography Mass Spectrometry

Proteomics is the study of the complete set of proteins expressed by the genome of a cell. This includes proteins with post transcriptional modifications, phosphorylation and glycosylation. As proteins are the 'nano-machines' of cells, their expression levels, functions and interaction network determine the state of the cell. It is more significant to study the changes in protein levels as compared to gene levels. Proteins are therefore, usually the target of drugs during drug-related therapies. The study of proteins first requires them to be resolved. Two platforms are often used: 1) Gel-based proteomics; 2) Chromatography-based proteomics. In gel-based proteomics, 2-D gel electrophoresis coupled to mass spectrometry (MS) is commonly employed. In this method, proteins are separated based on two dimensions. The first dimension separates proteins along a pH gradient while the second dimension further separates the proteins according to their molecular weight (SDS PAGE). By staining the proteins and comparing the protein patterns between gels of different samples, unique proteins may be identified. The protein spots of interest may be subsequently in-gel enzymatically digested with trypsin and sent for MS peptide sequence analysis. One disadvantage of this method is that proteins that are low in abundance may be missed during gel-staining.

On the other hand, chromatography-based staining circumvents the need for gel-staining and peptide extraction. It also ensures detection of low abundant proteins because the entire sample may be sent for MS screening with pre-purifying using liquid chromatography (LC). Hence, chromatography-based proteomics have since replaced the use of 2-D gel electrophoresis MS. Particularly, high performance liquid chromatography (HPLC) and capillary electrophoresis, a liquid-based technique, is a feasible approach used to identify low abundance and low resolution proteins. This method is able to effectively resolve the high degree of complexity of the cellular proteome and detect low abundance-proteins. Therefore, it is the method of choice in our study of cellular protein profiles. In this section, we will describe the theory and procedure of the liquid chromatography-mass spectrometry (LC-MS) technology for our protein profile analysis.

The coupling of gas chromatography to mass spectrometry (GC-MS) eventually led to the advent of the LC-MS. The LC-MS is more complicated than the GC-MS, due to the incompatibility of continuous liquid streams to the different MS ion sources. However, a vast development in MS has been achieved throughout the years, and by mid 1990s, the LC-MS was finally introduced into clinical biochemistry laboratories for functional studies. The main advantages of coupling LC to MS over the conventional detectors are its high specificity and ability to handle complex mixtures. A schematic diagram of an LC-MS equipment is shown in Figure 4.

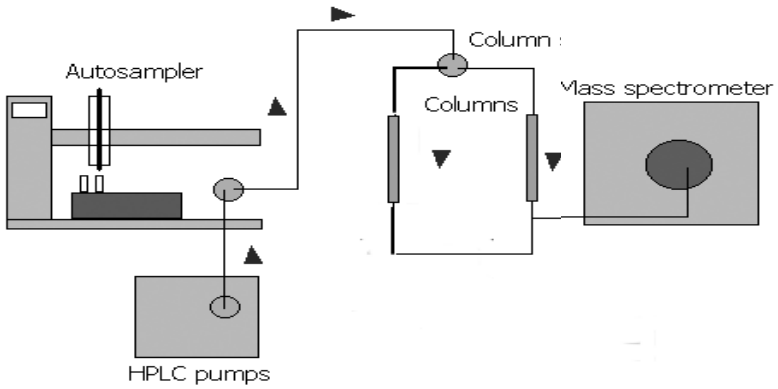

Figure 4. Schematic diagram of an LC-MS equipment. Samples enter the HPLC via the autosampler, gets pumped and separated through columns and finally detected by MS.

1.6.1 Liquid Chromatography

In this technique, the sample is first resolved by LC. There are many types of columns available for this purpose, each separating the samples according to different properties. Table 3 shows a list of common types of columns currently available.

Table 3. Specifically designed columns and their separating principles.

Type of Column	Separation Mode
Normal-Phase Columns	Polarity. Polar bound phase with nonpolar mobile phase
Reverse-Phase Columns	Polarity. Nonpolar bound phase with a polar mobile phase
Ion-Exchange Columns	Net charge. Retained ionized material eluted by different salt and salt gradients
Size-Separation Columns	Size (ie. Stokes radius).
Other Bonded-Phase Silica Columns	Structure (eg. Enantiomeric separation).

In particular, we shall explore the ion-exchange and reverse-phase columns a little further.

In ion-exchange chromatography, the stationary phase surface displays ionic functional

groups that interact with analyte ions of opposite charge. Ions of similar charge get eluted while oppositely charged ions are retained on the stationary phase of the column and later eluted by increasing the concentration of a similarly charged species that will displace the analyte ions from the stationary phase. This is an excellent way of separating proteins because proteins have many charged functional groups. By varying the pH and ionic concentration of the mobile phase, especially the pH, the proteins will be eluted out of the column as its net charge changes from one sign to another.

In reverse-phase chromatography, a hydrophobic stationary phase and a polar mobile phase of column is used. As a result, hydrophobic molecules in the polar mobile phase adsorb onto the hydrophobic stationary phase, and hydrophilic molecules in the mobile phase will pass through the column and get eluted first. Mixtures of water or aqueous buffers and organic solvents are used to elute the analytes from the reversed-phase column. The solvents must be miscible with water, and the most common organic solvents used are acetonitrile, methanol, and tetrahydrofuran (THF). Other solvents can include ethanol or 2-propanol (isopropyl alcohol). Elution may be performed isocratically or by using a solution gradient.

Two reasons why LC is encouraged prior to MS are because firstly, MS alone is unable to distinguish isomers due to their same mass. Many biological chemicals exist as isomers, with the same molecular mass but different structures. Hence, an additional step of LC would aid in differentiating between two isomers. Secondly, LC may be able to help avoid or at least alleviate ion suppression, a situation where molecules that are low in abundance or poorly ionised are undetected by MS due to the presence of other highly expressed

compounds. Pre-purification of the ionisation mixture can separate these components from each other so that the masking effects are minimized.

1.6.2 Mass Spectrometry

After separating the sample within the LC columns, the samples are next prepared for detection and identification in the MS. While the LC separates the components, it does not identify a compound. Therefore, MS coupled to LC performs this task of identifying the compounds present after some pre-purification. Mass spectrometers convert analyte molecules into an ionised state, and subsequently analyse them (and any fragment ions produced in the ionization process) based on the mass to charge ratio (m/z). One common method used to form ions from the analytes is electrospray ionisation (ESI). This method works well with moderately polar molecules and therefore is suitable in the study of peptides, metabolites and xenobiotics. Little fragmentation occurs under normal circumstances. The liquid sample is pumped and charged through a metal capillary, forming a fine spray of charged droplets. Heat and dry nitrogen dries the droplets by evaporating the liquid, and any electrical charge is transferred onto the analytes. The ionised analytes are next charged through a vacuum, through a series of small apertures and focusing voltages, and finally detected. Small molecules with a single charge-carrying functional group tend to carry a single charge while larger molecules with multiple charge-carrying functional groups (ie. Peptides and proteins) can carry multiple charges. This difference in ion charges within a sample can be used to determine analytes up to 100kDa. This is the basic working principle of ESI in MS. Many variations of ESI have been developed to improve on the quality of detection.

While ESI is useful for ionising biological molecules, neutral and low polarity molecules may not be efficiently ionised by this method. Instead, atmospheric pressure chemical ionisation (APCI) may be a better option. In this method, gas and solvent that have been ionised in the ion source react with the analyte and transfers their charge to it. Alternatively, atmospheric pressure photo-ionisation (APPI) uses photons to excite and ionise molecules. These options are useful for small, thermally stable molecules not easily ionised by ESI.

Following ionisation, the ions are accelerated through a mass analyser. The quadrupole analyser is the component in a MS responsible for filtering sample ions based on their m/z value. This is achieved by using a combination of constant and varying voltages, resulting in a mass spectrum. Stepping voltages may be used to focus the detection a range of ions of a certain m/z value. While the ionisation process itself produces little or no fragmentation, ions may be made to fragment by passing them through a collision cell. In the collision cell, the ions collide with an inert gas such as nitrogen or argon. A collision cell may be placed between two mass analysers, also known as a triple quadrupole mass spectrometer. One main benefit of using a tandem MS is the increased specificity in its detection. The product ion scans contain both structural information about the analyte and confirms its identity with greater certainty [81]. Tandem MS is frequently used in LC-MS applications.

Another popular mode of analyser is the time-of-flight (TOF). Ions are accelerated through a high voltage and reach the detector at different times, depending on their m/z value. Ion trap analysers introduce an inert gas into the trap and ions are fragmented several times before the final mass spectrum is obtained. Hybrid analysers combine the

different analysers in the MS. When the third quadrupole of a triple quadrupole MS is replaced by a TOF analyser, a hybrid MS (QTOF) is produced. QTOF is widely used in proteomics. If an ion trap analyser is replaced for the third quadrupole, a QTrap MS is formed.

In our study, we employ a QTOF MS. It has a high sensitivity, high resolution and mass accuracy. Q1 in a QTOF MS is operated in the mass filter mode to transmit only the parent ion of interest. These ions are accelerated before they enter the collision cell Q2, where they get fragmented due to collision with inert gas molecules. If no collision is desired, a single mass spectrum can be obtained by setting the collision energy to below 10eV. The fragmented ions are cooled, re-focused and re-accelerated into the ion modulator of the TOF analyser. A pulsed electric field applied across the modulator gap changes the direction of the ions to a path perpendicular to that of its original direction, where they accelerate in the accelerating column and mass separation occurs. Ions reach the ion mirror and get deflected to the TOF detector where the mass spectra are recorded [82]. Figure 5 shows the trajectory of ions in a typical QTOF MS.

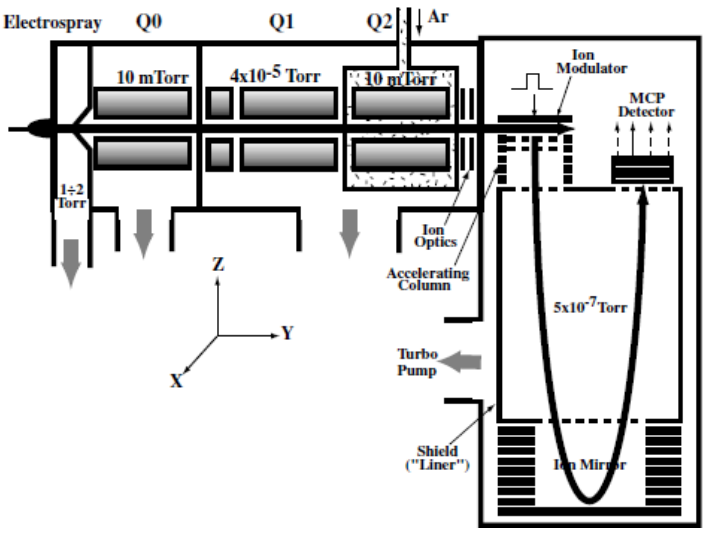

Figure 5. Schematic diagram of a tandem QTOF MS [82]. Ions are accelerated and collided with inert gas molecules to form daughter ions in Q1 and Q2 of the QTOF. The fragmented ions are re-accelerated in the ion-modulator and a subsequent electric pulse applied such that it changes the direction of the ions perpendicularly, where they then accelerate and separate. They are finally deflected into the TOF detector where mass spectra are recorded. (Permission from ref.81 was obtained from publisher to use this figure).

1.6.3 LC/MS Software

Data analysis software is employed to extract and interpret information from MS datasets. Molecules detected by MS are next identified through a MS database search. At present, the standard libraries of mass spectral data that are commonly used include Swiss-prot, NIST and Wiley et al. Current limitations of the LC-MS technique lie primarily in the separation speed, peak resolution, data analysis and cost.

1.6.4 Applications of LC-MS/MS

The LC-MS/MS technology may be used in a variety of applications. Millington et al. utilised this technology in the screening of neonatal dried blood spots for errors of metabolism. Dried blood spots are extracted and derivatised and scanned for a number of marker amino acids and acyl carnitines. This may also be applied to screening other

conditions, such as sickle cell anaemia, galactosaemia, lysosomal disorders, disorders of porphyrin, purine and pyrimidine, peroxisomal and bile acid metabolism. Also, instead of measuring the levels of metabolites, the amounts of enzymes may be measured instead.

Apart from the biochemical screening for genetic disorders, LC-MS may also be applied in therapeutic drug monitoring and toxicology. The study of drug therapy and their variable cross-reactivity with metabolites have been improved with the tandem use of the LC-MS. LC-MS can be used not only to confirm the structure of the final metabolite product and its impurities, but also to study the precursor purity, intermediate compounds in the synthesis pathway, and the completeness of the drug conversion. It has been used to assay multiple drugs at the same time, due to the capacity to multiplex LC-MS assays, making it a more convenient assay as compared to immunoassays.

Many other types of studies may be performed with the LC-MS. Vitamins, steroid hormones and proteins are a few of them that may be studied. Some studies use LC-MS for the analysis of specific proteins from complex biological samples. Chang group developed a LC–MS/MS method for the quantitation of a large peptide, T-20 and its metabolite in human plasma. The method was developed and used for analysing pharmacokinetic profiles and metabolite of samples treated by the HIV fusion inhibitor peptide drug [83]. Lin described a LC–MS/MS method for the determination of levovirin in rat and Cynomolgus monkey plasma, and the assay was validated and used in pharmacokinetic studies in rats and monkeys [84]. Feng et al. [85] has shown the feasibility of using this method of protein profiling by applying the iTRAQ-coupled 2-D LC-MS/MS analysis to reveal and quantify the differences of protein expression levels of normal HepG2 cells and those transfected with HBx of three different genotypes (A, B

and C). Their results showed that HBx alters the expression levels of proteins involved in metabolic enzymes, signalling pathway and cytoskeleton regulation. Proteins regulating cell migration were also successfully identified via this comparative proteomics approach. The same group did another study [86] using this approach in the identification of secreted proteins in their cell-based HBV replication system to establish potential biomarkers of liver disease development. Zhang et al. [87] identified enzymes associated with angiogenesis in HBV replicating RPHs and HepG2 cells by 2-D LC-MS/MS analysis. The identified proteins may lead to a novel anti-angiogenic HCC therapy based on tumour vascular targeting.

These studies highlight the significance of the LC-MS/MS approach in protein profiling, as it is able to identifying novel markers indicative of diseases as well as explain the mechanisms involved in disease development. In this project, a similar method of proteomics analysis will be applied in the identification of differentially expressed proteins upon the transfection of miR-181a in HepG2 cells. Their functions and effects will then be explored.

1.6.5 Quantitative Proteomics

As mentioned earlier, the coupling of LC to MS enables the detection and identification of unknown compounds like drugs, proteins, etc. Proteomics refers to the entire complement of proteins expressed in a given cell, tissue or organism. In our study, we are interested in the proteomics of HepG2 cells transfected with miR-181a. While it is useful to identify the proteins present in the samples, a quantitative proteomics approach is able to yield the difference in protein levels of different samples. MS itself is not inherently quantitative; inaccuracies may occur due to the differences in ionisation efficiencies, and the peaks

obtained in a mass spectrum is not a good indicator of the amount of analyte in a sample. Relative quantitation is still possible using MS alone, but may be less sensitive to experimental bias. Moreover, only one sample may be analysed in a single run, making it a relatively inconvenient method to study larger sample sizes.

One way to circumvent these problems would be to incorporate stable isotope labels, such as isotopic tags, to the samples. What this does is to cause a mass shift of a labelled protein or peptide in the mass spectrum. Differentially labelled samples are combined and analysed together, and the differences in the peak intensities of the isotope pairs accurately reflect the difference in the abundance of their corresponding proteins. Known concentrations of labels may be added to samples for absolute quantification of target proteins. Many types of labels are available, including isotope-coded affinity tags (ICAT), tandem mass tags (TMT), isobaric tags for relative and absolute quantitation (iTRAQ), metal-coded tags, and stable isotope labelling with amino acids in cell culture (SILAC). Table 4 shows the principles of these labelling methods.

Table 4. Principles of ICAT, iTRAQ, metal-coded tags and SILAC.

Labelling Method	Principle
ICAT	Two-sample simultaneous quantitation. One sample is labelled with light hydrogen while the other, with a heavier version (ie. Deuterium).
iTRAQ	Up to eight samples may be studied simultaneously. Samples are labelled with reagents as in Figure 6.
Metal-coded tags	A macrocyclic metal chelate complex loaded with different lanthanides (metal (III) ions) forms the essential part of the tag.
SILAC	Two-sample simultaneous quantitation. Labelling occurs at cell culture level. Cells of one sample is fed with growth medium containing normal

amino acids while cells of the other sample is fed with growth medium containing amino acids labelled with stable (non-radioactive) heavy isotopes.

There are three major types of labelling: 1) Metabolic labelling; 2) Protein labelling; 3) Peptide labelling. Peptide labelling has the advantage over protein labelling by increasing the specificity and accuracy of proteins identified.

Of all the developed stable isotope-based quantification methods, iTRAQ has gained much popularity as it allows up to eight samples to be examined within one experiment. The reagents are composed of an amino reactive NHS group coupled to a balancer and reporter group. Using iTRAQ 4-plex to illustrate, up to four samples can be done in a single experiment, with four different reporter groups (MW: 114Da, 115Da, 116Da, 117Da). Accordingly, the molecular weights of the balancers are: 31Da, 30Da, 29Da, 28Da. Each reporter group is linked to a balancer, contributing to a total molecular weight of 145. The NHS group labels all peptides at the 22 lysine side chain. At the first MS, the same peptides (from different samples) will elute at the same retention time as they have the same molecular weight. At the second MS (MS/MS), the balancer is lost and the label dissociates and releases the reporter group as a single charged ion of masses 114Da, 115Da, 116Da, or 117Da, respectively. The relative peak areas of the reporter groups indicate the contribution of each sample to the total peptide present, providing a measure of relative abundance. The principle of iTRAQ labelling is shown in Figures 6 and 7. Briefly, sample proteins are extracted and digested into their peptides and labelled with iTRAQ reagents. Different samples are labelled with different iTRAQ reagents, each with a different reporter group. The underlying principle is that, the mass difference resulting

from the introduction of the individual stable isotope provides a ratio for the reporters, and this is directly corresponds to the ratio of the analytes. The samples are then pooled and separated sequentially on the multi-dimensional columns of the LC based on charge or hydrophobicity of the ionized analytes and eluted into the MS for identification and quantification. On-line libraries of information and sequence structures of polypeptides are available to aid in quickly identifying the peptide sequence, and a bottom-up approach is taken to identify the original protein. Generally, two or more unique peptides are usually sufficient to recognize a protein. In our study, an iTRAQ LC-MS/MS was applied in studying the biological effects of miR-181a in HepG2 cells.

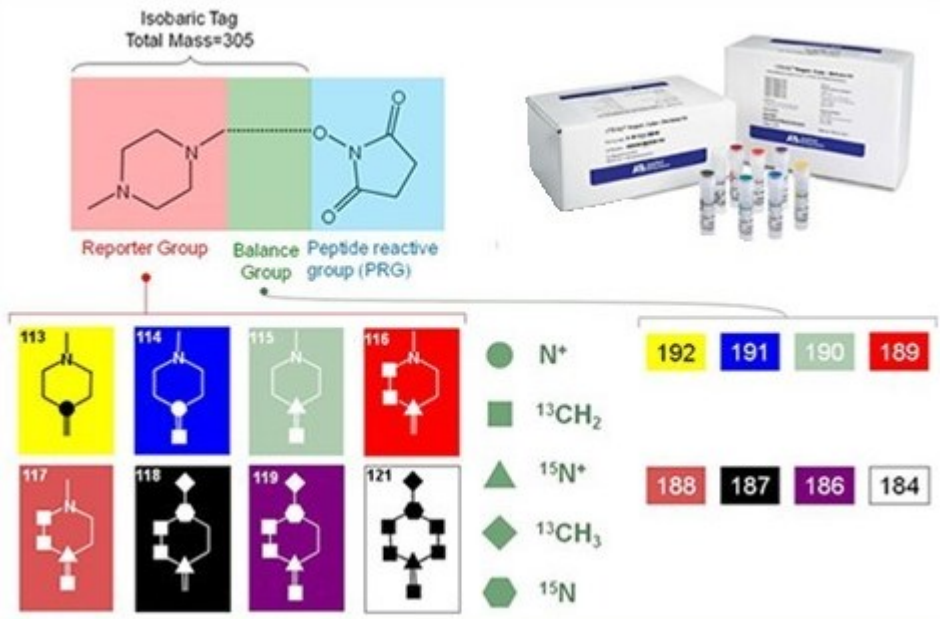

Figure 6. iTRAQ reagents and their chemical structures. Up to 8 samples may be labelled per experiment (Applied Biosystems). The labelling reagent consists of a quantification (reporter) group (N-methylpiperazine), a balance group (carbonyl), and a hydroxyl succinimide ester group that reacts with the N-terminal amino groups of peptides and the amino groups of lysine. (Adapted from **http://www.creative-proteomics.com/iTRAQ.htm**)

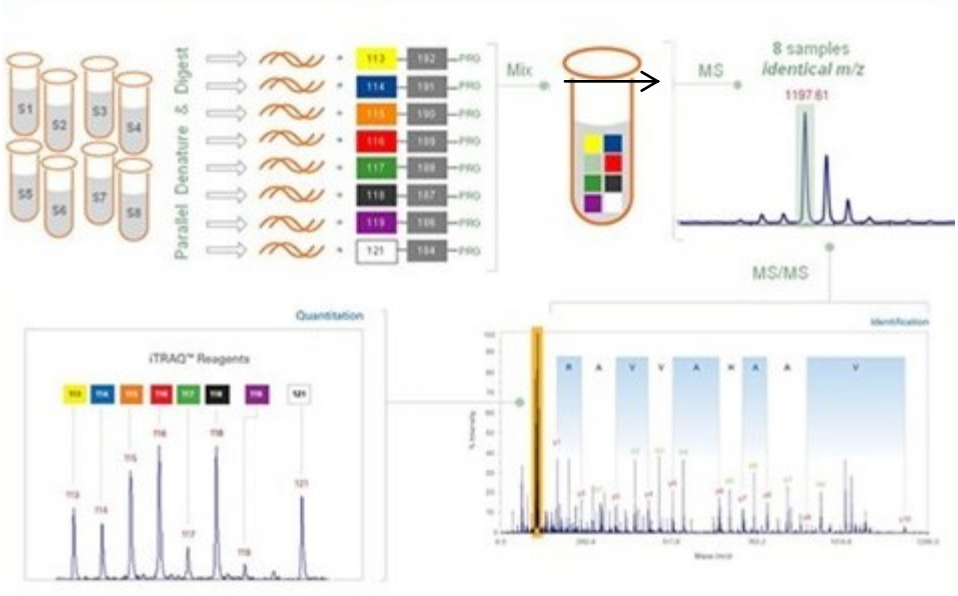

Figure 7. Summary of iTRAQ-based LC-MS. Proteins from each sample are denatured, reduced and digested into peptides, and labelled with an iTRAQ reagent. Samples are pooled and sent for LC-MS analysis, where the peptides are identified and quantified simultaneously. The signal intensity ratios of the reporter groups indicate the ratios of the peptide quantities. The MS/MS spectra of the individual peptides show signals reflecting amino acid sequences and also show reporter ions reflecting the protein contents of the samples. A database search is performed using fragmentation data to identify the labelled peptides and hence the corresponding proteins whilst the iTRAQ mass reporter ion relatively quantifies the peptides. (Adapted from **http://www.creative-proteomics.com/iTRAQ.htm**)

A mass spectrum consists of both fragmentation and quantitation data of the peptides detected. As the peptides enter the MS, they are ionised and fragmented in the collision cell into daughter ions, which are subsequently accelerated through the TOF and detected. There are several bonds that may be broken during fragmentation. The spine of a peptide consists of three bonds: C-C, C-N and N-C. Breaking any of these bonds would result in daughter ions that may be known as A, B, C X, Y or Z ions. Figure 8 shows the possible ions formed when any of these bonds are broken. The most common types of ions formed are the B and Y ions.

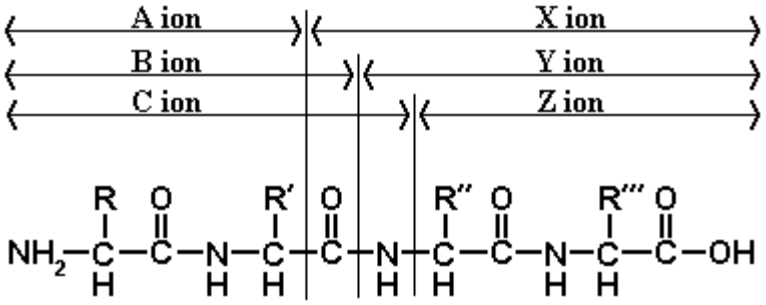

Figure 8. Possible daughter ions after peptide fragmentation. Depending on which bonds are broken during collision in the MS, ions A, B, C, X, Y or Z may be formed. Their masses are detected and correspond to the molecular mass of the ions (**http://www.weddslist.com/ms/tandem.html**). (Permission from owner of website was obtained to use this figure).

Based on the mass detected by the MS, the daughter ions and their structures may be inferred. A bottom-up approach is used to piece the original peptide back together and it can then be identified and quantified. The corresponding protein may be subsequently identified and quantified, and protein expression in different samples compared.

2. Aims and Objectives

2.1 Global study of miR-181a in HepG2 cells

The first aim of this project is to investigate the overall effects of miR-181a in HepG2 cells. We will employ the use of the LC-MS/MS to obtain a protein profile of the cells transfected with either a control miRNA, miR-181a or its inhibitor. The differential expression of proteins obtained that are both significant and pivotal in cancers would give us a preliminary outlook on what "class" of miRNAs miR-181a may belong to (ie. An oncogene or a tumour suppressor). Following protein profiling, we next assess how miR-181a affects critical cancer-related processes. We will focus on cell proliferation and cell cycle as these are important processes often found altered in cancers.

2.2 Molecular Study of miR-181a in HepG2 cells

With the results obtained from the studies performed above, we will then delve into the molecular level and identify the direct mRNA targets of miR-181a in HepG2 cells, both *in vitro* and in the cellular environment. This may be able to explain some of the observed phenotypes in earlier experiments. Apart from direct targets, because of the non-specific nature of miRNAs and the interconnectedness of the protein network in cells, we would also expect other downstream effects of the introduction of a single miRNA in cells. Therefore, we propose to also study the effect of important cancer-related pathways and their transcription factors when miR-181a is transfected into HepG2 cells. We will also carry out a PCR array analysis to try to identify more targets of miR-181a, taking in mind that the action of miRNAs is usually found at the translational level. All these, when taken together, would hopefully be able to elucidate the general function of miR-181a in HepG2 cells.

3. Materials and Methods

2.1 Cell Culture

HepG2 (Human hepatoma cell line) cells were obtained from American Type Culture Collection (ATCC), maintained and passaged in Minimal Essential Medium (MEM) (Gibco, Invitrogen), supplemented with 10% fetal bovine serum (FBS) (Gibco, Invitrogen), 1% anti-mycotic (penicillin, streptomycin, and amphotericin) (Invitrogen) at 37°C in a 5% CO_2 incubator. Cells were passaged every 2–3 days at 80–90% confluency.

Subculturing of cells was carried out using 0.25% trypsin-EDTA (Gibco, Invitrogen). Briefly, at confluence, complete growth media was aspirated and the adherent cell monolayer gently washed with warm sterile phosphate-buffered saline (PBS, 8 g/L NaCL, 1.44 g/L Na_2HPO_4, 0.24 g/L KH_2PO_4, pH 7.4) (Lonza). PBS was next aspirated and 1ml of 0.25% trypsin-EDTA added to the cell monolayer grown in 100mm petri dishes (Greiner Bio-One). Cells were incubated in a 37^oC, 5% CO_2 incubator until most of the cells became detached. 4ml complete media was added to neutralize the trypsin, cells collected in a tube and centrifuged for 4 min at 1000 rpm at room temperature using a bench-top centrifuge (Sigma Aldrich). The cell pellet was then resuspended in complete growth media and divided into individual tissue culture wares.

For cryopreservation of cells, cells were trypsinized and pelleted as above. Resuspended cells were aliquoted into 2ml plastic cryogenic vials (IWAKI) and tissue culture grade dimethylsulphoxide (DMSO) (Sigma Aldrich) was added to a final concentration of 10%. The cryovials were put into the 4^oC fridge for 30min, then -20^oC freezer for 4h, overnight at -80^oC and finally transferred and stored in liquid nitrogen the following day.

2.2 Determination of Cell Number

Manual Counting

Cells were manually counted using a Neubauer haemocytometer (Baxter Scientific). After trypsinization and neutralization, the cells were appropriately diluted down and 10µl of cell suspension loaded into one chamber of the haemocytometer. Excess liquid was blotted off and the cells were allowed to settle on the slide for 30s. The number of cells in each of the four corner and central squares was counted under an inverted microscope

(Olympus) under a 10X magnification using a hand-held counter. The number of cells per millimetre and total cell number were determined using the following calculation:

$$Cells/ml = \frac{\#cellscounted.X.10^4.X.dilutionfactor}{\#squarescounted}$$

$$Total\#cell = Cells/ml.X.suspensionvolume$$

2.3 Cell Transfection

Transfection of cells was carried out via different techniques, depending on the subsequent analysis carried out. Most of the transfections were carried out using electroporation, as this method has shown to be of high efficiency. In this method, cells were transfected in Cell Line Nucleofector Solution V (Lonza). 24h prior to transfection, 2.5×10^6 cells were seeded in 100mm tissue culture dishes. Upon adherence and confluence, the cells were serum starved with 2% FBS MEM for 16-24h before being transfected with various concentrations of synthesized miRNAs (Dharmacon). We chose to perform a starvation step for this length of time because it has been shown by other studies that the longer the starvation period (up to 72h), the larger the proportion of cells in the G0/G1 stage, therefore successfully synchronizing the cells according to the baseline level of the cell cycle [88]. This is important in our study because we are interested in cell cycle analysis and minimal interference would be preferred. Many other studies have also used serum starvation as a form of synchronization such that cells are at the same 'starting point' before the actual experiment is conducted [89]. However, we note that despite the advantage of this, serum starvation itself may pose as a form of stress for the cells, indirectly causing unwanted cellular reaction like apoptosis. Therefore, a final starvation duration of 16h was chosen for our studies. Briefly, HepG2 cells were

resuspended in 100µl Nucleofector Solution V. miRNAs were added and transferred into the specialized cuvettes provided. Electroporation was carried out using Program T-28 (HepG2 high efficiency). 500µl warm complete growth media was added to the transfected mix and carefully transferred, using the plastic pipettes provided, into 100mm tissue culture dishes containing 10ml complete growth media. The transfected cells were allowed to grow at 37°C, in a 5% CO_2 incubator for an appropriate amount of time before harvesting or continuing with subsequent assays.

2.4 miRNA Quantification

To ensure successful transfection of miR-181a in the cells, a real-time reverse transcription polymerase chain reaction (RT-PCR) was carried out to quantify the amount of miR-181a in the cells. The miScript PCR system (Qiagen) was used for the precise real-time quantification of miR-181a. Specifically, the miRNeasy mini kit (Qiagen), miScript PCR starter kit (Qiagen) and the miScript primer assay (Qiagen) were used according to the manufacturer's instructions for this purpose.

2.4.1 Total RNA Extraction

Total RNA was extracted using the miRNeasy mini kit. Cells were harvested, pelleted and disrupted by vortexing in 700µl QIAzol lysis reagent for 1min. The homogenate was left on the bench-top for 5min at room temperature. 140µl chloroform was added to the homogenate, vortexed for 15s and left on the bench-top for 3min at room temperature. The mixture was centrifuged at 4^{o}C at 12,000 x *g* for 15min. The upper aqueous phase was collected into a new collection tube (supplied) and 1.5 volumes of 100% ethanol added and mixed.700µl of sample was added into an RNeasy Mini spin column in a 2ml

collection tube and centrifuged at 14,000rpm for 15s at room temperature. The flow through was discarded and the procedure repeated with the remaining sample. 700ul Buffer RWT was added to the column and centrifuged at 14,000rpm for 15s and the flow through discarded. 500µl Buffer RPE was next loaded onto the column and centrifuged as before. Another 500µl Buffer RPE was loaded again and centrifuged for 2min. To elute RNA, the column was transferred to a new 1.5ml collection tube and 40µl RNase-free water added directly on the membrane. The tube was centrifuged at 14,000rpm for 1min and repeated again with another 40µl RNase-free water to obtain a total RNA elution volume of 80µl. The RNA was quantified using a nanodrop spectrophotometer.

2.4.2 Reverse Transcription of Total RNA

The cDNA was synthesized using the miScript HiFlex buffer instead of the HiSpec buffer because a concurrent quantification of mRNA was performed. Each reaction of reverse transcription master mix was prepared on ice as follows: 4µl 5X miScript HiFlex Buffer, 2µl 10X miScript Nucleics Mix, 2µl miScript Reverse Transcriptase Mix, 1µg RNA template and a variable amount of RNase-free water to make up a total volume of 20µl. The mixture was incubated at 37^{o}C for 60min and 95^{o}C for 5min and immediately proceeded with real-time PCR.

2.4.3 Real-time PCR

For detection of the mature miRNA, each reaction mix was prepared by adding 12.5µl 2x QuantiTect SYBR Green PCR Master Mix, 2.5µl 10x miScript Universal Primer, 2.5µl 10x miScript Primer Assay and an appropriate amount of cDNA template and RNase-free water. The mix was transferred to 0.2ml white strip tubes (Bio-Rad) and sealed with

optical flat strip caps (Bio-Rad). The real-time PCR was carried out on the IQ5 Multicolor Real-time PCR detection system (Bio-Rad). The cycling program was: 95^{o}C for 15min (PCR initial activation step); repeat 40 times the following: 94^{o}C 15s, 55^{o}C 30s, 70^{o}C 30s.

Microsoft Excel formatted data, including the amplification analysis, experimental report, melting curve analysis and threshold cycle number (C_t) were automatically provided by IQ5 optical system software version 2.0 (Bio-Rad). The fold changes were calculated as follows:

Sample $\Delta C_t = C_{t\ sample} - C_{t\ \beta\text{-actin}}$; $\Delta\Delta C_t$ = Sample ΔC_t - Control ΔC_t;

Fold change (Sample vs Control) $= 2^{-\Delta\Delta C_t}$

2.5 Protein Profile Preparation and Labeling with iTRAQ Reagents

Cell pellets were lysed in 200µl 8M urea, 4% (W/v) CHAPS and 0.05% SDS (W/v) on ice for 20min with regular vortexing. Cell lysate was centrifuged at 12,800rpm for 45min at 4°C, supernatant collected, and protein quantified using the Bradford Protein Assay (Biorad). A standard curve was established using BSA as a control (Further details under the Materials and Methods for 'Western blot Validation of LC-MS/MS Results'). 100µg of each sample was protein precipitated by the addition of 4 volumes of cold acetone and stored at -20° C for 1h. The samples were centrifuged for 5min at 12,040rpm and supernatant removed. Precipitated proteins were dissolved in the dissolution buffer, denatured and cysteine-blocked as described in the iTRAQ protocol (Applied Biosystems). Each sample was then digested with 20µl of 0.25µg/µl sequence grade modified trypsin (Promega) solution at 37°C overnight and labelled with the iTRAQ tags as follows:

HepG2 transfected with miR-mimic control: iTRAQ 114; HepG2 transfected with miR-inhibitor control: iTRAQ 115; HepG2 transfected with miR-181a: iTRAQ 116; HepG2 transfected with miR-181a inhibitor: iTRAQ 117. Labelled samples were pooled before analysis. To verify that sample preparation techniques do not interfere with digestion and labeling procedures, BSA standard solution (Pierce) was also enzymatically digested with trypsin and labelled with the iTRAQ reagents as previously stated. These differentially labelled digests were mixed at a ratio of 1: 2: 1.5: 2 and analysed by LC-MS/MS.

2.5.1 On-line 2D Nano-LC-MS/MS Analysis

The Agilent 1200 nanoflow LC system (Agilent Technologies) was used along with the 6530 Q-TOF mass spectrometer (Agilent Technologies) for this purpose [90]. A total of 3µl of the pooled sample peptide mixture was loaded onto the PolySulfoethyl A strong cation exchange column (SCX) (0.32 x 50 mm, 5 µm). The peptides that do not bind to the SCX column is subsequently trapped in the ZORBAX 300SB-C18 enrichment column (0.3x5mm, 5um) and washed isocratically with loading buffer 1 (5% acetonitrile, 0.1% formic acid) at 0.5 ml/min for 100min to remove any excess reagent. Next, the enrichment column is switched into the solvent path of the nanopump. Peptides were eluted using buffer 2 (0.1% formic acid) and buffer 3 (95% acetonitrile, 0.1% formic acid) with a nanoflow gradient increasing from 5%-80% buffer 3 over 100 min at a flow rate of 500 nl/min for each analysis. An increasing concentration of acetonitrile elutes the concentrated sample and further separation is achieved onto the analytical Zorbax 300SB C-18 reversed-phase column (75umx50mm, 3.5um). Survey scans were acquired from m/z 300-1500 with up to two precursors selected for MS/MS from m/z 100-2000. Following the completion of the first analysis, the enrichment column is switched again

into the solvent path of the SCX. Increasing concentrations of buffer 4 (KCl salt solution from 10mM to 500mM) is used to elute the retained peptides from the SCX column by sequential injection, followed by valve switching and reversed phase chromatography, respectively.

2.5.2 Data Analysis and Interpretation

Following the separation of peptides, we proceeded in the identification and quantification of proteins detected. The Spectrum Mill MS Proteomics Workbench (Agilent Technologies, Software Revision A.03.03.084 SR4) was used to identify proteins and to quantify their relative abundance. Each MS/MS spectrum was searched for the species of 'Homosapiens' in the UniProt_sprot_20100123 database. The searches were run using the following parameters: fixed modification of methylmethanethiosulfate-labelled cysteine, fixed iTRAQ modification of free amine in the amino terminus and lysine. Other parameters such as tryptic cleavage specificity, precursor ion mass accuracy, and fragment ion mass accuracy were in-built as functions of the Spectrum Mill software. The protein profile results were filtered with a protein score greater than 11 and peptide score of at least 6, giving a confidence value of more than 99%. Relative quantification of proteins in the case of iTRAQ was performed on the MS/MS scans and displayed as the ratio of the areas under the peaks at 114 and 115 Da, which were the masses of the tags that corresponded to the iTRAQ reagents. The relative amount of a peptide in each sample was calculated by the ratio of the peak areas observed at 115.1 m/z over that of 114.1 m/z. Sequence coverage was calculated as a result of the number of amino acids observed divided by the protein amino acid length. Standard deviation was calculated by analyzing protein ratios between the miR-transfected cells and control transfected cells rather than

peptide ratios. The following criteria were required to consider a protein for further statistical analysis: more than two unique peptides with high confidence (95%) had to be identified, and the-fold differences of integral proteins had to be greater than 1.1.

2.6 Western blot Validation of LC-MS/MS Results

2.6.1 Protein Quantification

The Bradford dye-binding assay was used to measure the total protein concentration in the cell lysates. Bovine serum albumin (BSA) (Sigma) (1mg/ml) was used to prepare protein standards. 0, 5, 10, 15, 20, 25 and 30µl of BSA were individually pipetted into 1ml disposable plastic PLASTIBRAND® cuvettes (Brand). The volume was topped up to 1ml with Bradford reagent and mixed by pipetting gently till a homogeneous solution is formed. Absorbance at 595nm was measured using a spectrometer. The absorbance values were used to plot a BSA standard curve.

For measurement of sample protein concentration, 10µl of protein sample was diluted in 990µl of Bradford reagent. 1ml of Bradford reagent without proteins added was used as the blank control. The OD was read at 595nm and protein concentration was determined against the BSA standard curve.

2.6.2 Gel Electrophoresis

SDS-PAGE was performed on the Bio-Rad mini-protean electrophoresis system. Each 1mm thick gel consists of a stacking gel and separating gel. Separating gels were prepared by mixing appropriate amounts of 40% acrylamide/bisacrylamide solution (37.5:1, acrylamide/bis; Bio-rad) (1.875 ml for 7.5% gel, 3.125 ml for 12.5% gel and 3.75 ml for

15% gel) with 2.5 ml of 1.5 M Tris·Cl (pH 8.8), 100µl of 10% SDS, and 100µl of 10% fresh ammonium persulfate (APS) (Bio-rad) and H_2O to a total volume of 10ml. The volumes can be adjusted accordingly. 5µl of N, N, N', N'-tetramethylethylenediamine (TEMED) (Bio-rad) was added just prior to pouring the gel into the gel apparatus setup. 100µl pure ethanol was immediately placed over the separating gel to rid of bubbles. After polymerization, the ethanol was decanted, and a 5% stacking gel was poured on top of the separating gel. 4ml of 5% stacking gel was prepared by mixing 0.5ml of 40% acrylamide/bisacrylamide solution with 0.5ml 1.0 M Tris·Cl (pH 6.8), 40µl of 10% SDS, 40µl of 10% APS, 4µl TEMED and H_2O. A comb was inserted at the top and the gel allowed to polymerize completely before preparing for gel electrophoresis.

30µg protein per sample was mixed with 1 x loading buffer (62.5 mM Tris·Cl pH6.8, 10% glycerol, 2% SDS, 0.05% bromophenol blue), and 100 mM dithiothreitol (DTT) (Sigma) and denatured at 90^{o}C for 5min. For non-reducing condition, the DTT was omitted. After loading the samples into the wells, the gel was run under constant current (20mA) condition until satisfactory protein separation was observed. 10µl Novex Sharp Protein Standard (Life Technologies) was loaded per lane to verify protein size.

2.6.3 Gel transfer

The separated proteins were electrophoretically transferred to a Hybond-P Polyvinylidene Fluoride (PVDF) membrane (Amersham-Pharmacia) using Mini-PROTEAN 3 Electrophoresis System (Bio-rad). The polyacrylamide gel obtained after electrophoresis was rinsed in water, placed in-between layers of Whatman paper and membrane, cut to exact size of the gel, and inserted with 8 layer filter papers soaked in transfer buffer (0.3%

Tris, 1.45% glycine and 20% methanol), with the membrane facing the anode. The bubbles were carefully and completely removed by rolling across a glass spreading rod. The transfer was performed in 1x transfer buffer at 21V for 50min. The blotted membrane was marked and washed with 1x Tris-buffered saline (TBS) (20mM Tris·Cl pH 7.4, 150mM NaCl) buffer and stored at 4°C if not used immediately.

2.6.4 Immunoprobing

The antibodies used in this study were as follows: (1) 14-3-3σ protein (SC 7681, Santa Cruz), (2) α-enolase (SC 100812, Santa Cruz), (3) Hsp-90β (SC1057, Santa Cruz), (4) NPM1 (SC 47725, Santa Cruz), (5) p27 (SC 528, Santa Cruz), (6) E2F7 (AB56022, Abcam, Biomed Diagnostics), (7) *β*-actin mouse monoclonal IgG (Sigma A5441). Bands were analysed and quantified by ImageJ software.

The immunoprobing was carried out following the standard protocol. Briefly, the membrane was wetted with 1X TBS buffer before being blocked with 5% nonfat milk powder in 0.1% TBST (0.1% Tween-20 in 1x TBS) for 1h at room temperature. Following blocking, the membrane was incubated with the recommended amount of primary antibody in 5% nonfat milk powder in 0.1% TBST overnight at 4°C on a roller. After that, it was washed three times with 0.1% TBST for 10min each time. After the washings, the membrane was incubated in anti-goat, anti-mouse or anti-rabbit IgG HRP-conjugated secondary antibody (Thermo) in 5% nonfat milk powder in 0.1% TBST for 1h at room temperature on a roller. The membrane was then washed three times as before and incubated in the SuperSignal West Pico Substrate solution (Pierce) by mixing equal

volumes of the two reagents for 3min and then exposing to Hyperfilm X-ray films (Amersham-Pharmacia) for the desired amount of time.

2.6.5 Stripping and Re-Probing

Where re-probing was done, the membrane was stripped after chemiluminescent detection and re-probed with other primary antibodies. Briefly, the membrane was washed in TBST for 5min and incubated in sufficient volume of Re-Blot Plus Strong Stripping Solution (Merck, Millipore) at room temperature for 15min. The membrane was then blocked and re-probed as before.

2.7 WST-1 Cell Viability Assay

Assessment of HepG2 cell viability was carried out using the WST-1 reduction test. Briefly, HepG2 cells electroporated with miRNAs were seeded a 96-well plate and incubated for 24h, 48h or 72h. At the end of these time points, 10µl WST-1 solution (Roche Applied Science) was added to each well containing $3x10^4$ cells each. The plate was incubated at 37ºC for 1h and absorbance measured using a microplate reader (Benchmark Plus) at 450nm.

For HepG2 cells transfected with miRNAs and subsequently treated with *cisplatin*, the transfected cells were seeded in 96-well plates for the various incubation times and then treated with 21µg/ml *cisplatin* for 24h. This concentration of *cisplatin* was chosen as it is found to be slightly less than the LC_{50} of *cisplatin* at 24h. This is because we do not wish for the cells to fully undergo apoptosis at the point of readout, as a cell viability test

requires cells to still be active, albeit weakened by the treatment. Readout was then measured as before.

2.7.1 *Cisplatin* Concentration Determination

HepG2 cells were seeded in 96-well plates in complete growth media and a range of *cisplatin* concentrations (0-21µg/ml) added to each well. The WST-1 assay was used to measure cell viability 24h after *cisplatin* treatment. LC_{50} here refers to the lethal concentration of a chemical (ie. *Cisplatin*) such that 50% of the population are killed off after a given duration of time. A concentration of *cisplatin* was chosen as the experimental concentration such that the cells are still viable, albeit weakened by *cisplatin* treatment.

2.8 Cell Cycle Analysis

Transfected cells were harvested and washed in PBS. They were then fixed in -20°C methanol (by adding drop wise to the cell pellet while vortexing) for 30min at 4°C. The fixed cells were washed twice in PBS and treated with 25µl 20µg/ml Ribonuclease A (Biomed Diagnostics). 500µl propidium iodide (Sigma Aldrich) (100µg/ml) was added to the cells and left to incubate in the dark at 37°C for at least 30min. The cells were then analysed by flow cytometry (BD FACSCalibur™).

2.9 Bioinformatics Study of mRNA Target Prediction

Human miRNA target predictions for miRNA families were obtained from TargetScan 6.2 (http://www.targetscan.org/) as well as miRanda (http://www.microrna.org/microrna/home.do) database. miRò, the miR-ontology database was also used as a convenient source of categorizing miRNAs and their targets by

diseases, functions or processes that they are involved in. Relevant targets predicted by both TargetScan and miRanda were chosen for wet lab experimentation. Putative miRNA:mRNA interaction, in TargetScan, was based on the total context score and probability of conserved targeting (P_{CT}). The more negative the context score and the higher the P_{CT}, the higher the probability of miRNA:mRNA binding.

Apart from interaction around the seed region, a secondary source of concern, in terms of possible miRNA:mRNA binding, would be the extent of RNA folding around the binding site. The Mfold web server is an online software that calculates free energies of folding (ΔG_{Fold}). The more negative the $\Delta G_{Fold,}$ the higher the probability of RNA folding.

2.10 Surface Plasmon Resonance (SPR) assay.

Surface plasmon resonance (SPR) is a real-time platform for detecting the binding of specific molecules to a partner. Protein interactions, small molecules, nucleic acids, cells and viruses and carbohydrates are some of the compounds that can be studied with SPR [91]. It typically takes place on the sensor surface of a chip, and its working principle is based on the change in refractive index of the interface when the surface condition changes. When positive binding occurs, the sensorgram registers a change in angle due to the increase in mass bound at the surface. A real-time profile of binding followed by subsequent dissociation can be generated, and the kinetics of the binding characterised. This provides a quick yet precise method of screening potential mRNA targets of miR-181a. An illustration of the working platform is shown in Figure 9.

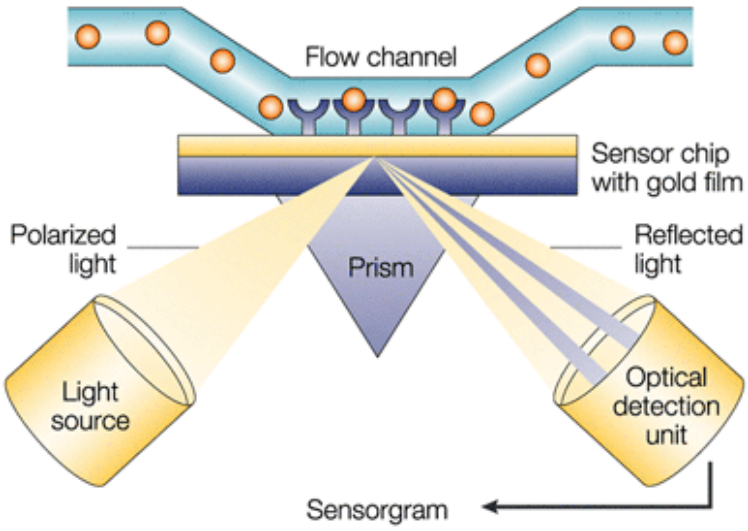

Figure 9. Working principles of SPR [92]. As polarized light hits the sensor-gold/buffer interface, it undergoes total internal reflection and the reflected light is eventually detected. At the same time, when the light hits the glass, the electrons from the gold layer absorbs the energy from the evanescent waves, generating plasmons, reducing the reflected light and hence causing a drop in the intensity of light detected. This happens at a certain angle, depending on the angle of incidence light. When binding occurs, the increase in mass bound to the interface causes a change in refractive index of the solution, thereby altering the angle of reflected light detected. (Permission from ref.89 was obtained from publisher to use this figure).

All SPR experiments were run with HBS-EP buffer (10mM HEPES, 150mM NaCl, 3.4mM EDTA and 0.005% P20 at pH 7.4) on a Biacore 3000 (BIAcore AB, GE Healthcare) with a carboxymethylated dextran coated sensor chip (CM5) at 25°C. Two surfaces were activated for 7min with 1:1 mixture of 0.2 M N-ethyl-N'-[3-(diethylamino)propyl]carbodiimide (EDC) and 50mM N-hydroxysuccinimide (NHS), before immobilization of 1500 RU of Neutravidin (Pierce, USA) in 10mM sodium acetate at pH 6.0 at the flow rate of 10µl/min by standard amine coupling procedure. The surfaces were then blocked with 0.5M ethanolamine-HCl at pH 8.5 for 7min. Biotin-labelled single-stranded RNA harboring 31bp 3'UTR of CDKN1β mRNA (5'-GGGAGUU**UUGAAUGU**UAAGAAUUGACCAUCUGC -3') and 34bp 3'UTR of E2F7 mRNA (5'- GGGUAUGACGAC**UUGAAUGU**UUAUACUUUUAUUC -3') were captured on sensor chip surface to 200 RU and 430 RU, respectively. Another two empty

channels serve as reference. A 2-fold serial injection of miR-181a (180nM, 359nM, 719nM, 1.44uM, 2.88uM, 5.75uM, 11.5uM, and 23uM) was injected at 10µl/min across all the surfaces for 2min, and was then allowed to dissociate for 15min. All the sensorgrams were corrected by subtraction of the responses of analytes on the empty channel and buffer blanks [93]. Processed data were globally analysed and fit into 1:1 interaction model to yield the affinity.

2.11 Transformation

Mammalian expression vectors (Firefly/renilla duo-reporter vector system) with the 3' UTR of CDKN1β and E2F7 cloned downstream of the secreted firefly luciferase reporter gene were obtained from GeneCopoeia. These have been sequenced and quality checked before subsequent usage. 1µl of DNA plasmid was mixed with 50µl competent cell *Ecoli* strain *TOP10* in a microcentrifuge tube. The tube was stored on ice for 10min. It was next heat shocked at 42^0C for 90s and returned to ice immediately for 2min. 450µl fresh LB was added and the cells incubated at 37^0C in a shaking incubator at 250rpm for 1h. LB/*kanamycin* agar plate (1% Tryptone, 0.5% yeast extract, 171mM NaCl, 1.5% agar, PH 7.0) was prepared and 100µl of transformed bacterial cells was spread on top and incubated at 37^0C overnight in an inverted position.

2.12 Mini-prep Purification of Plasmids

A single colony of *TOP10* was incubated in 5ml sterile LB medium with 100ng/ml Kanamycin in a 15ml falcon tube at 37℃ with agitation at 250rpm overnight. The bacteria were harvested directly by centrifuging at 2500 rpm for 15min (Beckman Allegra 64R). Plasmid extractions were carried out using QIAprep Miniprep plasmid kit (Qiagen). 250µl

buffer P1 was used to resuspend the bacterial pellet and transferred to a microcentrifuge tube. 250µl buffer P2 was added and mixed gently. 350µl buffer N3 was added, mixed and centrifuged at 13,000rpm for 10min. The supernatant was loaded on QIAprep Spin Column, centrifuged at 13,000rpm for 30s, and the flow-through discarded. 750µl buffer PE was added to the column and centrifuged at 13,000 rpm for 30s, discarding the flow-through. The column was centrifuged for an additional minute to remove residual buffer. The column was placed on a new microcentrifuge tube and 50µl buffer EB (10mM Tris.Cl, pH 8.5) added and incubated for 1min. The DNA plasmid was finally eluted out by centrifugation for 1min, quantified by nanodrop spectrophotometer and stored at -20℃ until further use.

2.13 Co-Transfection of Plasmids and miRNAs

The co-transfection of DNA plasmids and miRNAs was carried out via electroporation. Briefly, $1x10^6$ of overnight starved HepG2 cells were resuspended in 100µl nucleofection solution and co-transfected with 4µg DNA plasmid and either 10nM or 100nM miR-181a. An additional control vector was also used such that the sequence cloned downstream of the firefly luciferase reporter gene is of a random, non-specific targeting sequence. 100K transfected cells were seeded in each well of a 24-well plate and incubated with 500µl complete growth media at 37℃ overnight.

2.14 Luciferase Assay

Luciferase is a class of enzyme that is used in bioluminescence, or light production. Many different luciferases are available, but the most common ones are those of the fireflies.

Their presence, in addition to a substrate luciferin, causes a chemical reaction to occur such that light is produced:

Luciferin + ATP → Luciferyl adenylate + PP_i

Luciferyl adenylate + O_2 → Oxyluciferin + AMP + Light

In our study, we make use of this property of luciferase to test for the binding between miR-181a and its predicted mRNA targets. A plasmid coding for the firefly luciferase is used, modified with the different 3'UTRs of the mRNAs cloned downstream of the firefly luciferase reporter gene. Co-transfection of miR-181a and the plasmid into HepG2 cells allow for any binding to occur. If binding exists, the transcription of the reporter firefly luciferase gene would be inhibited, thereby leading to a lowered bioluminescence detected. Figure 10 shows the plasmid used. The plasmid is a firefly/Renilla Duo-Luciferase reporter vector (GeneCopoeia, USA), with the Renilla Luciferase reporter gene acting as the control reporter in which firefly luciferase is normalised against. Two different variations of the plasmids were used, corresponding to the different 3'UTRs of the mRNAs cloned downstream of the firefly luciferase reporter gene. An additional control vector (C1) (GeneCopoeia, USA) was used that incorporated a random sequence downstream of the firefly luciferase reporter gene.

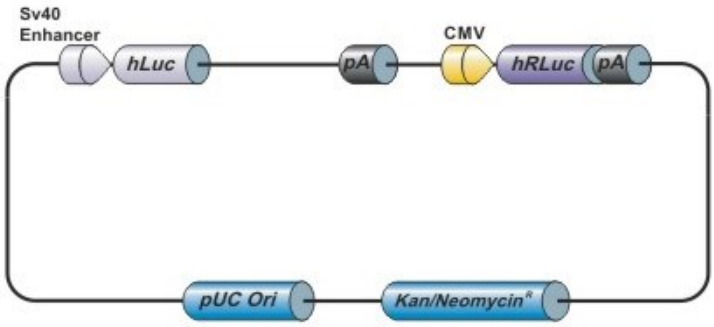

Figure 10. Schematic diagram of the firefly/renilla duo-luciferase reporter vector. The 3'UTRs of CDKN1β and E2F7 are cloned downstream of the firefly luciferase reporter gene, while a random sequence is cloned in the case of the control vector. Renilla luciferase activity is used as the internal control, and the firefly luciferase activity is normalised against that measured of renilla luciferase.

The luciferase assay was carried out using GeneCopoeia Luc-Pair™ miR Luciferase Assay kit. 24h after co-transfection of plasmids and miRNAs, growth media was aspirated and 300µl Solution 1 was added to each well and incubated at room temperature for 3min. 80µl of cell lysate was removed and transferred into a new 1.5ml microcentrifuge tube. Working Solution I and Working Solution II are prepared as follows. To prepare Working Solution I: Solution I and Substrate I are warmed up to room temperature and Substrate I diluted in Solution 1 in a ratio 1:40. Similarly, for Working Solution II, Substrate II was diluted in a ratio of 1:200 in Solution II. Prior to luciferase activity measurement, the GloMax 20/20 Luminometer (Promega) was set to measure luminescence for 2s. 20µl of Working Solution I was added to each of the 80µl sample and firefly luminescence measured (M1). 100µl of Working Solution II was subsequently added and renilla luminescence measured (M2). The firefly luciferase luminescence values obtained were normalized by taking M1/M2. The stability of the plasmids was also dutifully noted throughout the experiments to ensure that no aberrant measurements occurred, which

could imply plasmid instability or incompatibility with the cellular environment. This may be observed from the raw luminescence values (ie. M2) of the renilla reporter that was used in all three plasmids. Because it serves as a constitutively expressed control, the measured luminescence should be similar in all experiments where the same amount of plasmids was used. Any deviation from the values obtained within a single batch of experiments may indicate error and that measurement would not be used for further analysis. One thing to note, is that the transfection of the plasmid into the cells is a transient process and we are only investigating the interaction, if any, of the miRNA and its putative targets' mRNA 3'UTRs in the cellular environment. Hence, we would expect the plasmids' measured luminescence to be diluted with time.

2.15 Cignal Reporter Assay Analysis of Cancer Pathways Affected by miR-181a

The Cancer 10-pathway Reporter Luciferase Kit (Qiagen) in plate format was used in the measurement of ten cancer-related signaling pathways. Electroporation would not be possible with this assay format, therefore liposomal transfection was employed. A reverse transfection protocol was used as compared to the traditional forward transfection as this method of transfection has been found to be more efficient and reproducible.

This reporter array consists of ten cancer-related pathways that can be screened simultaneously. The signalling pathways included are Wnt, Notch, p53/DNA damage, TGFβ, Cell cycle, NFκB, Myc/Max, Hypoxia, MAPK/ERK and MAPK/JNK. Positive and negative controls were also included for quality control purposes. The assay came in a 96-well cell culture plate format, with each column being distinct from the next, distinguishable by the different transcription factor reporters dried down in each well. The

sample, negative control and positive control reporter transcription factors are as shown in Figure 11.

Figure 11. Illustration of the various reporter constructs used in the array. Mixture of constructs of each of the ten reporter assays (left), negative control (middle) and positive control (right).

Briefly, 2pmol of miRNA was diluted in 25µl of pure Opti-MEM (Life Technologies) growth media and added to each well of the plate to resuspend the plasmids. 0.6µl Attractene (Qiagen) was diluted in 25µl pure Opti-MEM in a separate microcentrifuge tube, incubated at room temperature for 5min and added to each well of the resuspended plasmids. The Attractene/plasmids-miRNA complex was allowed to form for 20min at room temperature. HepG2 cells growing in complete MEM media with 10% FBS were washed in PBS and trypsinized, centrifuged and supernatant discarded. The cell pellet was resuspended to $4X10^5$ cells/ml in Opti-MEM containing 5% FBS. After 20min of complex formation, 100µl of the prepared cell suspension was added to each well containing the constructs-miRNA-Attractene complexes, making up to a final volume of 150µl per well of a 96-well plate. The plate was mixed gently with a rocking motion and then incubated at 37℃ in a 5% CO_2 incubator for 16-24h. After 16-24h of transfection, the media was aspirated and changed to 75µl complete growth media (MEM with 10% FBS and 1% antimycotics) and further incubated at 37℃ for another 24h. The cells were checked with the positive control for GFP fluorescence using a fluorescent microscope. Following

successful transfection validation, the luciferase assay was developed by using Dual-Luciferase Reporter Assay System (Promega).

2.15.1 Developing Luciferase (Plate) Assay

Briefly, the Dual-Glo Luciferase buffer was added to Dual-Glo Luciferase Substrate to make up the Dual-Glo Luciferase Reagent. A calculated amount of Dual-Glo Stop & Glo Reagent was prepared by diluting the Dual-Glo Stop & Glo Substrate to the Dual-Glo Stop & Glo Buffer in a ratio of 1:100. 75µl Dual-Glo Luciferase Reagent was added to each well and firefly luminescence was measured after 10min (M1). 75µl of Dual-Glo Stop & Glo Reagent was added to each well and the renilla luminescence measured after 10min (M2). The ratio of luminescence (M1/M2) of firefly to renilla gives the normalized luminescent values per well. Luminescence was measured in a Tecan microplate reader with a Magellan Data Analysis Software.

2.16 Target Array Analysis of Direct mRNA Targets of miR-181a

2.16.1 RNA Extraction and Quantitation

RNA isolation was carried out using RNeasy mini kit (Qiagen). Briefly, cell pellets were resuspended in 350µl buffer RTL. (10µl β-Mercaptoethanol (β-ME) was added to 1ml buffer RTL). A 20-gange needle (0.9mm diameter) fitted to an RNase-free syringe was used to homogenize the sample, 1 volume 70% ethanol added and mixed well. Samples were transferred to RNeasy mini column placed in a 2ml collection tube, centrifuged at 13,000 rpm for 30s using a bench top centrifuge (Sorvall). The flow-through was discarded and 700µl buffer RW1 was added to column and centrifuged at 13,000rpm for 30s, discarding the flow-through. 500µl buffer RPE was added to column and centrifuged

at 13,000rpm for 30s, discarding the flow-through. Another 500µl buffer RPE was added and centrifuged at 13,000rpm for 2min. The column was placed in a new 2ml tube and centrifuged at 13,000rpm for 1min. The columns were transferred to a new 1.5ml collection tube. 30µl RNase-free water was directly added onto the membrane of column and centrifuged at 13,000rpm for 1min. The flow-through containing total RNA was quantified with a nanodrop spectrophotometer and stored at -80^{o}C until further use.

2.16.2 Reverse Transcription

Reverse transcription was carried out using the RT^{2} First Strand Kit (Qiagen). 0.5µg total RNA was added to the genomic DNA elimination mix, incubated at 42^{o}C for 5min and placed on ice. The reverse-transcription mix per reaction composed of 4µl 5x Buffer BC3, 1µl Control P2, 2µl RE3 Reverse Transcriptase Mix and 3µl RNase-free water. 10µl of this reverse-transcription mix was added to 10µl of genomic DNA elimination mix, pipetted to mix and incubated at 42^{o}C for 15min, followed by a 95^{o}C incubation for 5min. 91µl RNase-free water was added per reaction and the mixture either stored at 20^{o}C or immediately used for real-time PCR.

2.16.3 Real Time PCR

The PCR components mix per reaction consisted of 1350µl 2x RT^{2} SYBR Green Mastermix, 102µl cDNA synthesis reaction and 1248µl RNase-free water. 25µl of the mix was added to each well of the custom made RT^{2} Profiler PCR Array using an 8-channel pipettor. The array was sealed with optical thin-wall 8-caps strips. The platform used to carry out real-time PCR was Applied Biosystems 7500, with the following cycling conditions: 95^{o}C for 10min (1 cycle); 95^{o}C for 15s, 60^{o}C for 1min (40 cycles). An

automated baseline was used and the following calculation was used in the analysis of results: Sample ΔC_t=C_t Sample-C_t Housekeeping gene; $\Delta\Delta C_t$= Sample ΔC_t-Control ΔC_t; Fold change = $2 -\Delta\Delta C_t$

2.17 Statistical Analysis

All data are presented as mean ± SD. The Wilcoxon signed rank test was used for comparisons of fold changes in cell viability between HepG2 cells transfected with controls and miRNAs. 2-tailed Student's *t*-test was used for the other analyses where two experimental groups of values are being compared. Statistical significance was accepted at $p < 0.05$. Where the means of three or more groups were being compared for statistical difference, ANOVA was used. The value of n refers to the number of independent batch experiments performed for analysis.

3. A Quantitative Proteomics Approach in the Study of MicroRNA 181a in HepG2 Cells[1]

3.1 Introduction

Currently, not much of miR-181a is known about its role in HCC progression, apart from the fact that it is highly upregulated in HCC and HpSC-HCC, and that it is involved in the Wnt/β catenin signalling pathway, a pathway often found upregulated in many cancers. To study the effect of miR-181a in HCC, we first chose HepG2 cells as our model to represent HCC. It is a cell line commonly used in exemplifying HCC and is known to be a

[1] Reproduced in part with permission from [94] Y. Lin Jane Tan, N. A. Habib, W. Ning Chen, A Quantitative Proteomics Approach in the Study of MicroRNA 181a in HepG2 Cells, Current Proteomics, 9 (2012) 262-271. Reference copyright [2012]. Yi Lin Jane Tan designed and performed the experiments, analysed the data and wrote the paper.

good representation of human primary hepatocytes, therefore makes a good platform for an in depth study of this miRNA. The study of miR-181a in other established HCC cell lines would be the next step in the comparison and/or validation of the results of this study, but unfortunately is not going to be covered in this project as we are more interested in the potential effects of miR-181a as an initial investigation. The effect of miR-181a may be studied in two ways: To cause an upregulation of its expression in HepG2 cells or to inhibit its expression and examine the downstream effects of the perturbation. This can be done by either transfecting the cells with miR-181a or its inhibitor. As miRNAs are known to regulate many cellular processes through the binding of mRNAs, its introduction would have a profound effect in the protein profile of the cell. Because proteins are known to be the 'molecular machines' of cells, it is of great interest to study how the presence, or inhibition, of miR-181a would affect a cell's protein profile.

To do so, we make use of a modern and developed proteomics technique that is able to both identify and quantify the global protein profile of a given sample. The LC-MS/MS is a rapidly evolving platform for such a purpose, and in recent years, various methods have been used alongside this technology in elucidating the proteins that are present in biological samples. Among which, the iTRAQ method is the method of choice for our study.

3.2 Results and Discussion

3.2.1 RT-PCR of miR-181a in HepG2 Cells at 24h and 48h Post-Transfection

Before we begin to establish the protein profile, however, we first have to ensure that the HepG2 cells have been successfully transfected with miR-181a. Not only that, but we also

need to certify that the (new) levels of miR-181a is sustainable, at least for 48h, within the cell, because of the transient nature of its transfection. To do so, we have chosen electroporation as our method of transfection of miR-181a into HepG2 cells, because this technique has been consistently shown to produce a high transfection efficiency. Figure 12 shows the highly efficient transfection of GFP into HepG2 cells via electroporation.

After HepG2 cells were transfected with 100nM miR-181a and its inhibitor respectively, its relative amount in the cells were quantified by real-time RT-PCR. Figure 13 shows the levels of miR-181a at 24h and 48h post-transfection. A significant increase in levels of miR-181a is seen in cells transfected with miR-181a (by at least 3 times) while those that were transfected with the inhibitor exhibited much lower levels of the miRNA at both time points. This confirms the successful transfection via electroporation of miR-181a into HepG2 cells. The levels of miR-181a dropped slightly at 48h as compared to 24h post-transfection, albeit insignificant, but were still relatively high as compared to the control samples. This means that the transfection of miR-181a, although transient, but was still sustainable after a 48h time point at 100nM transfection concentration. We then proceeded to analyse the change in protein profile of HepG2 cells due to its transfection.

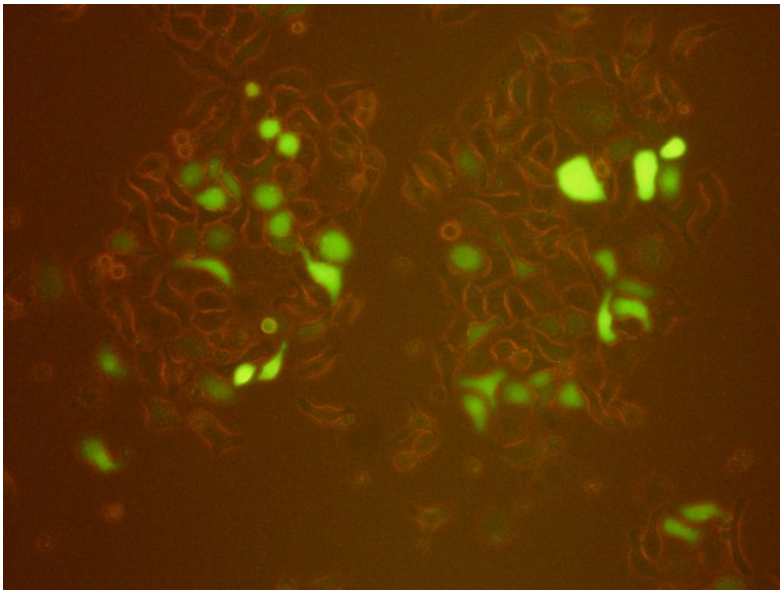

Figure 12. Phase contrast and fluorescence detection of HepG2 cells transfected with GFP plasmid at 24h post transfection. (10X magnification level) HepG2 cells were transfected with 4µg GFP by electroporation and incubated in complete growth medium. After a 24h incubation, the cells were viewed under a fluorescent microscope and compared with phase contrast microscopy. Most cells are observed producing green fluorescence, indicating the high transfection efficiency of this method on HepG2 cells.

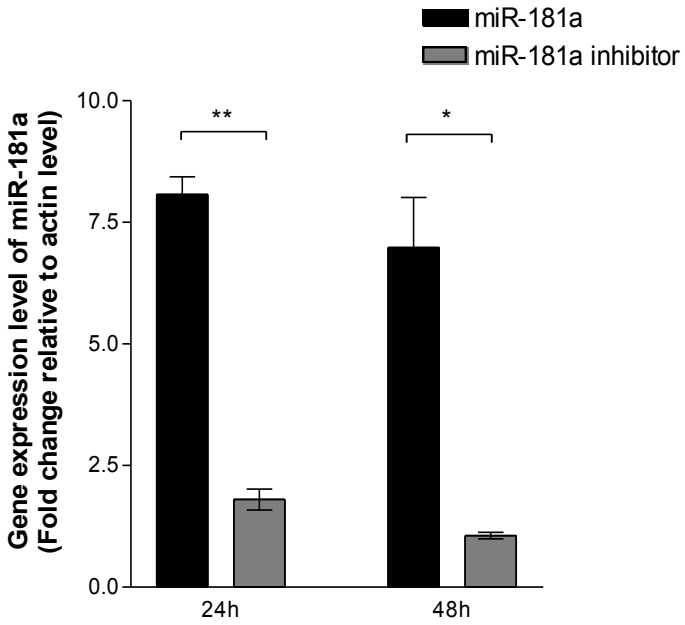

Figure 13. Real time RT-PCR of miR-181a gene expression levels at 24h and 48h post-transfection. Using a Student's *t*-test, the successful transfection of 100nM of miR-181a via electroporation caused a significant increase (p value= 0.0044 and 0.029 for 24h and 48h respectively) (n=3) in miR-181a levels in HepG2 cells as compared to those transfected with its inhibitor.

3.2.2 LC-MS/MS Analysis of Differentially Expressed Proteins

To understand the mechanisms and effects miR-181a induces in HepG2 cells, we proceeded to establish the protein profile of HepG2 cells transfected with this miRNA. HepG2 cells serum starved for 16h [95] were transfected with 100nM miR-181a or its inhibitor and harvested after a 24h incubation. This time point was chosen because the expression levels of miRNAs previously showed a slight decrease after that, albeit insignificant. Two different control miRNAs were used: One mimic control and an inhibitor control; each is a random sequence and serves as control for miR-181a and miR-181a inhibitor respectively. The transfected cells were lysed and proteins extracted and labelled with iTRAQ reagents. Experiments were carried out in triplicates and the MS result analysed by Spectrum Mill software using UniProt_sprot_20100123 database to identify and quantify the protein expression levels of the different samples. 208, 90 and 298 proteins were identified and quantified in the three experiments respectively. From these sets of data, proteins that were found to be consistently dysregulated due to the transfection of the miRNAs were chosen for further study. From this list, we further sieved out proteins involved in important cancer processes, for example, those involved in cell cycle, cell growth and apoptosis. Table 5 lists the proteins we have identified that are of interest.

11 proteins that were consistently found to be differentially expressed between the samples in all three independent experiments are listed and categorized according to their cellular functions. These included metabolic enzymes, stress proteins/molecular chaperones, binding/signalling proteins and transport proteins. The change in protein profile from the LC-MS/MS analysis shows a general upregulation of stress proteins in

HepG2 cells transfected with miR-181a. Inhibiting miR-181a, on the other hand, generally led to either a drop or no change in stress protein levels. Stress proteins act like molecular chaperones and tend to form a protective layer in the cell, shielding the cell from trauma, such that they become more resilient. These initial findings may suggest an oncogenetic role of miR-181a in HCC.

Among the proteins listed, a few garnered interest. Namely, heat shock protein 90β (Hsp-90β), nucleophosmin (NPM1) and 14-3-3σ protein. These proteins are heavily involved in cell survival (Hsp-90β) and cell growth (NPM1 and 14-3-3σ), which are crucial processes in the development of HCC. Expression of Hsp-90β was found to be increased in HepG2 cells transfected with miR-181a but decreased in cells transfected with its inhibitor. NPM1 was found to be increased in cells transfected with miR-181a but no significant change found in those transfected with the inhibitor. 14-3-3σ protein was found down-regulated in cells transfected with miR-181a. The roles and functions of these proteins will explained in further detail under '3.2.3 Western blot Validation of LC-MS/MS Identified Proteins'. Their representative peptides' MS are shown in Figure 14.

Table 5. List of 11 differentially expressed proteins characterized according to their function. The proteins were extracted from cell lysates and 100µg of total protein trypsinised and tagged with iTRAQ reagents 114, 115, 116 and 117. Peptide sequences were read in the MS and proteins quantified and identified. The ratio of expression of samples versus control provides the fold increase or decrease in protein expression.

Table 5 – Differentially expressed protein profile after miRNA transfections.							
Accession Number	**Protein name**	**%AA coverage**	**miR-181a/ control Mean±SD**	**miR-181a inhibitor/ Control Mean±SD**	**Peptide Count**	**Protein Score**	**Protein function**
P06733	Alpha enolase	40	1.31 ± 0.18	0.93 ± 0.17	12	195.71	Metabolic Enzyme
P14618	Pyruvate kinase isozymes M1/M2	33	0.93 ± 0.08	0.97 ± 0.08	13	196.07	Metabolic Enzyme

A5A6N7	L-lactate dehydrogenase B chain	16	1.47 ± 0.58	1.09 ± 0.43	4	44.22	Metabolic Enzyme
P15121	Aldose reductase	18	0.76 ± 0.27	0.96 ± 0.23	3	32.72	Metabolic Enzyme
P10809	60kDa heat shock protein, mitochondrial	49	1.32 ± 0.17	0.77 ± 0.17	17	291.66	Molecular Chaperone/ Stress Protein
P61603	10kDa heat shock protein, mitochondrial	23	1.18 ± 0.30	1.02 ± 0.15	2	23.79	Molecular Chaperone/ Stress Protein
P08238	Heat shock protein HSP 90-β	28	1.19 ± 0.12	0.87 ± 0.09	14	200.86	Molecular Chaperone/ Stress Protein
P06748	Nucleophosmin	28	1.37 ± 0.21	1.06 ± 0.53	6	93.7	Molecular Chaperone/ Stress Protein
P26599	Polypyrimidine tract-binding protein 1	24	1.84 ± 1.59	0.62 ± 0.12	5	74.97	Binding protein
P31947	14-3-3 protein sigma	31	0.72 ± 0.10	1.05 ± 0.37	4	51.99	Binding protein
O00410	Importin-5	5	1.01 ± 0.37	0.67 ± 0.20	3	39.92	Carrier/ Transport Protein

Panel A. Hsp-90β

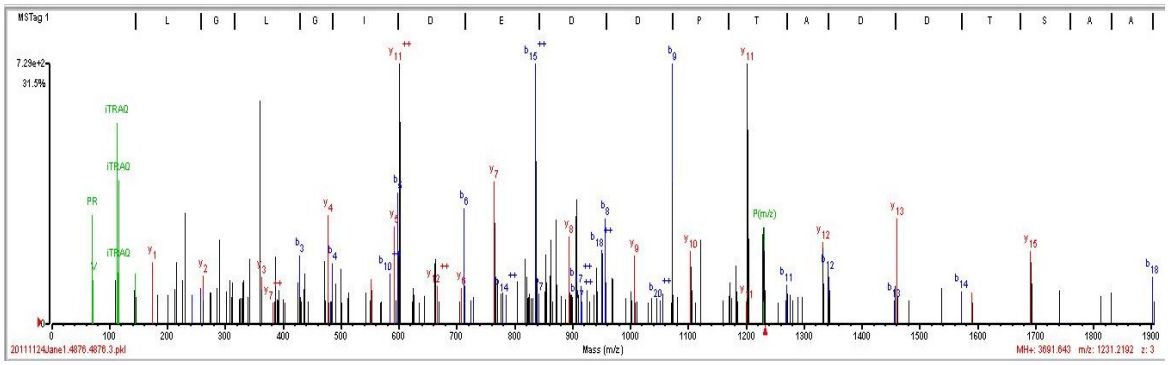

Panel B. NPM1

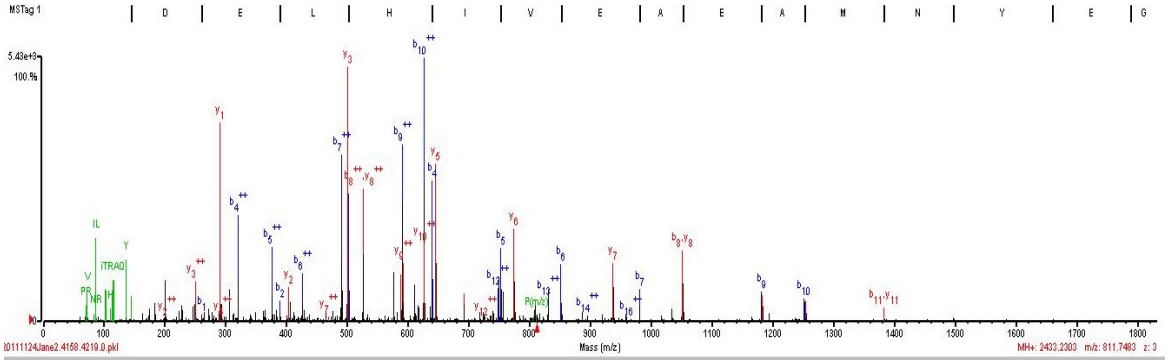

Panel C. 14-3-3σ

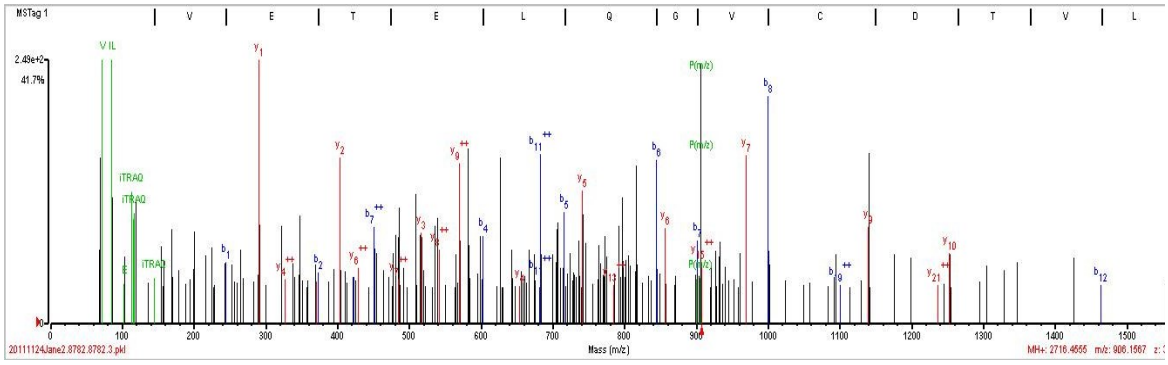

Figure 14. A representative MS/MS spectrum showing the peptides. The ion assignment were as follows: HepG2 transfected with miR-mimic control: iTRAQ 114; HepG2 transfected with miR-inhibitor control: iTRAQ 115; HepG2 transfected with miR-181a: iTRAQ 116; HepG2 transfected with miR-181a inhibitor: iTRAQ 117. Panels A, B and C represent spectrum of peptides identified and quantified that showed a consistent change in protein expression levels of Hsp-90β, NPM1 and 14-3-3σ protein respectively.

3.2.3 Western blot Validation of LC-MS/MS Identified Proteins

Expression levels of proteins identified from the LC-MS/MS analysis were next assessed and validated by a Western blot. Total protein from each sample was extracted from the cell lysate and 30μg per sample loaded into each well for gel electrophoresis. We have successfully probed for the expression of three proteins- Hsp-90β, NPM1 and 14-3-3σ (Figure 15 and 16). These three proteins were chosen for further validation because we found them to be pivotal and possess well established roles in cancer progression. Not only that, but they have been consistently detected in our LC-MS/MS studies, such that their expression levels show a trend when transfected with miR-181a, its inhibitor or both of them, albeit insignificant at this point in time. The other proteins listed in Table 5, despite also being detected in all three independent runs, do not have as strong a link to cancer, their trends are not as clear (high standard deviation) or have conflicting roles in cancer, as in the case of Hsp-60 [96]. The trends in expression of these three proteins will therefore give us a very preliminary outlook of the potential effect of miR-181a in cancer progression, which will then be validated with subsequent experiments. Hsp-90β protein expression level is seen to drop when miR-181a was inhibited while NPM1 protein expression levels increased when miR-181a was overexpressed.

Stress proteins include the heat shock proteins (HSPs), glucose-regulated proteins (GRPs) and ubiquitin. Stress in cells may include hyperthermia, hyperoxia, hypoxia, and other perturbations, which alter protein synthesis [97]. Under these conditions, the cells' protective mechanisms are activated, and HSPs in particular, would be highly produced to maintain cell integrity. An increase in expression of HSPs has been found in many cancers, leading to a shielded environment, allowing cancer cells to grow indefinitely. One reason

why HSPs may be overexpressed in cancer could be due to the physiopathological features of the tumour microenvironment (low glucose, pH, and oxygen), which tend toward HSP induction [98].

Among the HSPs, Hsp-90 plays a particularly versatile role in cell regulation, forming complexes with a large number of cellular kinases, transcription factors, and other molecules. Hsp-90β is a molecular chaperone that protects numerous key nodal proteins in cells and is especially involved in contributing to the robustness of cancer cells [99]. It plays a central role in many important processes like preventing apoptosis, insensitivity to anti-growth signals, sustained angiogenesis, limitless replicative potential, tissue invasion and metastasis as well as in the self-sufficiency of growth signals in cancer cells. It is therefore unsurprising, that the expression of Hsp-90β is often elevated in cancers. An example of a protein protected by Hsp-90β is NPM-ALK (a cause of malignant transformation) [99]. The decrease in Hsp-90β expression level in HepG2 cells when miR-181a was inhibited may cause a weakening in its inherent defence machinery.

On the other hand, miR-181a transfection causes an increase in the expression of NPM1 protein. NPM1 is a phosphoprotein found mainly in the nucleus. It is known to be involved in a multitude of cellular processes including the assembly and transport of ribosomal proteins, centrosome duplication and also acts as a molecular chaperone. When expressed at high levels, it is found to promote tumour growth by the inactivation of the p53/ARF pathway [100]. Not only that, but it is also found to interact with c-myc and NFκB transcription factors. Many studies link excessive levels of NPM1 to cellular transformation and are often found in many human cancers including those of the stomach, prostate, colon, bladder, and liver. NPM1 overexpression in tumour cells was also found

to lead to an increased proliferation and inhibition of apoptosis [101]. Although the study of NPM1 in carcinogenesis is well-documented, its mechanism of action lies largely unknown. The increase in NPM1 protein level by miR-181a may suggest the oncogenetic effect miR-181a exerts in HCC.

Lastly, 14-3-3σ was found to be down-regulated by miR-181a in HepG2 cells in the LC-MS/MS and upregulated when miR-181a was inhibited in the Western blot analyses. The 14-3-3 family of proteins consists of 7 different isoforms, with different functions in cell cycle and cell signaling, among which is 14-3-3σ. 14-3-3σ protein plays a role in cancer by participating in the cell cycle [102, 103]. It is known to be a negative regulator of the cell cycle by regulating the cyclin-dependent kinases (CDKs) and is found to be lowly or not expressed in HCC [104]. It is a p53 inducible gene following DNA damage and in turn also regulates the level of p53, thereby forming a positive feedback loop that reinforces each other. 14-3-3σ expression was found to lead to a stabilized expression of p53 and enhanced p53 transcriptional activity [103]. Additionally, it was found to antagonize the biological functions of Mdm2 by blocking Mdm2-mediated p53 ubiquitination and nuclear export [103]. It has been shown that the overexpression of 14-3-3σ protein in breast cancer cell lines inhibits cell proliferation and prevents anchorage-independent growth [105]. This suggests that 14-3-3σ may have a tumour suppressive role, and its increase in expression due to the inhibition of miR-181a in HepG2 cells could mean that inhibiting miR-181a leads to a mechanism in HepG2 cells that may decrease cancer cell growth and progression.

The Western blot results of these proteins that were probed for generally coincide with the LC-MS/MS data in terms of the trends of the proteins' expression when transfected with

the various miRNAs. However, it can be seen that the extent of change in expression levels are different from that of the LC-MS/MS results. This could be due to the differences in both types of quantification methods. The Western blot generally involves less processing and whole proteins are probed using antibodies while the iTRAQ-related LC-MS/MS requires much more processing prior to the actual identification and quantification of the proteins. Ideally, the processing of samples should not affect the protein levels, but the accumulation of errors in the processing steps may lead to a larger than necessary difference observed. Not only that, but the detection of proteins (eg. Specificity and sensitivity) in the mass spectrometer is dependent on the limitations and parameters set on the equipment, some of which cannot be controlled by the end user. Because of these reasons, a difference in the expression levels of proteins is expected. Despite this, the LC-MS/MS still remains to be a very useful tool in establishing a protein profile for subsequent analyses to be performed.

Gathering all the results obtained from the LC-MS/MS as well as Western blot analyses, the primary information obtained is that miR-181a may act as an oncogene in HepG2 cells. Inhibiting it, on the other hand, could possibly lead to an activation of pathways that are anti-proliferative. With this hypothesis in mind, we proceeded to conduct a cell viability test on HepG2 cells transfected with miR-181a as well as its inhibitor.

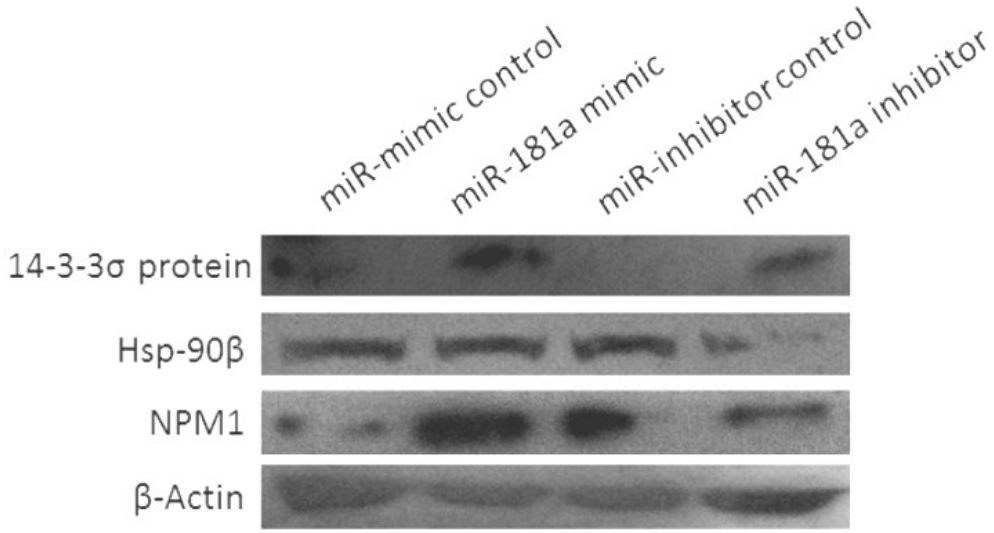

Figure 15. Western blot validation of LC-MS/MS results. HepG2 cells were transfected with miR-181a and its inhibitor and incubated for 24h and probed with various selected primary antibodies overnight at 4°C. miR-181a increased the expression of NPM1 while miR-181a inhibitor increased 14-3-3σ protein expression level and decreased NPM1 and Hsp-90β expression levels. β-actin served as a loading control. Brightness and contrast was adjusted to improve image clarity.

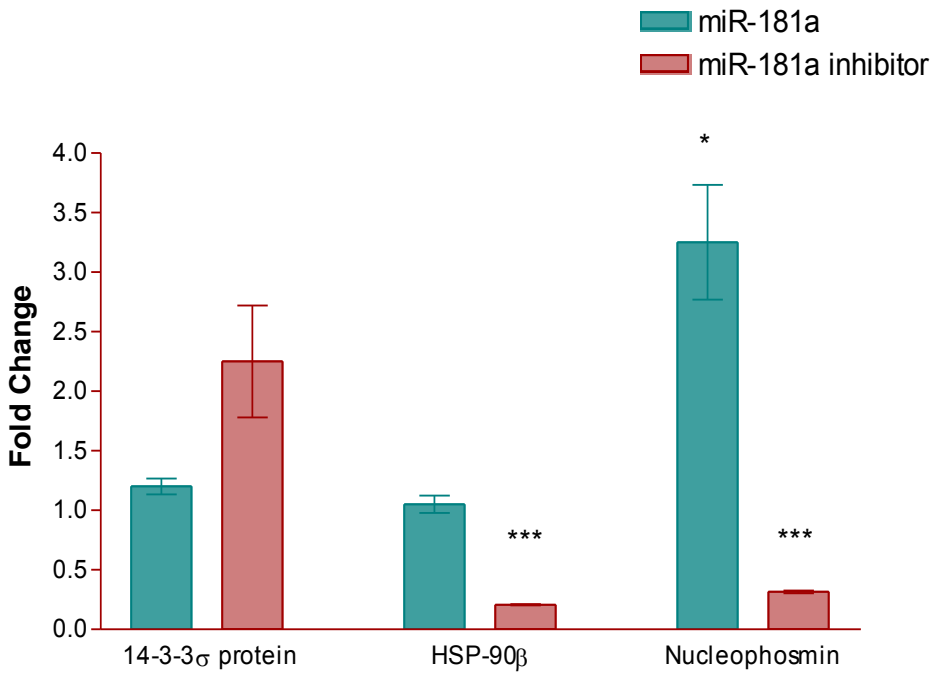

Figure 16. Quantification of Protein levels of 14-3-3σ, Hsp-90β and NPM1 in HepG2 cells. Proteins were quantified **using Image J software. The densities of the individual bands on the Western blots were analysed by the software and quantified.** The **fold changes were then obtained by normalizing the values of samples obtained against those of the controls. Using a** Student's ***t*-test, the protein levels of NPM1 protein was found to increase significantly when transfected with miR-181a (p value=** 0.043) (n=3). Both **NPM1 and HSP-90β was seen to decrease significantly (p value= 0.00027 and 0.000032 respectively) (n=3).**

3.2.4 Inhibiting miR-181a Significantly Reduced HepG2 Cell Viability and Sensitizes it to *Cisplatin* Treatment

Cell viability refers to the level of metabolism in cells and in some cases may extend to cell proliferation, because a proliferating cell generally has a higher metabolism than a resting cell. Cell viability assays measure the activity of cellular enzymes on their ability to reduce a tetrazolium dye to a coloured product (formazan) such that a colorimeter may be used to measure the concentration of coloured compounds formed. This gives a correlation of how active the cells are. Many cell viability assays have been developed using different types of dyes. In our study, we have chosen to use the Water soluble Tetrazolium salts (WST-1) assay. Among the assays available, this method is unique because the dye is reduced outside the cell, producing a soluble coloured formazan, so it does not require any addition of solubilizing reagents that may interfere with cell viability (unlike the other MTT assays).

HepG2 cells were electroporated with 100nM miR-181a and its inhibitor respectively, seeded onto 96-well plates over 3 day period and cell viability assessed every 24h. In addition to transfecting cells with miRNAs, we also investigated whether miRNA transfection could work in combination with drug treatment. Current liver cancer therapy makes use of drugs and/or radiation. However, the main setback of these methods is the fact they cause the death of healthy, untransformed cells by causing unwanted side effects. Not only that, but many cancers adapt and become resilient towards drugs. These reasons limit the use of drugs in chemotherapy. As miRNAs are endogenous cellular compounds, they are less likely to cause an immune response and may be better received by cancer cells during therapy.

Cisplatin is a drug widely used in chemotherapy and mainly acts in causing cell apoptosis through irreversible binding to specific grooves in the DNA, rendering cells unable to undergo subsequent transcription and ultimately be programmed for apoptosis following cell cycle checks. Another mechanism in which it acts to lead to apoptosis is through its binding to important cellular proteins [106]. With that, we first tested the optimal *cisplatin* concentration to be used in the experiments. A serial dilution of *cisplatin* concentrations was carried out on HepG2 cells seeded in 96-well plates. 24h after *cisplatin* treatment, their cell viabilities were measured using the WST-1 assay. Figure 17 shows the viabilities of HepG2 cells 24h after exposure to various concentrations of *cisplatin*.

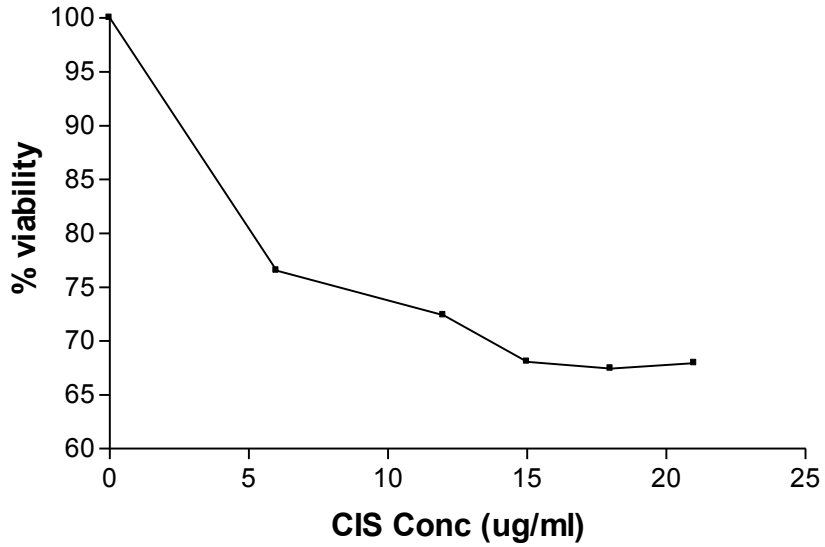

Figure 17. Growth curve of HepG2 cells treated with *cisplatin*. 30K HepG2 cells were seeded in each well of a 96-well plate and treated with various doses of *cisplatin*. Cell viabilities were measured after 24h of drug incubation. 21μg/μl *cisplatin* concentration was chosen as the experimental dosage because at this concentration, the cells are slightly weakened (35%) by the treatment but still viable enough for a WST-1 assay to work.

HepG2 cell viability is observed to decrease as the *cisplatin* dosage increases. As we are interested in performing a WST-1 cell viability assay on cells both transfected with the miRNA and treated with *cisplatin*, the cells should not be totally killed off by the drug treatment. Instead, the drug should exert a slight, weakening effect on the cells such that

its effects are still felt. With that, 21µg/µl *cisplatin* was chosen as the experimental concentration, because the cells at this drug concentration are weakened (cell viabilities are lowered to approximately 65% of control cells after a 24h incubation) but are still viable so that any additional change in viabilities due to the miRNAs *per se* may be still studied.

In the actual experiment, HepG2 cells were first transfected with the miRNAs and then incubated for 24h, 48h and 72h before treating them with 21µg/ml *cisplatin* for 24h. This 'transfect-then-treat' procedure was chosen over the 'treat-then-transfect' as the treatment of cells initially with *cisplatin* could mask the effects induced by subsequent transfection of cells with the miRNAs. Also, transfecting the cells firstly with the miRNAs would enable them to express the different proteins which may sensitize or desensitize the cells to drug treatment. Results of this experiment are shown in Figure 18.

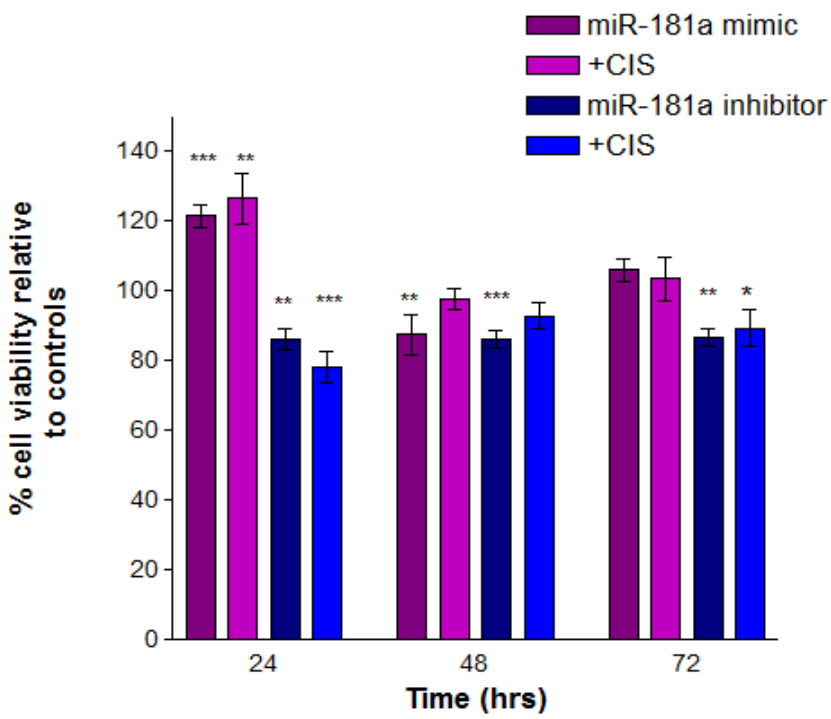

Figure 18. Comparison of miRNA-transfected HepG2 cell viabilities with and without *cisplatin* treatment. HepG2 cells were either transfected only with 100nM miR-181a/miR-181a inhibitor or subsequently treated with 21µg/ml *cisplatin* for 24h and their viability assessed via WST-1 assay. The different time points refer to the amount of incubation time of HepG2 cells post-transfection (pre-treatment). Absorbance readout of dye generated by assay was measured at 450nm. At the 24h time point, an increase in cell viablity in both cases (ie. Cells transfected with miR-181a only and cells tranfected as well as treated with *cisplatin*) (p value=0.0002 and 0.0024 respectively) were detected as compared to cells transfected with the control miRNA. Cell viability at 24h was seen to increase by about 20-30% for HepG2 cells transfected with miR-181a as compared to the control miRNA, both with and without *cisplatin* treatment. Conversely, there is a significant decrease of 20% in HepG2 cell viablity in both cases when transfected with miR-181a inhibitor (p value=0.0015), with a slight further decrease in viability (p value=0.0009) upon *cisplatin* treatment, leaving only 80% of viability measured as compared to that of the control samples. (n=3)

The transfection of miR-181a causes a significant increase in HepG2 cell viability by approximately 20% (p value= 0.0002) while inhibiting it reduces cell viability by a similar amount (p value=0.0015) at a 24h incubation period. At longer incubation periods of 48-72h, HepG2 cells transfected with miR-181a displayed a level of viability comparable to that of the control sample. This could be due to the fact that the transfection was transient in nature, therefore the cells that were present at longer time intervals (ie. 48-72h) could have been diluted with non-transfected cells (ie. Offspring of the original batch of cells),

therefore skewing the viabilities towards that of the control samples. This is very possible, since miR-181a causes an increase in cell viability/proliferation, thereby increasing the chances of such a dilution. The slight decrease in miR-181a expression levels after 24h could have also led to the drop in cell viability. Transfecting the cells with miR-181a inhibitor though, causes a sustained drop in cell viability through 72h of incubation, hovering that around 80% even at 72h post-transfection. Again, this could be due to the decrease in cell metabolism because of the inhibition of miR-181a, which could have led to a slowdown in cell proliferation, therefore the cells are 'less diluted' and their viability readouts do not skew towards that of the control samples as quickly. It would be expected, after a longer incubation time, for all the viabilities of all the samples to be similar to each other.

The treatment of HepG2 cells with *cisplatin* following the transfection of miR-181a inhibitor resulted in a further decrease in cell viability at a 24h incubation period as compared to the control (p value=0.0009). The same experiment carried out with miR-181a shows an increase in HepG2 cell viability (p value= 0.002). These results suggest that miR-181a desensitizes HepG2 cells while inhibiting miR-181a sensitizes them towards *cisplatin* treatment. The previous LC-MS/MS study could give some explanation to this observation. The LC-MS/MS identified and quantified Hsp-90β as a protein down-regulated while 14-3-3σ was up-regulated in HepG2 cells by the transfection of miR-181a inhibitor. Further analysis with Western blot confirmed this observation. The lowered expression of Hsp-90β, along with the increased expression of 14-3-3σ with the transfection of miR-181a inhibitor may be one of the modes in which inhibiting miR-181a works in reducing HepG2 cell viability, as confirmed with the WST-1 assay where

viability was found to be reduced by approximately 20% 24h post-transfection. The increase in 14-3-3σ protein could possibly have weakened the more active cells from proliferating by causing an initial cell cycle arrest, leading to lowered cell viability as compared to control cells.

In addition, cancer cells are more resistant in the face of extreme environmental stress, for example, during chemotherapy or radiation. These stresses generate free radicals that may cause substantial physical damage to cellular proteins that are normally protected by Hsp-90β [99]. The decreased expression of Hsp-90β may explain the further decrease in cell viability by sensitizing HepG2 cells to *cisplatin* treatment, as there would be less protection for cells and more damage done to cellular proteins due to the drug, leading to further lowered cell viability. Results of this experiment show that a combination of drugs and miRNAs could potentially be used as a better treatment option instead of solely relying on the use of drugs, as issues of drug-related resistance and/or toxicity may be addressed as compared to traditional chemotherapy. Drug dosages may be lowered when in use with appropriate miRNAs in treatments as well.

Also in our study, the transfection of miR-181a and its inhibitor led to an increase and decrease in NPM1 expression levels respectively. The increase in NPM1 when transfected with miR-181a could have possibly contributed to HepG2 cells with increased viability. The decrease in NPM1, on the other hand, could have reduced the cells' ability to inhibit apoptosis, therefore enabling the action of *cisplatin* to work better, thereby further reducing the cells' viabilities slightly more. The results from these experiments all suggest that inhibiting miR-181a could potentially play a tumour suppressive role in HCC.

3.2.5 Inhibiting miR-181a Delays HepG2 Cell Cycle Progression

As cell growth has been shown in our studies to be affected by the transfection of HepG2 cells with miR-181a and its inhibitor, we next investigated if miR-181a has any influence on cell cycle progression. HepG2 cells were transiently transfected with miR-181a, miR-181a inhibitor as well as their corresponding control miRNAs. Prior to transfection, they were synchronized by serum deprivation overnight. Serum starvation is one of the few cell synchronisation methods used in cell cycle analysis. Its rationale works on the basis that cells deprived of growth nutrients are forced into quiescence, therefore they would theoretically be at the same 'starting point' at the actual commencement of the experiment. Certainly, it does not come without its disadvantages, one being that it may pose as a form of stress for the cells if the cells are starved beyond a certain time point. Another method that may be used is via chemically reversible inhibitors to arrest the cells at specific stages of the cell cycle. This poses similar problems as serum starvation in that their over-exposure may cause unwanted side effects, and could potentially be even more than that of serum starvation due to the introduction of an exogenous compound to the cell population. Other methods exist but are more complicated, for example, the mitotic shake-off method or using centrifugal elutriation. Again, they each have their own drawbacks, the first having a low yield (of synchronised cells) and the second requiring special rotor. Taking into consideration these options and their respective drawbacks, we chose to use serum starvation as our method of choice due to its relative simplicity in carrying out and proven use in the literature. Whether or not this method of synchronization worked was not quantitatively verified here, partially due to the fact that it has previously been validated to work by other studies. However, on our part, it was noted by eye that the

HepG2 cells were growing at a much slower rate during the starvation period, very much visibly different from when they were exposed to 10% FBS. This was a good sign that they could be all slowing down in cell cycle. Also, at the end of the overnight incubation, there was little or no detachment of cells, meaning that the starvation was not too harsh such that cells started to detach from the surface.

24h post-transfection, the cells were harvested, fixed and sent for flow cytometry analysis using propidium iodide staining (PI). PI is a fluorescent molecule that is able to bind to double stranded nucleic acids. Therefore, with proper treatment with ribonucleases (RNases), it is able to quantify the amount of DNA in cells. As cells enter the various phases in the cell cycle, the amount of DNA changes, doubling as it enters S phase. Hence, the amount of DNA detected by PI corresponds to the proportion of cells undergoing cell cycle.

Results of the cell cycle analysis (Figure 19 and Table 6) show that inhibiting miR-181a delays cell cycle entry by about 10% while miR-181a has the opposite effect of promoting it, albeit to a lesser extent. Inhibiting miR-181a significantly increased the proportion of HepG2 cells in the G1 phase (p value= 0.0352) and reduced that of cells in the S and G2/M phases (p value= 0.0399) while the opposite was seen in the case of miR-181a transfection. This may explain why cells were seen to be more viable due to the transfection of miR-181a, as the entry into cell cycle could have indicated an increase in metabolism and/or increased cell proliferation by encouraging cells to go into DNA synthesis and subsequent mitosis. However, as the effect of miR-181a on cell cycle entry was not found to be statistically significant in this experiment, a more probable reason behind the increase in cell viability as seen in the previous cell viability test could have

been due to the increase in metabolic state of the cells instead of an increase in cell proliferation per se. Conversely, the delay in entering cell cycle caused by the transfection of miR-181a inhibitor could have slowed down HepG2 cell growth, thereby rendering the cancer cells to be less active and/or proliferative.

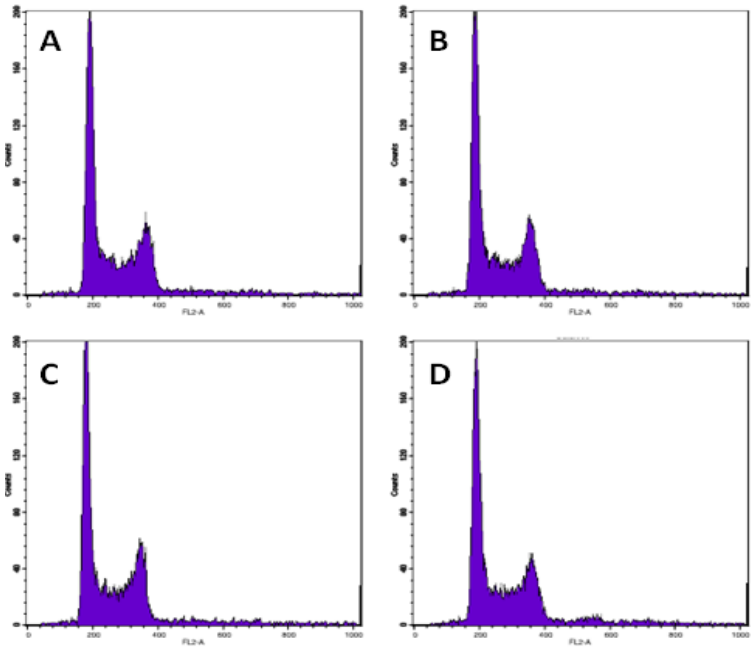

Figure 19. HepG2 cells transfected with miRNAs and analysed by flow cytometry. Panels A, B, C, D represent the cell cycle plots of HepG2 cells transfected with the mimic control, miR-181a, inhibitor control and miR-181a inhibitor respectively. Serum starved cells were harvested 24h post-transfection. Percentages of cells in G1, S and G2/M phases are indicated in Table 6. MiR-181a inhibitor significantly delayed cell cycle progression by increasing the proportion of cells in the G1 phase (p value= 0.0352) and significantly decreasing the cells in S phase (p value= 0.0399) (n=3).

Table 6.% of HepG2 cells in G1, S and G2/M phases of the cell cycle after transfection with various miRNAs.

Table 6. % of cells in the respective cell cycle phases (Mean±SD)				
Cell phase	**A** **miR-mimic control**	**B** **miR-181a mimic**	**C** **miR-inhibitor control**	**D** **miR-181a inhibitor**
G1	62.5 ± 3.67	56.8 ± 7.07	48.3 ± 8.71	60.4 ± 3.33
S	19.7 ± 4.49	24.9 ± 5.32	28.4 ± 2.79	20.8 ± 5.04
G2/M	19.1 ± 4.98	19.6 ± 3.08	24.9 ± 8.06	19.1 ± 1.32

3.2.6 Section Conclusion

Our results so far suggest that inhibiting miR-181a in HepG2 cells significantly lowers cell viability. This could possibly be through the increased expression of a number of important tumour suppressors like 14-3-3σ, as well as the decrease in other oncoproteins like Hsp-90β and NPM1. 14-3-3σ acts by activating p53 while the decrease of both Hsp-90β and NPM1 leads to a decrease in cellular protection in general, enhancing the action of *cisplatin* when the cells were subsequently treated with the drug. Cell cycle was also seen to be delayed. On the other hand, miR-181a increases the expression of tumour causing proteins like NPM1, leading to the observed increase in cell viability. Inhibiting miR-181a attenuates HCC through various pathways, and this should not be surprising as miRNAs are known to be unspecific, hence their presence in cells affects not just one, but numerous proteins and their subsequent pathways. This is useful in cancer therapy as most cancers have not just one or a few mutations, but thousands of mutated genes and pathways that using specific drugs or siRNAs prove to be insufficient in resulting in its eradication. In this first study, we see an overall anti-proliferative and tumour suppressive role when miR-181a is inhibited in HepG2 cells, while miR-181a itself results in HepG2 cells being more viable and less sensitive towards *cisplatin* treatment. The use of miR-181a inhibitor in HCC could potentially aid in eliminating more cancer cells.

4. Role of MicroRNA-181a in HepG2 Cells: Its Cell Cycle Targets

4.1 Introduction

The first section of this project elucidated an overall picture of the effects of overexpressing and inhibiting miR-181a in HepG2 cells. To gain a further understanding

of the functions of this miRNA, an in-depth molecular study on the direct targets of miR-181a will be investigated in this section. MiRNAs are generally known to perform their regulatory function through their binding to the 3′-UTRs of target mRNAs, ultimately leading to a repression of target protein expression levels. However, miRNAs, being non-specific in nature, are able to bind to multiple mRNAs in the cells and in the process, regulate many proteins simultaneously. Not only that, but because they usually bind with partial complementarity to mRNAs, it makes it more difficult to identify the direct targets of miRNAs. Nevertheless, we make use of bioinformatics as our first mode of narrowing down the choices of putative targets. From there, with our chosen targets, we carry out wet lab experiments to validate the targets both *in vitro* and *in vivo*.

4.2 Results and Discussion

4.2.1 Bioinformatics Screening of Putative mRNA Targets

Bioinformatics has evolved over the years and is now an important tool in generating new biological knowledge. It is an interdisciplinary field that develops and improves upon methods for storing, retrieving, organizing and analysing biological data. It plays many roles in biology, ranging from sequencing and annotating genomes, image and signal processing, organizing biological data, the analysis of gene and protein expression and regulation, etc. Of course, it is also involved in structural biology, aiding the simulation and modelling of DNA, RNA, and protein structures as well as molecular interactions. We thus make use of bioinformatics as a platform to help us identify possible mRNA targets of miR-181a based on sequence complementarity as well as mRNA folding. Three online software and databases, namely, TargetScan 6.2, miRanda and PicTar, were used in the first step to elucidate potential mRNA targets of miR-181a. Putative targets that were

predicted in at least two of the software were chosen for further study. Additionally, among the many possible targets predicted and listed, those that are involved in important cancer-related processes were selected for subsequent wet lab analysis. Two such targets of interest are cyclin-dependent kinase inhibitor 1B (CDKN1β) and transcription factor E2F7 (E2F7). Figures 20 through 22 show the putative binding sites and binding scores of miR-181 family to the 3' UTRs of CDKN1β and E2F7 based on TargetScan, miRanda and PicTar respectively. The locations of the predicted binding sites are similar for the three independent software.

	predicted consequential pairing of target region (top) and miRNA (bottom)	seed match	site-type contri-bution	3' pairing contri-bution	local AU contri-bution	position contri-bution	TA contribution	SPS contribution	context+ score	context+ score percentile	conserved branch length	P_{CT}
Position 745-751 of CDKN1B 3' UTR hsa-miR-181c	5' ...GGUGCUUGGGAGUUUUGAAUGUU... 3' UGAGUGGCUGUCCAACUUACAA	7mer-m8	-0.120	0.003	-0.072	0.022	0.020	0.049	-0.10	72	0.007	< 0.1
Position 745-751 of CDKN1B 3' UTR hsa-miR-181d	5' ...GGUGCUUGGGAGUUUUGAAUGUU... 3' UGGGUGGCUGUUGUUACUUACAA	7mer-m8	-0.120	0.003	-0.072	0.022	0.020	0.049	-0.10	71	0.007	< 0.1
Position 745-751 of CDKN1B 3' UTR hsa-miR-181a	5' ...GGUGCUUGGGAGUUUUGAAUGUU... 3' UGAGUGGCUGUCGCAACUUACAA	7mer-m8	-0.120	0.003	-0.072	0.022	0.020	0.049	-0.10	71	0.007	< 0.1
Position 745-751 of CDKN1B 3' UTR hsa-miR-4262	5' ...GGUGCUUGGGAGUUUUGAAUGUU... 3' GUCCAUCAGACUUACAG	7mer-m8	-0.120	0.003	-0.072	0.022	0.020	0.049	-0.10	71	0.007	< 0.1
Position 745-751 of CDKN1B 3' UTR hsa-miR-181b	5' ...GGUGCUUGGGAGUUUUGAAUGUU... 3' UGGGUGGCUGUCGUUACUUACAA	7mer-m8	-0.120	0.003	-0.072	0.022	0.020	0.049	-0.10	71	0.007	< 0.1

	predicted consequential pairing of target region (top) and miRNA (bottom)	seed match	site-type contri-bution	3' pairing contri-bution	local AU contri-bution	position contri-bution	TA contribution	SPS contribution	context+ score	context+ score percentile	conserved branch length	P_{CT}
Position 561-567 of E2F7 3' UTR hsa-miR-181c	5' ...CAGGGUAUGACGACU---UGAAUGUU... 3' UGAGUGGCUGUCCAACUUACAA	7mer-m8	-0.120	-0.025	-0.077	0.018	0.020	0.049	-0.14	82	3.119	0.79
Position 561-567 of E2F7 3' UTR hsa-miR-181b	5' ...CAGGGUAUGACGACU-UGAAUGUU... 3' UGGGUGGCUGUCGUUACUUACAA	7mer-m8	-0.120	-0.016	-0.077	0.018	0.020	0.049	-0.13	79	3.119	0.79
Position 561-567 of E2F7 3' UTR hsa-miR-181d	5' ...CAGGGUAUGACGACU-UGAAUGUU... 3' UGGGUGGCUGUUGUUACUUACAA	7mer-m8	-0.120	-0.016	-0.077	0.018	0.020	0.049	-0.13	79	3.119	0.79
Position 561-567 of E2F7 3' UTR hsa-miR-181a	5' ...CAGGGUAUGACGACU-UGAAUGUU... 3' UGAGUGGCUGUCGCAACUUACAA	7mer-m8	-0.120	-0.016	-0.077	0.018	0.020	0.049	-0.13	79	3.119	0.79
Position 561-567 of E2F7 3' UTR hsa-miR-4262	5' ...CAGGGUAUGACGACUUGAAUGUU... 3' GUCCAUCAGACUUACAG	7mer-m8	-0.120	0.003	-0.077	0.018	0.020	0.049	-0.11	74	3.119	0.79

Figure 20. TargetScan's predicted binding sites of miR-181a to the 3'UTRs of CDKN1β and E2F7. The total context score is based on six features: site-type contribution, 3' pairing contribution, local AU contribution, position contribution, TA (target site abundance) contribution and SPS (seed-pairing stability) contribution. The more negative the context score, the higher the probability of mRNA binding. The probability of conserved targeting, P_{CT}, refers to the likelihood of the sequence being conserved so as to allow regulation by the miRNA. The higher the P_{CT}, the higher the chance of miRNA:mRNA binding.

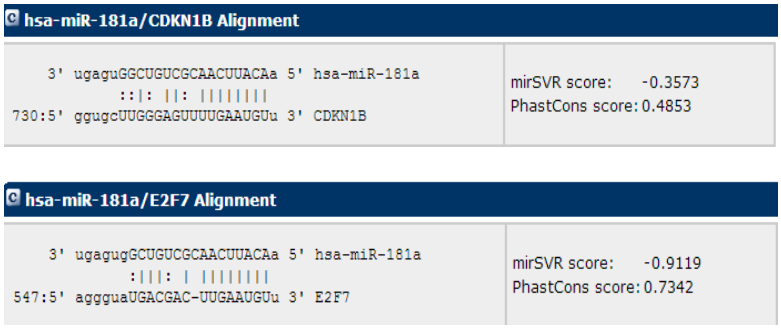

Figure 21. MiRanda's predicted binding sites of miR-181a to the 3'UTRs of CDKN1β and E2F7. The mirSVR score is based on seed-site pairing, site context, free-energy, and conserved targeting. The more negative the mirSVR score, the higher the probability of mRNA binding. PhastCons score refers to the likelihood of the sequence being conserved so as to allow regulation by the miRNA. The higher the P_{CT}, the higher the chance of miRNA:mRNA binding.

Org	PicTar score	PicTar score per species	microRNA	Probabilities	Nuclei mapped to alignments	Nuclei mapped to sequence	Free Energies kcal/mol	Structure of predicted duplex
hs	1.87	0.86	hsa-miR-181a	0.58	652	562	-19.7	UUCA____UGACG_C_UUGAAUGUU_:_GAGU____GCUGU_G_AACUUACAA

Figure 22. PicTar's predicted binding site of miR-181a to the 3'UTR of E2F7. Similar to TargetScan, PicTar also predicts miRNA-mRNA interaction based on identical seed sequences. The PicTar algorithm score is based on seed complementarity, thermodynamics and a combinatorial prediction for common targets in sets of co-expressed miRNAs. There was no prediction for the binding of miR-181a to the 3'UTR of CDKN1β mRNA.

According to TargetScan 6.2, the more negative the context score of an interaction, the more favourable it is for binding to occur. The context score is based on six types of interactions found both at the seed region and around the seed region. It seems that there is a more extensive base pairing between miR-181a and E2F7 as compared to CDKN1β due to the presence of predicted base interactions beyond the seed region, leading to a more negative context score. This same result was seen in miRanda as well, where the mirSVR score is more negative in the binding of miR-181a to the 3'UTR of E2F7 than CDKN1β mRNA.

Not only is binding at the seed region crucial, but the way the mRNAs fold, especially at areas around the seed region, also plays a part in miRNA accessibility and binding. Secondary structures of mRNA may prevent miRNA targeting (if too much steric hindrance is present), even though their sequences may support a positive interaction. We next performed another bioinformatics study on the possibility of RNA folding around the

seed regions of the two binding sites identified. To do this, we make use of the public software 'The Mfold Web Server' [107] to elucidate the structure of the RNAs at the site of binding. Figure 21 shows the possible predicted secondary structures of CDKN1β and E2F7 mRNAs at their binding regions to miR-181a.

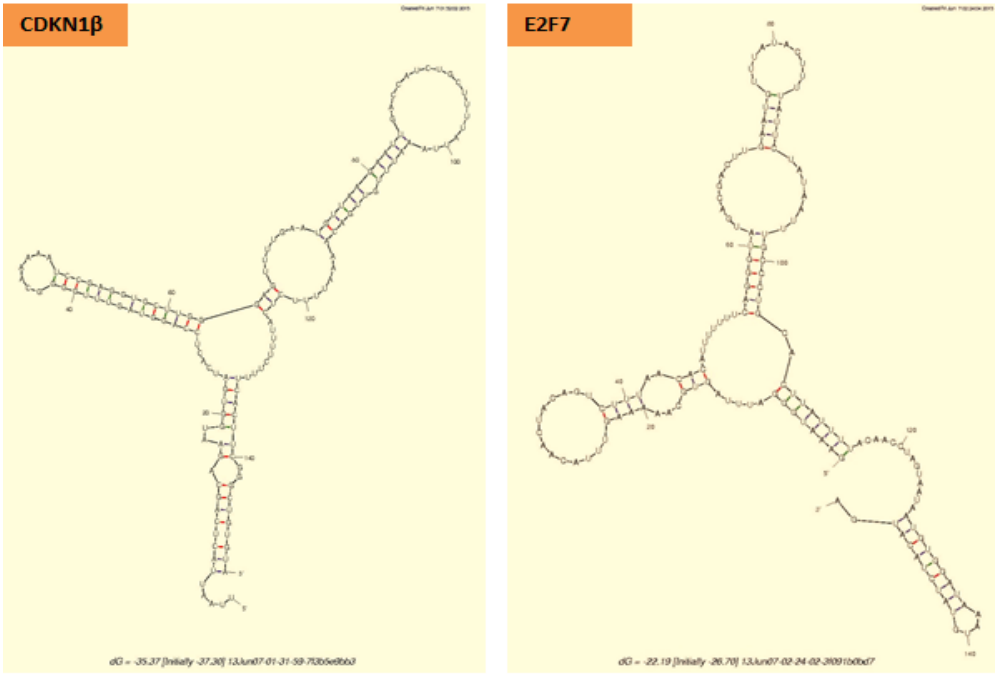

Figure 23. Predicted secondary structures of CDKN1β and E2F7 around the binding regions of miR-181a. Both structures are predicted to possess some RNA folding, but it does not appear to cause much steric hindrance at areas around the seed regions.

Some RNA folding is predicted around the areas surrounding the binding regions between miR-181a and both the CDKN1β and E2F7 mRNA 3'UTRs. However, it does not appear to cause much steric hindrance as the structures look open, with no major blockage near the predicted interaction sites. As this was just carried out as a brief, qualitative analysis on the 3' UTRs of the two mRNAs around their specific sequences of interest, it does not take into account the possible hindrance that may stem from further upstream or downstream sequences along the same mRNA that may be present in the cellular environment. However, as a first step and with the preliminary RNA structures we have

obtained, we shall assume that these two binding regions are open for miRNA binding. Therefore, using information from our bioinformatics study as the first step, we proceeded to validate for any actual binding between the two RNAs.

4.2.2 *In vitro* Binding of miR-181a to the 3'UTR of CDKN1β and E2F7 via Surface Plasmon Resonance

Based on the results of the bioinformatics analysis, we proceeded to use SPR to monitor miR-181a:mRNA interactions, if any. Single-stranded RNA and DNA nucleotides carrying the putative binding 3'UTR seed regions and flanking nucleotides were synthesized and immobilized in separate flow channels. Although we are interested in studying the interactions between mRNAs and miR-181a, because of the inherent instability of RNAs as opposed to DNAs, we also incorporated the DNA version of the synthesized nucleotides in our study, with the only difference being that the DNA strands contain deoxyribose instead of a ribose unit. The sequences in the synthesized DNA is the exactly the same as that of the RNA, both containing only the AUGC nucleotides. This served as a type of control in case of any RNA degradation during the experiment. Synthesized miR-181a at different concentrations was subjected in a single run. Kinetic binding constants were determined. Sensorgrams for the two flow channels containing the binding portions of the 3'UTRs of CDKN1β and E2F7 RNA shows that they both interacted significantly with miR-181a. As shown in Figure 22, the experimental curves of the binding between miR-181a and CDKN1β and E2F7 fit closely to a 1:1 binding model (Panels A and C). The slight discrepancy between the theoretical and experimental curves is likely to be due to the aggregation of miR-181a at high concentrations. The dissociation constants (K_D) for the binding between miR-181a and CDKN1β and E2F7 are 272.5 ±

0.008 nM and 1.186 ± 0.009 uM respectively, indicating that the binding between miR-181a and CDKN1β is stronger than that with E2F7, although a more extensive binding was predicted between miR-181a and E2F7. Both DNA versions of the synthesized oligomers, on the other hand, did not show any *in vitro* binding with miR-181a (Panels B and D). The deoxyribose unit in the backbone may have caused a change in oligo structure and positioning as compared to its ribose counterpart, such that binding to miR-181a is impossible.

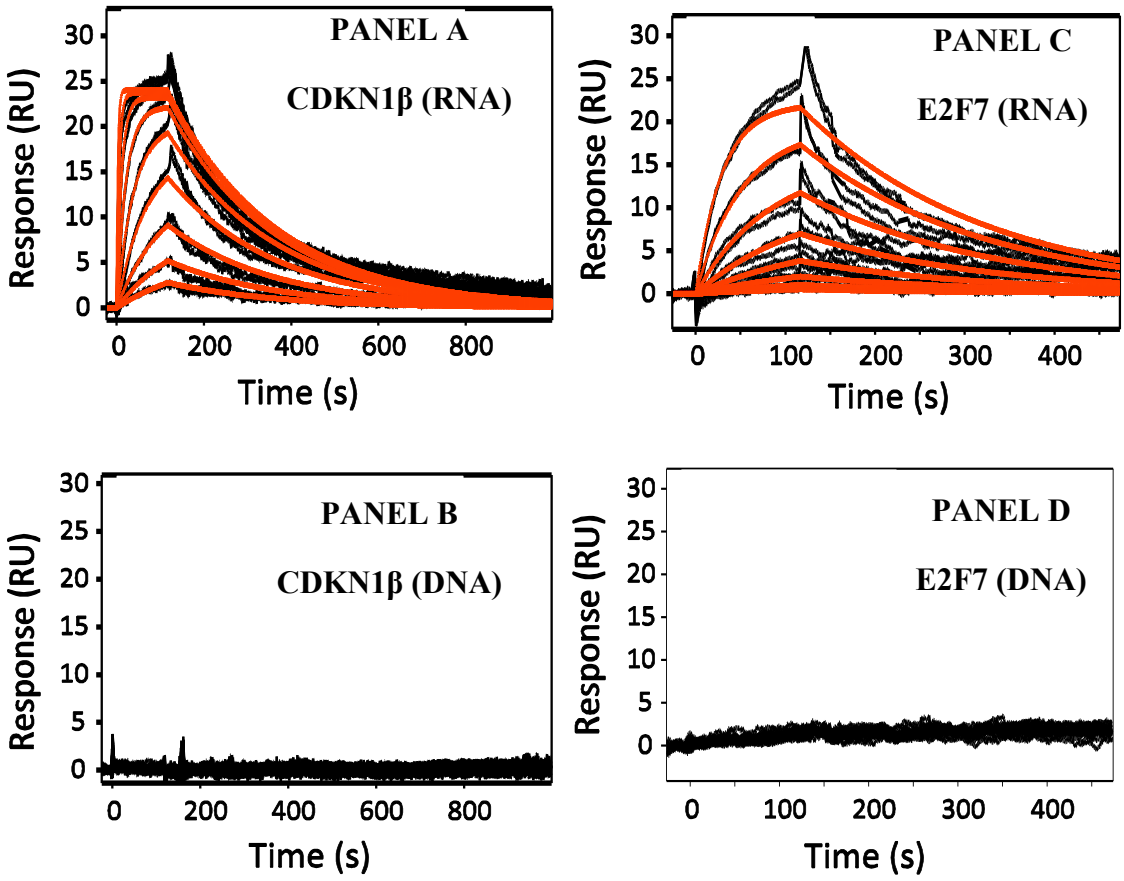

Figure 24. Experimental curves of the bindings between miR-181a and CDKN1β and E2F7 (both RNA and DNA backbone). A positive 1:1 binding is observed between both miR-181a and CDKN1β (RNA) and E2F7 (RNA) (Panels A and C) with dissociation constants 272.5 ± 0.008 nM and 1.186 ± 0.009 uM respectively. The DNA versions of CDKN1β and E2F7 (Panels B and D) did not show any binding to miR-181a.

4.2.3 *In vivo* Binding Confirmation of miR-181a to the 3'UTR of CDKN1β and E2F7

The successful detection of interaction between miR-181a and the two seed regions (and the sites flanking them) of the 3'UTRs of CDKN1β and E2F7 mRNAs *in vitro* next led us to study if the interactions are also positive in the cellular environment. As the cellular environment is very much different from that *in vitro*, in order to ensure that positive binding occurs between the miR-181a and the mRNAs in cells, we investigated the binding via a luciferase assay.

Results (Figure 23) show that miR-181a binds to both the 3'UTRs of CDKN1β and E2F7 in HepG2 cells, confirming the previous findings of *in vitro* binding. A tenfold dilution of miR-181a was studied and in general, it seems that miR-181a does bind to the control plasmid to an extent, because the normalised firefly luciferase activity was lowered as the concentration of miR-181a increased from 10nM to 100nM. However, comparing data within the same miR-181a concentration shows that miR-181a binds to a larger extent to the 3' UTRs of CDKN1β and E2F7 mRNAs as compared to the control plasmid, evident from the decrease in firefly luciferase activity detected. Not only that, but it seems that *in vivo*, miR-181a binds more strongly to the 3' UTR of E2F7 than of CDKN1β mRNA. This is in contrast with the results of the *in vitro* SPR experiment, which demonstrated positive miR-181a binding to both seed region sequences of the two mRNAs, but more strongly towards that of CDKN1β instead of E2F7. It could be that the cellular environment was able to facilitate further, the binding of the miRNA to the 3'UTR of E2F7, due to the presence of various enzymes and RNA-induced silencing complex

(RISC) that could aid strengthening the bond between miR-181a and the 3'UTR of E2F7, or that the ionic concentration *in vitro* had affected binding affinity. A more extensive binding between miR-181a and E2F7 was also previously predicted as compared to that of CDKN1β by bioinformatics analysis. In any case, miR-181a seems to target both mRNAs significantly, with p values= 0.0022 and 0.0008 for 100nM miR-181a targeting the 3'UTRs of CDKN1β and E2F7 respectively, and p values= 0.0057 and <0.0001 for 10nM miR-181a targeting the 3'UTRs of CDKN1β and E2F7 respectively.

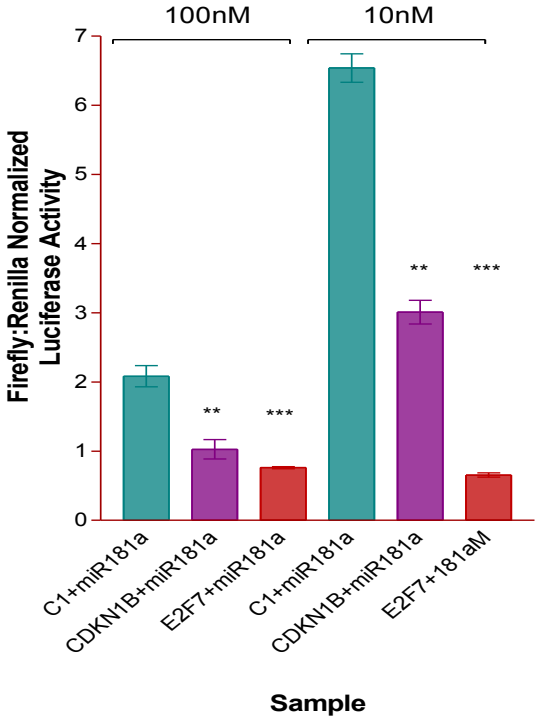

Figure 25. *In vivo* luciferase assay study of HepG2 cells co-transfected with the reporter plasmids and different concentrations of miR-181a. HepG2 cells were electroporated with 4μg of reporter plasmids and 10nM or 100nM miR-181a and seeded on 24 well plates. They were harvested after a 24h incubation and assayed for firefly and renilla luminescence using a manual luminometer. Results show that miR-181a binds to some extent, to the control vector, because of its dose dependent reduction in firefly luciferase activity upon transfection with the control vector. However, as compared to the control, miR-181a shows a significantly stronger binding to both the plasmids containing the 3'UTRs of CDKN1β and E2F7, with a further decrease in firefly luciferase activity by about two times when transfected with 10nM miR-181a (p value= 0.0057 and <0.0001 respectively) (n=3) and up to six times when transfected with 100nM miR-181a (p value= 0.0022 and 0.0008 respectively) (n=3), as compared to when transfected with the control reporter plasmid.

4.2.4 Western blot Verification

Binding of miR-181a to the 3'UTRs of CDKN1β and E2F7 *in vivo* may result in either the degradation of the mRNAs, the translational inhibition of the mRNAs to proteins or the temporary storage of the mRNAs in processing bodies (P-bodies) of cells and ultimately either degraded or released for delayed translation [108]. To study whether the protein levels of CDKN1β and E2F7 are affected by the transfection of miR-181a, we performed a Western blot analysis. Figures 24 and 25 show that the transfection of 10nM miR-181a downregulates the protein levels of CDKN1β and E2F7, but only the protein levels of E2F7 was statistically shown to be significantly downregulated (p value= 0.03). These two proteins were chosen in this study because our previous findings indicate that miR-181a, a miRNA found upregulated in HCC, causes a significant increase in HepG2 cell viability and may also play a part in cell cycle. These two proteins have been predicted by bioinformatics to be potential targets of miR-181a, and both partake in the negative regulation of the cell cycle and proliferation. CDKN1β is a well-known protein that prevents the activation of cyclin E-CDK2 and cyclin D-CDK4 complexes, thereby leading to a G1 cell cycle arrest [109]. E2F7 is a relatively newly discovered member of the E2F family of transcription factors that are highly involved in cell cycle progression, DNA repair and mitosis. In contrast to other well-studied E2F transcription factors (eg. E2F1, E2F2 and E2F3), E2F7 acts in the cell cycle by being a transcriptional repressor and negatively regulates cell proliferation [110]. The downregulation of these two proteins by miR-181a could have been one of the reasons that led to the increase in HepG2 cell growth as seen in our previous study. We also notice that miR-181a downregulated E2F7

protein more than CDKN1β. This is in line with the luciferase results obtained, where it was shown that a stronger binding occurred between miR-181a and the 3'UTR of E2F7. Also, in the earlier bioinformatics study, it was predicted that miR-181a forms a more extensive interaction with the 3'UTR of E2F7 than CDKN1β. Not only that, but the Mfold results on RNA folding also showed a more negative free energy of folding (ΔG_{fold}) at the binding region between miR-181a and the 3'UTR of CDKN1β, indicating a possibility of more secondary structures there. In this section, we show that miR-181a targets both mRNAs, but binds to the 3'UTR of E2F7 and downregulates its protein to a larger extent.

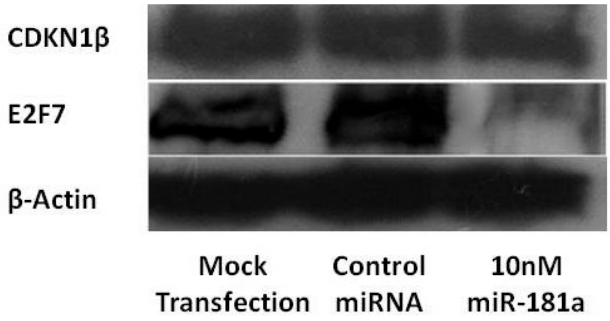

Figure 26. CDKN1β and E2F7 protein expression levels detection via a Western blot analysis. HepG2 cells were starved, electroporated with 10nM miR-181a and harvested after 24h incubation. 30μg total protein extract was loaded onto each well of an SDS-PAGE and probed with various selected primary antibodies overnight at 4°C. Mir-181a reduced the protein expression levels of both CDKN1β and E2F7; with the reduction of E2F7 to a greater extent. β-actin served as a loading control.

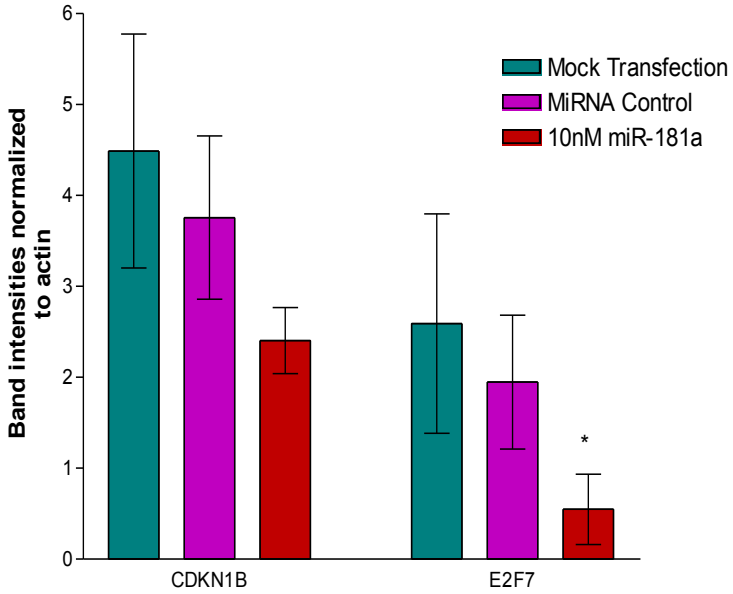

Figure 27. Protein levels of CDKN1β and E2F7in HepG2 cells following miR-181a transfection. Quantification of protein levels was analysed using Image J software. The transfection of miR-181a into the cells seems to decrease the amounts of these two proteins, but only the protein expression of E2F7 was statistically significant. ANOVA analysis of the three groups (done separately for each protein) showed a difference in means for that of E2F7 but not CDKN1β (p value= 0.03) (n=3). On closer inspection with a Student's *t*-test, the levels of E2F7 is shown to be significantly decreased when the cells were transfected with miR-181a as compared to the control (p value= 0.03) (n=3).

4.2.5 Section Conclusion

MiR-181a is found to target cell cycle proteins CDKN1β and E2F7. Their interactions were shown to be positive both *in vitro* and *in vivo*, using SPR and luciferase assays to validate respectively. However, a positive binding does not necessarily lead to protein downregulation. Although miRNAs are known to bind to mRNAs and affect protein levels, the exact mechanisms of protein regulation is still not well understood. The general consensus is that miRNAs bind to mRNAs and cause either mRNA degradation or a protein translation. However, there are also studies that show that the mRNAs may be temporarily stored and translated at a later time; the protein may still be expressed, albeit delayed. Also, because of the non-specific nature of miRNAs, binding to a certain mRNA may decrease the protein expression due to that particular binding. However, other

pathways and transcriptional factors activated by the same miRNA may cause an opposite effect of increasing transcription and/or stabilization of the target mRNA/protein. Therefore, the study of miRNAs is not as direct as we would like it to be. In order to study whether the proteins of the two target mRNAs are affected by miR-181a, a Western blot analysis was conducted. A slight, statistically insignificant downregulation of CDKN1β protein was observed while E2F7 protein appeared to be affected more, possibly due to the stronger binding between miR-181a and its 3'UTR. From this section, we have found that miR-181a plays a role in cell cycle by targeting cell cycle genes. This could be one of the reasons as to why cell viability was seen to be affected. We next look at other important pathways that this miRNA affects in a cell.

5. MiR-181a in Cancer Related Pathways: Its Effect on Important Transcription Factors

5.1 Introduction

As we are interested in how miR-181a is involved in liver cancer, we expanded the investigation to include not just its direct targets, but also how it affects the expression or activity levels of important transcription factors involved in cancer. Because many such proteins are implicated, the most efficient method of evaluation would be via a microarray analysis. The main advantage of using microarrays is in its ability to examine large amounts of biological material because of its high throughput.

Each of the ten reporter assays used in this microarray consists of a mixture of an inducible transcription factor responsive firefly luciferase reporter and a constitutively

expressing Renilla construct. The negative control consists of a mixture of a non-inducible responsive firefly luciferase reporter and a constitutively expressing Renilla construct, while the positive control consists of a mixture of constitutively expressing GFP construct, constitutively expressing firefly luciferase reporter and a constitutively expressing Renilla construct.

5.2 Results and Discussion

5.2.1 MiR-181a Significantly Activated the MAPK/JNK Pathway while Inhibiting it Significantly Reduced HIF-Related Hypoxia

The constructs, as described above, were dried-down to the bottom of each well of the 96-well plate, resuspended in OPTI-MEM growth media and reverse co-transfected with miR-181a or its inhibitor. The dual-luciferase activities were measured 48h after transfection The normalised firefly:Renilla luciferase activity was then plotted for three independent experimental repeats. Figure 26 shows the effects of the transfection of miR-181a and its inhibitor in the various cancer-related signalling pathways, normalized with readouts obtained from the transfection of HepG2 cells with a control miRNA. Pathways that are shown to be significantly up or downregulated will be further discussed. Among the ten pathways analysed, miR-181a causes the activation of activating protein 1 (AP-1) transcription factor most significantly (p value= 0.029), by approximately two folds, while inhibiting it abolished this observation. AP-1 is a transcriptional factor involved in the mitogen-activated protein (MAP) kinase signalling pathway. It contains two components, c-Jun and c-Fos, which are both crucial regulators of liver tumour development. C-Jun has been shown to promote the growth of tumour through the positive regulation of cell-cycle (eg. Cyclin D1) or through the repression of its negative regulators (eg. p16) [111]. It is

also able to antagonize apoptosis in liver tumours. In addition to the increase in activity or expression levels of AP-1, other transcriptional factors were also shown to be affected by miR-181a in HepG2 cells. Transcription factors involved in NFκB, Myc and Hypoxia also showed an increase, albeit lowered significance, in transcriptional activities overall. These are signalling pathways often found activated in cancers. It should be noted that the three independent measured activity readouts of the transcription factor for the MAPK/ERK pathway, Elk-1/SRF, have produced a large standard deviation. It is also not shown to be statistically significant, although the general trend may seem like it is activated when transfected with miR-181a. On further inspection of the raw values obtained, it is noticed that one of the repeats had produced an abnormally large firefly luminescence readout, almost twice that of the average value recorded. The other two repeats were of 'normal range'. This outlier could be due to various reasons: a rare abnormality in the construct such that the firefly reporter is more highly expressed than normal (eg. Promoter-related) or an unexpected change in environment that occurred in that particular well of the array that may have caused a sudden, acute activation of Elk-1/SRF. In either case, it would be safe to say that no conclusion may be drawn from our experiments for this particular pathway when miR-181a was transfected into HepG2 cells.

One interesting observation though, is that we have shown that miR-181a binds to the 3'UTRs of CDKN1β and E2F7 (and lowers their protein expression levels), and also that miR-181a transfection leads to an increase in AP-1 transcription factor activity, this could technically mean that miR-181a has a positive role to play in cell cycle. However, the pathway in the microarray analysis containing the E2F-DP1 transcription factor did not show any significant change as compared to the control sample. This could be due to the

concurrent activation of contradicting pathways following miR-181a transfection. From the microarray results, the transfection of miR-181a leads to the activation of TGF-β and Notch pathways, albeit of lowered significance. This translates to an increase in SMAD2/3/4 and RBP-Jk transcriptional activities, which has a cell cycle inhibition effect and growth arresting effect (in HCC) respectively [112, 113]. It is the overall balance of these different reinforcing and contradicting pathways that leads to the final outcome on the expression levels of the proteins. Indeed, our previous study showed that cell cycle was not significantly affected when miR-181a was transfected. However, the transfection of its inhibitor showed a significant slowdown in cell cycle by about 10%. The E2F transcription factor activity was seen to be lowered from the microarray study when miR-181a was inhibited.

In contrast to the increase in hypoxia-inducible factors (HIF) transcriptional activity by miR-181a, inhibiting it caused a corresponding significant decrease by approximately 40% (p value=0.027). Hypoxia is a condition in cells where oxygen concentration becomes low, leading to a massive transcription of genes by HIF proteins involved in angiogenesis, metabolism, cell proliferation and survival [114]. This is often seen in the case of many cancers, where oxygen concentration within cancer cells drop due to the spurt of cancer cell growth and HIF protein is overexpressed to accommodate this increase in cell proliferation. The lowered activity or expression levels of HIF in HepG2 cells transfected with miR-181a inhibitor could potentially decrease cell viability due to the reduction of this protective layer. Apart from the decrease in HIF, inhibiting miR-181a also caused a significant increase in SMAD protein activity (p value=0.0024). This protein is involved in TGF-β signalling, which can act as a tumour suppressor by causing a G_1 cell cycle

arrest [112]. Also, the increase and decrease in p53 and E2F proteins may respectively contribute to the lowered cell proliferation and viability of HepG2 cells when transfected with miR-181a inhibitor. However, the significant activation of the NFκB pathway (p value=0.041), may negate some of the anti-proliferative effects of the other tumour suppressive pathways, due to the ability of the NFκB pathway to induce cancer-causing cellular alterations like increasing insensitivity to growth inhibition, self-sufficiency in growth signals, evasion of apoptosis immortalization, angiogenesis and metastasis [115]. This could also be the reason why inhibiting miR-181a showed a limited therapeutic effect when transfected into HepG2 cells in our previous study, where cell viability reduced by only 20%. The combination of miR-181a inhibitor with specific siRNAs to target such tumour-promoting proteins could potentially further increase the eradication of HCC. Table 7 shows a summary of the transcription factors assayed and their roles in cancer.

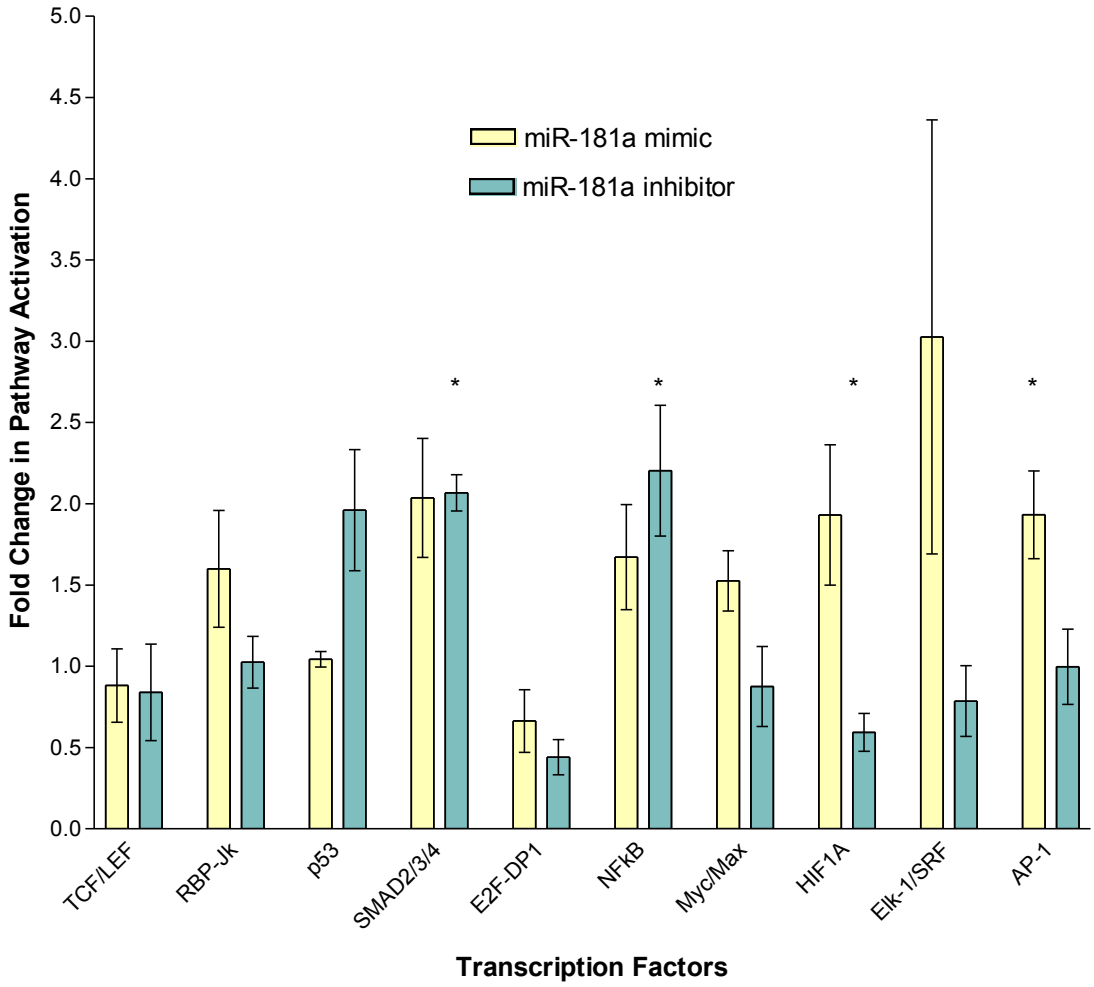

Figure 28. Microarray analysis of the expression levels/activities of ten important cancer-related transcription factors. HepG2 cells were reverse co-transfected with 100nM miR-181a or 100nM miR-181a inhibitor, along with the dried down transcription factor reporter plasmids and incubated for 24h in 96-well plates. Cells were assayed for luciferase activity 48h after reverse transfection using a plate luminometer. The values plotted are that of firefly luminescence normalized against that of renilla, which was used as the internal control. Among the ten pathways investigated, miR-181a caused a significant activation in the MAPK/JNK pathway, as seen by the increase in expression levels/activity of AP-1 protein (p value= 0.029) (n=3). Inhibiting miR-181a significantly activated the NFκB (p value= 0.041) (n=3) and TGF-β (p value= 0.0024) (n=3) pathways and lowered the HIF protein expression level/activity (p value= 0.027) (n=3).

Table 7. Transcription factors and their regulation by miR-181a and miR-181a inhibitor. The overall effects after regulation are listed alongside. Regulations in bold and labelled with an asterisk (*) refer to results that are significant. An increase in both tumour suppressive and tumour causing pathways are seen in both transfections. MiR-181a activates mainly tumour enhancing pathways while inhibiting it activates mostly tumour suppressive pathways.

Transcription Factor	Pathway(s) Involved	miR-181a		miR-181a Inhibitor	
		Regulation	Effect After Regulation	Regulation	Effect After Regulation
TCF/LEF	Wnt	-	-	-	-
RBP-Jk	Notch	↑	Growth Arrest	-	-
p53	p53/DNA Damage	-	-	↑	Cell Cycle Inhibition
SMAD2/3/4	TGFβ	↑	Cell Cycle Inhibition	↑*	**Cell Cycle Inhibition**
E2F/DP1	Cell cycle/ pRb-E2F	-	-	↓	Cell Cycle Inhibition
NFκB	NFκB	↑	Insensitivity to growth inhibition, self-sufficiency in growth signals, evasion of apoptosis immortalization, angiogenesis and metastasis	↑*	**Insensitivity to growth inhibition, self-sufficiency in growth signals, evasion of apoptosis immortalization, angiogenesis and metastasis**
Myc/Max	Myc/Max	↑	Proliferation	-	-
HIF1A	Hypoxia	↑	Survival/ Angiogenesis	↓*	**Decreased Survival/ Angiogenesis**
Elk-1/SRF	MAPK/ERK	↑	Proliferation	-	-
AP-1	MAPK/JNK	↑*	**Positive Cell Cycle Regulation**	-	-

5.2.2 Section Conclusion

As shown in the microarray analysis, miR-181a affects not just its direct targets but also, indirectly, many important transcription factors involved in cancer. This alone is sufficient in highlighting the impact miRNAs has in cells, and that their effects are not just limited to their protein targets alone. Ten cancer-related pathways were studied in HepG2 cells,

among which many of them were found to be affected by the overexpression of miR-181a or by its inhibition. MiR-181a causes a significant activation of the MAPK/JNK pathway by causing an increase in expression level or activity of AP-1 protein, a protein involved in positive cell cycle regulation and angiogenesis. It also causes activation of Hypoxia, MAPK/ERK, Myc, NFκB, TGFβ and Notch, but to a lesser extent for these. While the activation of MAPK/JNK, Hypoxia, MAPK/ERK, Myc and NFκB pathways directs the cell towards proliferation and survival, the simultaneous activation of TGFβ and Notch signalling leads the cell towards growth inhibition. MiR-181a seems to overall activate mainly the tumour-promoting signalling pathways probed for in the assay.

Inhibiting miR-181a, on the other hand, causes a significant decrease in hypoxia and promotes cell cycle inhibition by decreasing and increasing HIF1A and SMAD2/3/4 transcription factors respectively. It also causes a moderate increase of p53 and a corresponding decrease in E2F proteins. The overall effects of these tend to direct the cell towards a lowered cell proliferation. However, we also see a significant increase in the NFκB pathway, which has a counteracting effect by causing cells to become insensitive towards anti-growth signals.

Our previous studies showed that miR-181a significantly increased HepG2 cell viability while inhibiting it significantly decreased cell viability, by approximately 20%. The regulation of these important cancer-related pathways could have contributed to the overall cell viability observed. Because of the contradicting pathways activated when miR-181a was introduced or inhibited, the observed increase or decrease in viability was limited to a certain extent (ie. 20%). Specific targeting using siRNAs could aid in

deactivating pathways that enhance cancer cell growth, and the use of miRNAs and siRNAs could potentially improve current therapies in HCC.

6. Identification of Other mRNA Targets of miR-181a: High Throughput Approach using Microarrays

6.1 Introduction

We previously identified two targets of miR-181a in HepG2 cells, namely, CDKN1β and E2F7. To do so, we employed bioinformatics as our first platform and then validated the results with SPR, luciferase assays and a Western blot analysis as described in Section 4 of this thesis. In order to identify a larger range of targets, we made use of a custom-made microarray—miR-181 Targets RT^2 Profiler PCR Array (Qiagen). In this microarray analysis, the expression of 84 hsa-miR-181a-5p target genes was profiled. This panel of 84 genes includes currently known experimentally verified plus bioinformatically predicted target genes regulated by hsa-miR-181a-5p. The array also includes target genes regulated by other miRNAs that have the same seed sequence as hsa-miR-181a-5p, including hsa-miR-181b-5p, hsa-miR-181c-5p, hsa-miR-181d, and hsa-miR-4262. MiR-181a target gene expression analysis provides further insight into the function of this miRNA. A set of controls present on each array enables data analysis using the ΔΔCT method of relative quantification as well as assessment of reverse transcription performance, genomic DNA contamination and PCR performance. Using real-time PCR, we analyse the expression of a focused panel of genes likely to be regulated by miR-181 with this array. The array layout is shown in Table 8 and the full list of gene identification attached under the Appendix.

Table 8. Layout of miR-181 Targets RT^2 Profiler PCR Array. 84 genes may be studied simultaneously in this array, along with five housekeeping genes, one genomic DNA contamination control, three reverse transcription controls and three positive controls. A real-time RTPCR approach will be used to study the gene expression of these selected genes in HepG2 cells transfected with miR-181a and its inhibitor.

ACVR2A A01	ADARB1 A02	ADCY1 A03	AICDA A04	ATG5 A05	ATM A06	BCL2 A07	BCL2L11 A08	BDNF A09	BMPR2 A10	C16orf87 A11	C6orf62 A12
CAPRIN2 B01	CASP3 B02	CBLB B03	CBX7 B04	CD69 B05	CDKN1B B06	CDX2 B07	COPS2 B08	CXCR3 B09	CYLD B10	DDIT4 B11	DISC1 B12
DOCK4 C01	DUSP5 C02	DUSP6 C03	EIF4A2 C04	ENKUR C05	ETV6 C06	FBXL3 C07	FKBP1A C08	FOS C09	GABRA1 C10	GATA6 C11	GLS C12
GRIA1 D01	GRIA2 D02	GRIK1 D03	HIPK2 D04	HK2 D05	HMGB2 D06	IGF1R D07	IL1A D08	KANK1 D09	KAT2B D10	KCNA4 D11	KIAA0195 D12
KLHL2 E01	KRAS E02	LRBA E03	MAP1B E04	MAP3K10 E05	MGMT E06	NARF E07	NLK E08	NMT2 E09	NOTCH4 E10	NPEPPS E11	PLAG1 E12
PLAU F01	PLCL2 F02	PRKCD F03	PROX1 F04	PTPN11 F05	PTPN22 F06	RALA F07	RLF F08	RNF2 F09	SIRT1 F10	SLC2A1 F11	STAT1 F12
TANC2 G01	TBPL1 G02	TCERG1 G03	TCL1A G04	TMEM131 G05	VSNL1 G06	YTHDC1 G07	ZFP36L1 G08	ZFP36L2 G09	ZNF180 G10	ZNF37A G11	ZNF83 G12
ACTB H01	B2M H02	GAPDH H03	HPRT1 H04	RPLP0 H05	HGDC H06	RTC H07	RTC H08	RTC H09	PPC H10	PPC H11	PPC H12

6.2 Results and Discussion

6.2.1 BMPR2, GATA6, NOTCH4 and ZNF180 were among the 84 Genes Significantly Regulated by miR-181a or miR-181a inhibitor

HepG2 cells were transfected with 100nM miR-181a or 100nM miR-181a inhibitor and incubated for 24h before harvesting for RNA extraction. Extracted RNA was reverse transcribed and allowed to undergo PCR in the microarray plate format as shown in Table 6, with SYBR Green used as the reporter dye due to its ability to bind to double stranded DNA and its high sensitivity. Each run was done in triplicate. Figure 27 shows the typical amplification plot and melting curve obtained during each run of PCR.

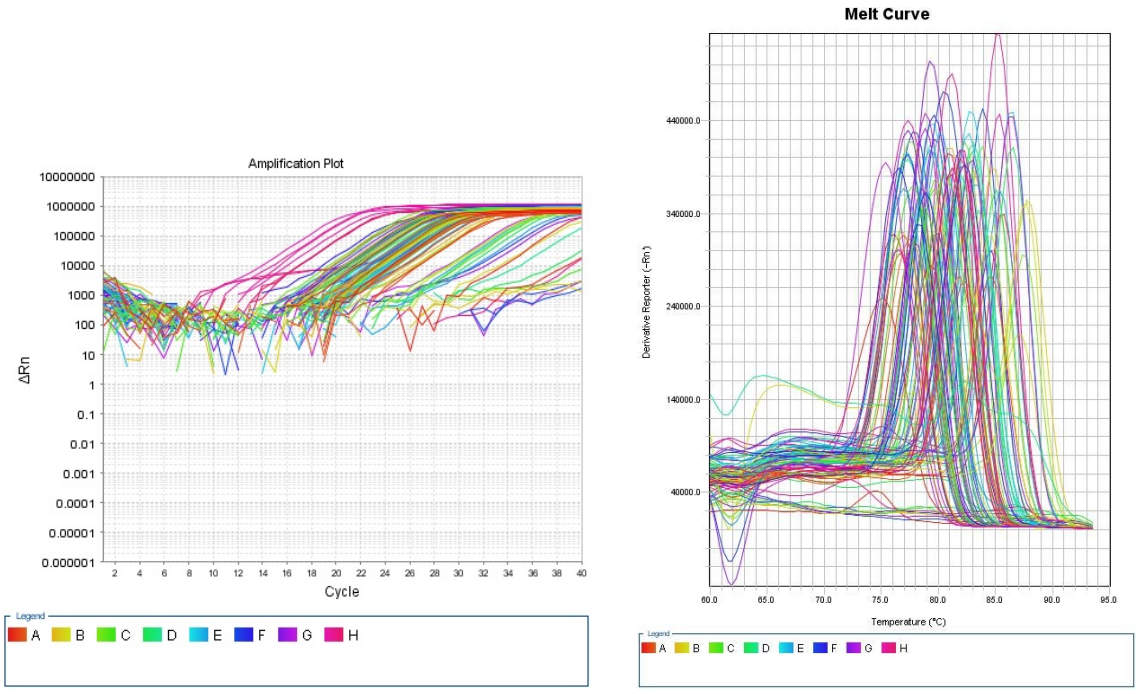

Figure 29. Amplification Plot (left) and Melting Curve (right). The amplification plot shows the variation of log (ΔRn) with PCR cycle number, while a unique melting curve checks for specificity of the PCR product.

Tables 9 and 10 show the fold changes and p values of the test samples (ie. HepG2 cells transfected with miR-181a or miR-181a inhibitor) vs control samples (ie. HepG2 cells transfected with control miRNA) for all the genes probed for in the microarray. P values in bold indicate significance (ie. P value<0.05). The overall changes in gene expression are represented as a 3D plot in Figures 28 and 29.

Table 9. Fold change and p values of genes probed in HepG2 cells transfected with miR-181a. HepG2 cells were transfected with 100nM miR-181a, total RNA extracted and reverse transcribed. PCR was done on the cDNAs in the microarrays using SYBR Green as the reporter dye. ΔCt represents Ct(Gene of interest)-AvgCt(housekeeping genes), while the fold change is represented by ΔΔCt= 2^(- Delta Ct)) in the Test Sample divided the normalized gene expression (2^(- Delta Ct)) in the Control Sample. n=3 for each gene.

Symbol	Well	AVG ΔC_t (Ct(GOI) - Ave Ct (HKG))		$2^{-\Delta C_t}$		Fold Change	*t*-test	Fold Up- or Down-Regulation
		miR-181aM	Control Sample	miR-181aM	Control Sample	miR-181aM /Control Sample	p value	miR-181aM /Control Sample
ACVR2A	A01	8.32	8.57	3.1E-03	2.6E-03	1.19	0.267537	1.19

ADARB1	A02	5.45	5.91	2.3E-02	1.7E-02	1.37	0.457283	1.37
ADCY1	A03	19.40	18.91	1.4E-06	2.0E-06	0.71	0.456841	-1.41
AICDA	A04	17.22	19.77	6.6E-06	1.1E-06	**5.87**	0.182613	**5.87**
ATG5	A05	7.25	7.55	6.6E-03	5.3E-03	1.23	0.498072	1.23
ATM	A06	10.39	10.94	7.5E-04	5.1E-04	1.47	0.291322	1.47
BCL2	A07	10.40	10.80	7.4E-04	5.6E-04	1.32	0.165535	1.32
BCL2L11	A08	8.94	8.80	2.0E-03	2.2E-03	0.91	0.438811	-1.10
BDNF	A09	9.03	9.38	1.9E-03	1.5E-03	1.27	0.207232	1.27
BMPR2	A10	8.16	8.87	3.5E-03	2.1E-03	1.64	**0.019618**	1.64
C16orf87	A11	6.46	6.36	1.1E-02	1.2E-02	0.93	0.659065	-1.07
C6orf62	A12	3.80	4.14	7.2E-02	5.7E-02	1.27	0.500807	1.27
CAPRIN2	B01	9.16	9.49	1.7E-03	1.4E-03	1.26	0.485955	1.26
CASP3	B02	7.47	5.95	5.7E-03	1.6E-02	0.35	0.313767	-2.86
CBLB	B03	8.42	9.09	2.9E-03	1.8E-03	1.59	0.402325	1.59
CBX7	B04	10.77	11.23	5.7E-04	4.2E-04	1.37	0.840424	1.37
CD69	B05	19.42	20.93	1.4E-06	5.0E-07	2.85	0.347530	2.85
CDKN1B	B06	5.24	5.46	2.7E-02	2.3E-02	1.17	0.540722	1.17
CDX2	B07	17.64	14.34	4.9E-06	4.8E-05	**0.10**	0.373920	**-9.86**
COPS2	B08	4.56	4.59	4.2E-02	4.1E-02	1.03	0.983017	1.03
CXCR3	B09	15.80	17.23	1.7E-05	6.5E-06	2.69	0.091385	2.69
CYLD	B10	7.70	7.79	4.8E-03	4.5E-03	1.06	0.122809	1.06
DDIT4	B11	6.84	6.31	8.7E-03	1.3E-02	0.69	0.443617	-1.44
DISC1	B12	12.28	13.37	2.0E-04	9.4E-05	2.14	0.154479	2.14
DOCK4	C01	12.18	12.82	2.2E-04	1.4E-04	1.57	0.540829	1.57
DUSP5	C02	6.42	7.21	1.2E-02	6.7E-03	1.73	0.235421	1.73
DUSP6	C03	9.63	8.72	1.3E-03	2.4E-03	0.53	0.404475	-1.88
EIF4A2	C04	2.87	2.95	1.4E-01	1.3E-01	1.06	0.949822	1.06
ENKUR	C05	14.96	14.96	3.1E-05	3.1E-05	0.99	0.751036	-1.01
ETV6	C06	7.53	8.11	5.4E-03	3.6E-03	1.49	0.140128	1.49
FBXL3	C07	5.32	3.73	2.5E-02	7.5E-02	0.33	0.379105	**-3.02**
FKBP1A	C08	5.50	5.11	2.2E-02	2.9E-02	0.77	0.464486	-1.31
FOS	C09	8.19	8.37	3.4E-03	3.0E-03	1.13	0.829436	1.13
GABRA1	C10	19.32	20.93	1.5E-06	5.0E-07	**3.05**	0.367941	**3.05**
GATA6	C11	7.72	8.27	4.7E-03	3.2E-03	1.46	0.255139	1.46
GLS	C12	4.69	5.04	3.9E-02	3.0E-02	1.27	0.331817	1.27
GRIA1	D01	20.78	17.44	5.5E-07	5.6E-06	**0.10**	0.373936	**-10.13**
GRIA2	D02	20.78	18.01	5.5E-07	3.8E-06	**0.15**	0.371367	**-6.82**
GRIK1	D03	12.89	13.84	1.3E-04	6.8E-05	1.93	0.071683	1.93
HIPK2	D04	14.19	14.04	5.3E-05	5.9E-05	0.90	0.833027	-1.11
HK2	D05	4.69	4.93	3.9E-02	3.3E-02	1.18	0.486988	1.18
HMGB2	D06	4.07	4.30	5.9E-02	5.1E-02	1.17	0.392232	1.17

IGF1R	D07	6.77	6.17	9.2E-03	1.4E-02	0.66	0.444346	-1.51
IL1A	D08	8.54	8.80	2.7E-03	2.2E-03	1.20	0.922057	1.20
KANK1	D09	5.95	5.18	1.6E-02	2.7E-02	0.59	0.336143	-1.70
KAT2B	D10	8.75	8.71	2.3E-03	2.4E-03	0.97	0.980091	-1.03
KCNA4	D11	18.40	18.23	2.9E-06	3.3E-06	0.89	0.820454	-1.12
KIAA0195	D12	8.08	8.53	3.7E-03	2.7E-03	1.36	0.341902	1.36
KLHL2	E01	8.15	8.27	3.5E-03	3.2E-03	1.09	0.589740	1.09
KRAS	E02	6.13	6.40	1.4E-02	1.2E-02	1.20	0.674682	1.20
LRBA	E03	7.65	7.98	5.0E-03	4.0E-03	1.26	0.447922	1.26
MAP1B	E04	9.48	9.75	1.4E-03	1.2E-03	1.21	0.627909	1.21
MAP3K10	E05	8.14	8.83	3.5E-03	2.2E-03	1.62	0.269571	1.62
MGMT	E06	6.45	7.67	1.1E-02	4.9E-03	2.34	0.374145	2.34
NARF	E07	6.59	6.29	1.0E-02	1.3E-02	0.81	0.348006	-1.23
NLK	E08	7.80	8.08	4.5E-03	3.7E-03	1.21	0.654475	1.21
NMT2	E09	8.20	7.67	3.4E-03	4.9E-03	0.69	0.323736	-1.45
NOTCH4	E10	13.23	13.69	1.0E-04	7.5E-05	1.38	0.280996	1.38
NPEPPS	E11	5.88	5.96	1.7E-02	1.6E-02	1.06	0.849837	1.06
PLAG1	E12	16.85	15.56	8.5E-06	2.1E-05	0.41	0.158431	-2.44
PLAU	F01	16.76	18.32	9.0E-06	3.1E-06	2.94	0.277788	2.94
PLCL2	F02	6.90	5.96	8.4E-03	1.6E-02	0.52	0.320174	-1.91
PRKCD	F03	8.56	9.75	2.7E-03	1.2E-03	2.29	0.060598	2.29
PROX1	F04	20.78	18.99	5.5E-07	1.9E-06	**0.29**	0.374823	**-3.46**
PTPN11	F05	4.13	4.18	5.7E-02	5.5E-02	1.04	0.656689	1.04
PTPN22	F06	14.13	10.42	5.6E-05	7.3E-04	**0.08**	0.373865	**-13.05**
RALA	F07	5.20	5.36	2.7E-02	2.4E-02	1.12	0.634097	1.12
RLF	F08	7.30	7.47	6.3E-03	5.6E-03	1.13	0.156487	1.13
RNF2	F09	6.51	6.85	1.1E-02	8.7E-03	1.26	0.495303	1.26
SIRT1	F10	6.76	7.00	9.3E-03	7.8E-03	1.18	0.701498	1.18
SLC2A1	F11	4.62	4.75	4.1E-02	3.7E-02	1.09	0.436090	1.09
STAT1	F12	2.73	4.64	1.5E-01	4.0E-02	**3.75**	0.169613	**3.75**
TANC2	G01	6.98	7.29	7.9E-03	6.4E-03	1.23	0.940822	1.23
TBPL1	G02	7.90	7.80	4.2E-03	4.5E-03	0.93	0.820814	-1.08
TCERG1	G03	4.73	4.20	3.8E-02	5.4E-02	0.69	0.535745	-1.44
TCL1A	G04	16.76	15.85	9.0E-06	1.7E-05	0.53	0.693015	-1.88
TMEM131	G05	6.44	6.78	1.1E-02	9.1E-03	1.26	0.318019	1.26
VSNL1	G06	15.20	20.03	2.7E-05	9.4E-07	**28.34**	0.128277	**28.34**
YTHDC1	G07	5.76	5.91	1.8E-02	1.7E-02	1.11	0.808541	1.11
ZFP36L1	G08	4.34	3.76	4.9E-02	7.4E-02	0.67	0.409457	-1.50
ZFP36L2	G09	4.68	4.22	3.9E-02	5.4E-02	0.73	0.461535	-1.38
ZNF180	G10	7.79	8.10	4.5E-03	3.7E-03	1.23	0.257589	1.23
ZNF37A	G11	6.66	7.38	9.9E-03	6.0E-03	1.65	0.248678	1.65

ZNF83	G12	12.00	12.12	2.4E-04	2.2E-04	1.09	0.778311	1.09
ACTB	H01	-1.68	-2.17	3.2E+00	4.5E+00	0.71	0.280654	-1.41
B2M	H02	-0.21	0.02	1.2E+00	9.9E-01	1.17	0.634824	1.17
GAPDH	H03	-1.27	-0.92	2.4E+00	1.9E+00	1.28	0.722400	1.28
HPRT1	H04	4.23	3.78	5.3E-02	7.3E-02	0.73	0.468227	-1.36
RPLP0	H05	-1.07	-0.71	2.1E+00	1.6E+00	1.28	0.087210	1.28

Table 10. Fold change and p values of genes probed in HepG2 cells transfected with miR-181a inhibitor. HepG2 cells were transfected with 100nM miR-181a inhibitor, total RNA extracted and reverse transcribed. PCR was done on the cDNAs in the microarrays using SYBR Green as the reporter dye. ΔCt represents Ct(Gene of interest)-AvgCt(housekeeping genes), while the fold change is represented by ΔΔCt= 2^(- Delta Ct)) in the Test Sample divided the normalized gene expression (2^(- Delta Ct)) in the Control Sample. n=3 for each gene.

Symbol	Well	AVG ΔC_t (Ct(GOI) - Ave Ct (HKG))		$2^{-\Delta C_t}$		Fold Change	*t*-test	Fold Up- or Down-Regulation
		miR-181a inhibitor	Control Sample	miR-181a inhibitor	Control Sample	miR-181a inhibitor /Control Sample	p value	miR-181a inhibitor /Control Sample
ACVR2A	A01	8.16	8.57	3.5E-03	2.6E-03	1.33	0.178884	1.33
ADARB1	A02	5.62	5.91	2.0E-02	1.7E-02	1.22	0.681159	1.22
ADCY1	A03	19.15	18.91	1.7E-06	2.0E-06	0.85	0.927969	-1.18
AICDA	A04	19.09	19.77	1.8E-06	1.1E-06	1.60	0.575954	1.60
ATG5	A05	7.43	7.55	5.8E-03	5.3E-03	1.09	0.881300	1.09
ATM	A06	10.52	10.94	6.8E-04	5.1E-04	1.34	0.432982	1.34
BCL2	A07	10.47	10.80	7.0E-04	5.6E-04	1.25	0.191383	1.25
BCL2L11	A08	8.81	8.80	2.2E-03	2.2E-03	1.00	0.949859	-1.00
BDNF	A09	9.41	9.38	1.5E-03	1.5E-03	0.98	0.883756	-1.02
BMPR2	A10	8.14	8.87	3.6E-03	2.1E-03	1.66	0.261549	1.66
C16orf87	A11	6.73	6.36	9.4E-03	1.2E-02	0.77	0.488151	-1.30
C6orf62	A12	4.13	4.14	5.7E-02	5.7E-02	1.00	0.869187	1.00
CAPRIN2	B01	9.43	9.49	1.5E-03	1.4E-03	1.05	0.822617	1.05
CASP3	B02	7.70	5.95	4.8E-03	1.6E-02	**0.30**	0.294857	**-3.36**
CBLB	B03	8.53	9.09	2.7E-03	1.8E-03	1.47	0.532407	1.47
CBX7	B04	9.99	11.23	9.8E-04	4.2E-04	2.35	0.185352	2.35
CD69	B05	19.39	20.93	1.5E-06	5.0E-07	2.91	0.323067	2.91
CDKN1B	B06	5.77	5.46	1.8E-02	2.3E-02	0.81	0.430697	-1.24
CDX2	B07	18.56	14.34	2.6E-06	4.8E-05	**0.05**	0.373911	**-18.68**
COPS2	B08	4.75	4.59	3.7E-02	4.1E-02	0.90	0.658805	-1.11
CXCR3	B09	17.18	17.23	6.7E-06	6.5E-06	1.04	0.792632	1.04
CYLD	B10	7.73	7.79	4.7E-03	4.5E-03	1.04	0.630303	1.04
DDIT4	B11	7.21	6.31	6.8E-03	1.3E-02	0.54	0.405868	-1.86

DISC1	B12	12.76	13.37	1.4E-04	9.4E-05	1.53	0.256660	1.53
DOCK4	C01	12.71	12.82	1.5E-04	1.4E-04	1.08	0.775658	1.08
DUSP5	C02	6.66	7.21	9.9E-03	6.7E-03	1.47	0.468794	1.47
DUSP6	C03	9.91	8.72	1.0E-03	2.4E-03	0.44	0.368368	-2.28
EIF4A2	C04	3.65	2.95	7.9E-02	1.3E-01	0.62	0.192413	-1.62
ENKUR	C05	14.45	14.96	4.5E-05	3.1E-05	1.42	0.480452	1.42
ETV6	C06	7.78	8.11	4.6E-03	3.6E-03	1.26	0.294626	1.26
FBXL3	C07	4.82	3.73	3.5E-02	7.5E-02	0.47	0.417681	-2.13
FKBP1A	C08	5.36	5.11	2.4E-02	2.9E-02	0.84	0.570747	-1.19
FOS	C09	8.56	8.37	2.6E-03	3.0E-03	0.88	0.664234	-1.14
GABRA1	C10	19.23	20.93	1.6E-06	5.0E-07	**3.26**	0.309785	**3.26**
GATA6	C11	7.35	8.27	6.1E-03	3.2E-03	1.89	**0.043807**	1.89
GLS	C12	4.46	5.04	4.5E-02	3.0E-02	1.49	0.092393	1.49
GRIA1	D01	19.43	17.44	1.4E-06	5.6E-06	**0.25**	0.377106	**-3.95**
GRIA2	D02	17.50	18.01	5.4E-06	3.8E-06	1.43	0.502535	1.43
GRIK1	D03	13.46	13.84	8.9E-05	6.8E-05	1.31	0.488462	1.31
HIPK2	D04	13.78	14.04	7.1E-05	5.9E-05	1.20	0.620013	1.20
HK2	D05	4.61	4.93	4.1E-02	3.3E-02	1.25	0.426343	1.25
HMGB2	D06	4.16	4.30	5.6E-02	5.1E-02	1.10	0.548619	1.10
IGF1R	D07	6.95	6.17	8.1E-03	1.4E-02	0.58	0.410657	-1.72
IL1A	D08	9.57	8.80	1.3E-03	2.2E-03	0.59	0.539420	-1.71
KANK1	D09	5.86	5.18	1.7E-02	2.7E-02	0.63	0.364501	-1.59
KAT2B	D10	8.53	8.71	2.7E-03	2.4E-03	1.13	0.603511	1.13
KCNA4	D11	18.16	18.23	3.4E-06	3.3E-06	1.05	0.718505	1.05
KIAA0195	D12	7.95	8.53	4.1E-03	2.7E-03	1.49	0.212327	1.49
KLHL2	E01	8.06	8.27	3.7E-03	3.2E-03	1.15	0.434422	1.15
KRAS	E02	6.42	6.40	1.2E-02	1.2E-02	0.98	0.841916	-1.02
LRBA	E03	7.80	7.98	4.5E-03	4.0E-03	1.13	0.608517	1.13
MAP1B	E04	9.48	9.75	1.4E-03	1.2E-03	1.21	0.630339	1.21
MAP3K10	E05	8.09	8.83	3.7E-03	2.2E-03	1.67	0.189699	1.67
MGMT	E06	7.58	7.67	5.2E-03	4.9E-03	1.07	0.638796	1.07
NARF	E07	6.40	6.29	1.2E-02	1.3E-02	0.93	0.605548	-1.08
NLK	E08	7.63	8.08	5.1E-03	3.7E-03	1.36	0.367233	1.36
NMT2	E09	8.20	7.67	3.4E-03	4.9E-03	0.69	0.326794	-1.45
NOTCH4	E10	13.32	13.69	9.8E-05	7.5E-05	1.30	**0.020019**	1.30
NPEPPS	E11	5.75	5.96	1.9E-02	1.6E-02	1.16	0.572568	1.16
PLAG1	E12	17.56	15.56	5.2E-06	2.1E-05	**0.25**	0.142215	**-3.98**
PLAU	F01	16.33	18.32	1.2E-05	3.1E-06	**3.97**	0.237507	**3.97**
PLCL2	F02	6.46	5.96	1.1E-02	1.6E-02	0.71	0.561881	-1.41
PRKCD	F03	8.67	9.75	2.4E-03	1.2E-03	2.11	0.219765	2.11
PROX1	F04	20.49	18.99	6.8E-07	1.9E-06	0.35	0.383044	-2.82

PTPN11	F05	4.48	4.18	4.5E-02	5.5E-02	0.81	0.286405	-1.23
PTPN22	F06	15.65	10.42	1.9E-05	7.3E-04	**0.03**	0.373580	**-37.54**
RALA	F07	5.00	5.36	3.1E-02	2.4E-02	1.28	0.219388	1.28
RLF	F08	7.14	7.47	7.1E-03	5.6E-03	1.26	0.183147	1.26
RNF2	F09	6.38	6.85	1.2E-02	8.7E-03	1.39	0.250751	1.39
SIRT1	F10	6.78	7.00	9.1E-03	7.8E-03	1.16	0.762576	1.16
SLC2A1	F11	4.70	4.75	3.8E-02	3.7E-02	1.03	0.595572	1.03
STAT1	F12	3.24	4.64	1.1E-01	4.0E-02	2.64	0.424496	2.64
TANC2	G01	7.04	7.29	7.6E-03	6.4E-03	1.19	0.977385	1.19
TBPL1	G02	7.45	7.80	5.7E-03	4.5E-03	1.27	0.451731	1.27
TCERG1	G03	3.96	4.20	6.4E-02	5.4E-02	1.18	0.898740	1.18
TCL1A	G04	18.44	15.85	2.8E-06	1.7E-05	**0.17**	0.209868	**-6.04**
TMEM131	G05	6.65	6.78	1.0E-02	9.1E-03	1.09	0.640466	1.09
VSNL1	G06	17.34	20.03	6.0E-06	9.4E-07	**6.45**	0.226328	**6.45**
YTHDC1	G07	5.73	5.91	1.9E-02	1.7E-02	1.13	0.826471	1.13
ZFP36L1	G08	4.36	3.76	4.9E-02	7.4E-02	0.66	0.400925	-1.52
ZFP36L2	G09	4.34	4.22	4.9E-02	5.4E-02	0.92	0.646202	-1.08
ZNF180	G10	7.48	8.10	5.6E-03	3.7E-03	1.53	**0.013637**	1.53
ZNF37A	G11	6.39	7.38	1.2E-02	6.0E-03	1.98	0.068227	1.98
ZNF83	G12	12.77	12.12	1.4E-04	2.2E-04	0.64	0.328636	-1.57
ACTB	H01	-1.79	-2.17	3.5E+00	4.5E+00	0.77	0.405856	-1.31
B2M	H02	-0.20	0.02	1.1E+00	9.9E-01	1.16	0.652129	1.16
GAPDH	H03	-1.23	-0.92	2.3E+00	1.9E+00	1.24	0.796353	1.24
HPRT1	H04	4.14	3.78	5.7E-02	7.3E-02	0.78	0.484904	-1.28
RPLP0	H05	-0.93	-0.71	1.9E+00	1.6E+00	1.16	0.418096	1.16

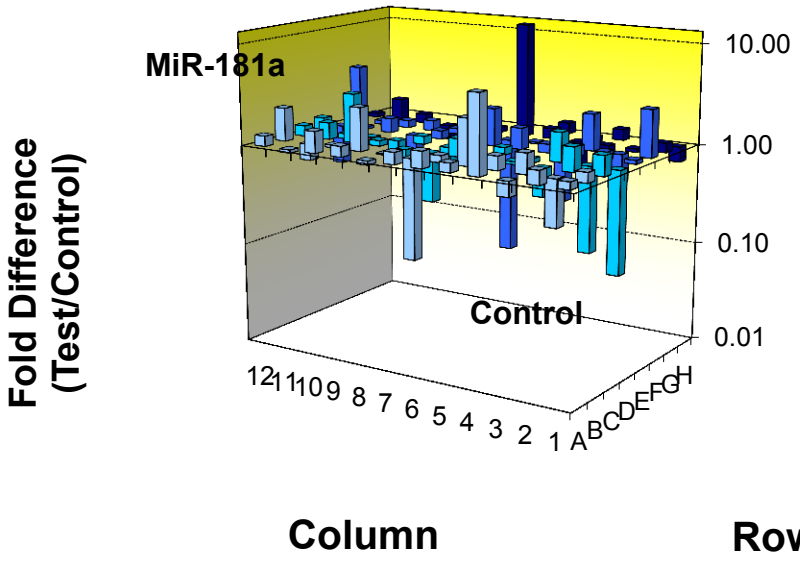

Figure 30. Overall gene regulation of miR-181a in HepG2 cells. HepG2 cells were transfected with 100nM miR-181a and total RNA extracted, reverse transcribed and underwent PCR. 84 genes were probed by real-time PCR and their fold change (test sample/control sample) plotted in a 3D graph. Both an increase and decrease in genes were detected, in contrast to only down-regulation in the case of mRNA targeting and degradation by miR-181a. This shows that miRNAs may regulate cellular activities at the translational instead of transcriptional level. BMPR2 gene expression levels showed a significant and consistent up-regulation in all three experimental repeats.

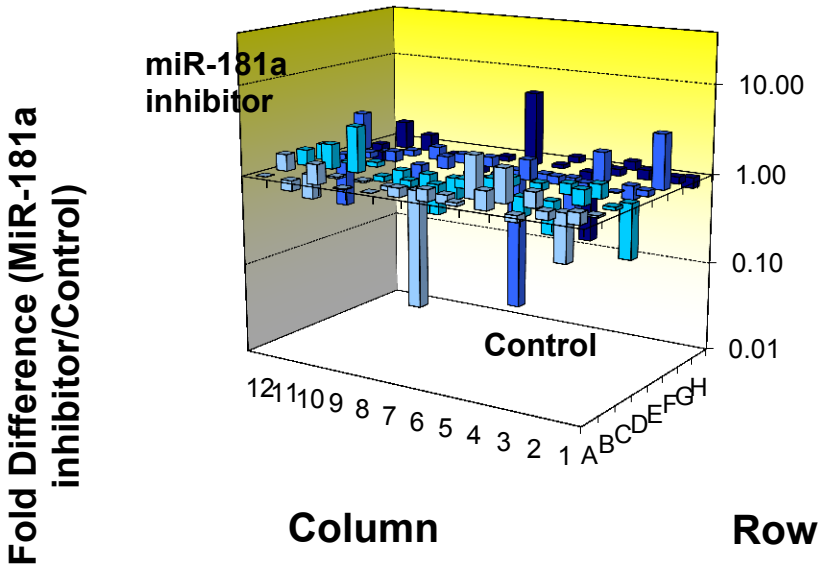

Figure 31. Overall gene regulation of miR-181a inhibitor in HepG2 cells. HepG2 cells were transfected with 100nM miR-181a inhibitor and total RNA extracted, reverse transcribed and real-time RT PCR carried out in the microarray. 84 genes were probed by real-time PCR and their fold change (test sample/control sample) plotted in a 3D graph. Similar to Figure 28, a combination of both up and down-regulation of genes is found when miR-181a was inhibited in HepG2 cells. GATA6, NOTCH4 and ZNF180 were genes found to be significantly and consistently upregulated when miR-181a was inhibited in HepG2 cells in all three experimental repeats.

Overall, we do see fold changes in most of the genes, both up and down regulated. The microarray is custom-made to probe for predicted genes targeted by miR-181a. Instead of downregulating most genes, we see a mix of both up and downregulation. This highly supports the general consensus that most human miRNAs affect gene expression at the translational level instead of causing mRNA degradation, since considerable amount of mRNA could still be detected. Not only that, but evidently from our previous transcription factor microarray study, the transfection of miR-181a causes a change in the expression levels or activities of transcription factors in HepG2 cells that are not known to be its direct targets. This in turn means that miRNAs are able to affect gene expression of mRNAs directly or indirectly, due to the vast interconnectedness of biological molecules in the cell. Therefore, in the analysis of this study, we broaden the scope of the term 'targets' to include not just the possible direct targets, but the overall gene expression of HepG2 cells due to the direct or indirect effects of miR-181a and its inhibitor.

We will discuss the effects of miR-181a and its inhibitor on genes that have shown significant up or down regulation. Only one gene showed a consistent and significant change in expression level when miR-181a was transfected into HepG2 cells. Bone morphogenetic protein receptor type 2 (BMPR2) mRNA expression level is shown to be significantly upregulated by a factor of 1.64 (p value=0.02) as compared to the control sample. The protein expressed by this gene is a serine/threonine receptor kinase that binds to bone morphogenetic proteins (BMPs) that leads to the transduction of cell signals involved in the SMAD, MAPK, NFκB, LIM domain kinase 1 (LIMK) and dynein, light chain, Tctex-type 1 (TCTEX) and v-src sarcoma viral oncogene homolog (SRC) signalling pathway [116]. As found earlier in our previous microarray pathway analysis,

SMAD2/3/4, NFκB, Elk-1/SRF and AP-1 transcription factors corresponding to SMAD, NFκB, and MAPK signalling pathways were found to be over-activated in HepG2 cells due to the transfection of miR-181a. The increased gene expression of BMPR2 due to miR-181a could have led to the overall activation of these pathways as its binding to BMPs aids in mediating these signal transductions. One interesting observation is that miR-181a also seemed to increase the gene expression of CDKN1β, albeit to an insignificant extent (p value= 0.54). It was previously noted that miR-181a slightly decreased the protein level of CDKN1β, although also insignificantly. This conflicting result could be due to the fact that miRNAs are known to regulate protein levels through mRNA translation rather than at the transcription level, therefore the level of CDKN1β mRNA did not reflect the corresponding protein level. Regardless, the two experiments have shown that the mean mRNA and protein levels of CDKN1β do not differ from that of their controls, therefore this gene might not play an important role in the downstream effects of miR-181a in HepG2 cells as much as E2F7.

When miR-181a was inhibited in HepG2 cells, three genes showed a significant change in expression. GATA6, NOTCH4 and ZNF180 mRNA were found to increase by 1.89, 1.30 and 1.53 times respectively (p values= 0.0438, 0.0200 and 0.0136). A study [78] has shown that miR-181a downregulates GATA6 protein in Hep3B cells and also binds to its mRNA. It also showed that the inhibition of miR-181a restored the expression of GATA6 protein. Our studies on HepG2 cells show that inhibiting miR-181a significantly increases the expression of GATA6 mRNA. This may, or may not be through direct mRNA regulation. However, this supports the previous findings from other studies that miR-181a may target GATA6 mRNA. GATA6 is one of the regulators of hepatic cell differentiation.

It is also believed that the loss of expression of this gene leads to the 'stemness' of HpSC-HCC, thereby giving hepatic cancer stem cells (CSCs) the ability to proliferate indefinitely. The increased gene expression of GATA6 due to the inhibition of miR-181a may lead to a reduction in 'stemness' of HpSC-HCC, thereby making it more vulnerable to HCC therapy.

The inhibition of miR-181a caused a significant increase in NOTCH4 mRNA. While NOTCH1 is a relatively well-studied gene that when activated, causes apoptosis and inhibition of HCC proliferation, NOTCH4 is less understood. There are studies that have shown that NOTCH4 expression inhibits angiogenesis, endothelial sprouting and migration through collagen [117]. Other studies however, show that NOTCH4 is upregulated in neoplastic hepatocytes with respect to normal liver cells [118]. Its functional implication, however, is still not known. Similar to NOTCH4, ZNF180 is found to be significantly upregulated when miR-181a was inhibited in HepG2 cells from our microarray analysis. However, its role in HCC is not well understood. Its plays a role mainly in the physiological and pathological processes, but their mechanisms of actions are still not known [119].

6.2.2 Section Conclusion

Out of 84 genes probed, we obtained a significant upregulation in four such genes. Out the four genes, two of them are relatively well-studied and their functions understood, while the other two are comparatively more obscure. The transfection of miR-181a into HepG2 cells caused an increase in BMPR2 mRNA expression level, whose protein when expressed is a receptor that mediates in the transduction of the SMAD, MAPK and NFκB

pathways. This observation was supported by our previous microarray study on cancer pathways, where an increase in expression and/or activities of all four transcription factors participating in these three pathways was observed. This could be one of the mechanisms in which miR-181a exerts its effect on in HepG2 cells. The increased expression of miR-181a found in many HCC cases may enable liver cancer cells to activate these pathways due to the elevated BMPR2 gene expression level.

The inhibition of miR-181a increased the expression level of GATA6. This gene aids in cellular differentiation, and its loss in expression has been found to lead to 'stemness', a quality of stem cells that makes them 'immortal' and with 'unlimited growth potential'. The increased expression of GATA6 by inhibiting miR-181a could reduce this 'stemness' quality of liver cancer cells, which may be useful in liver cancer therapy.

The two other genes found to be significantly upregulated when miR-181a was inhibited, NOTCH4 and ZNF180, are not well understood yet, and their role (if any) in cancers are also not well studied. In this study, we may have identified one of the mechanisms in which miR-181a acts in activating the pathways involved in cancer, by the increased expression of BMPR2.

7. Conclusion

HCC is currently one of the top cancers with the highest mortality rate. Popular treatment options include surgical resection or liver transplantation, radiotherapy and chemotherapy, TACE, etc. While surgical resection and liver transplantation are effective in eradicating liver cancer in patients at the early stages of the disease, patients diagnosed at the mid or terminal stages usually have very low survival rates under TACE, chemotherapy or radiotherapy. These treatment methods cause unwanted side effects and therefore have limited effectiveness. MiRNAs have been shown to be able to regulate many cellular processes, including proliferation, differentiation, angiogenesis, cell development, etc. Its main mode of regulation is through the binding of multiple target mRNAs, leading to the translational inhibition of the mRNAs into their proteins. Therefore, miRNAs are able to affect the protein profile of a cell. In this study, we investigated the role of miR-181a in HCC. MiR-181a has been shown to be upregulated in HCC and HpSC-HCC, and found to be involved in cellular differentiation. Its role in cancer, however, has yet to be investigated upon. In the first part of this project, we aim to elucidate the overall effects miR-181a exerts in HepG2 cells. Particularly, we made use of LC-MS/MS technology in identifying and quantifying proteins dysregulated when miR-181a was overexpressed or inhibited in HepG2 cells. We chose to study the protein profile because proteins are known to be the 'molecular machines' of cells, and cellular phenotype, whether diseased or healthy, is largely due to the cellular protein expression levels. From the LC-MS/MS analysis, we found that the overexpression of miR-181a in HepG2 cells led to a significant increase in NPM1 protein, while its inhibition lowered the expression levels of Hsp-90β protein. NPM1 is found in many human cancers including those of the stomach, prostate,

colon, bladder, and liver. NPM1 overexpression in tumour cells was also found to lead to an increased proliferation and inhibition of apoptosis. Inhibiting miR-181a, on the other hand, led to a decrease in Hsp-90β, a chaperone usually highly expressed by cancer cells to help protect and ensure proper folding and functioning of its proteins. The decrease in Hsp-90β due to the inhibition of miR-181a may lead to a reduction in protection of cancer cells. These initial results from the protein profile analysis of HepG2 cells may suggest that miR-181a acts as an oncogene while its inhibition could produce tumour suppressing effects. The expression levels of these two proteins in HepG2 cells transfected with miR-181a and its inhibitor were subsequently validated with a Western blot analysis, and are in line with the results obtained from the LC-MS/MS.

Based on results from the protein profile analysis, we infer that miR-181a may have effects in important cancer-related pathways like cell growth. A cell viability assay shows that miR-181a causes a significant increase in HepG2 cell viability while inhibiting it significantly reduces viability by about 20%. As cell cycle is closely related to cell viability, we also employed flow cytometry to study if cell cycle is affected by miR-181a. While miR-181a itself did not cause a significant change in cell cycle, inhibiting it caused a significant decrease in proportion of cells in the S phase, while at the same time, increasing the proportion of cells in the G1 phase. Inhibiting miR-181a, therefore, may reduce HepG2 cell viability by delaying cell cycle entry. From these studies, our results suggest that miR-181a causes an increase in cell viability, possibly through exerting some effect in the cell cycle as one of the mechanisms and the upregulation of proliferative proteins as another.

We next delved into the molecular level and investigated the direct mRNA targets of miR-181a. Because there can be many potential targets, we made use of bioinformatics to aid in target prediction. Among the targets predicted, CDKN1β and E2F7 were chosen for further study because they are both important cell cycle genes, and as shown in our earlier study, miR-181a may have an effect on the cell cycle. We first tested out the miRNA:mRNA interactions *in vitro* using SPR technology. The predicted binding sites in the 3'UTRs of the mRNAs were synthesized and localized onto the SPR platform while miR-181a was injected as the flow through. SPR results show a positive binding between miR-181a and the 3'UTRs of both CDKN1β and E2F7, with a higher affinity and stronger binding between miR-181a and the 3'UTR of CDKN1β (lower dissociation constant). After a positive validation of interaction *in vitro*, we proceeded to test for any binding *in vivo* via luciferase assay. The 3'UTRs of both CDKN1β and E2F7 were cloned into a duo-luciferase reporter plasmid and co-transfected along with miR-181a into HepG2 cells. A significantly lower luciferase activity was detected in both reporter plasmids as compared to the control plasmid, suggesting a positive binding of miR-181a to the 3'UTRs of both CDKN1β and E2F7 *in vivo*. *In vivo*, however, it seems that the binding between miR-181a and E2F7 is stronger than with CDKN1β, because of the lower luciferase activity detected. It could be due to the various enzymes and molecular machinery present in the cells, as well as the more extensive sequence complementarity that favour the binding of miR-181a to the 3'UTR of E2F7. The positive interaction between miR-181a and the 3'UTRs of both mRNAs led us to further study whether the binding may cause a decrease in their respective protein expressions. A Western blot study showed that the protein levels of CDKN1β and E2F7 were lowered, with E2F7 expressed at a much lower level than the

control sample as compared to CDKN1β, when HepG2 cells were transfected with miR-181a. This supports the notion that the binding between miR-181a and E2F7 may have been stronger than that of miR-181a and CDKN1β.

We next investigated the effects miR-181a has on important transcription factors involved in cancer-related pathways, because ultimately, we are interested to get an overview of the effects of miR-181a in cancer. The transcription factors included in the study may not be direct targets of the miRNA. Using a microarray analysis, we studied ten different cancer pathways and their transcription factors. What was interesting in our findings is that the SMAD, MAPK and NFκB signalling pathways were found to be activated, with a significant activation in the MAPK/JNK pathway when HepG2 cells were transfected with miR-181a. The significant activation of AP-1 transcription factor in the MAPK/JNK pathway positively regulates the cell cycle and antagonizes apoptosis in liver tumours, possibly leading to an increase in cancer cell viability in the process. Inhibiting miR-181a, on the other hand, overall activates most tumour suppressing pathways and inactivates tumour-promoting ones. Hypoxia was found to be significantly reduced while SMAD was significantly activated. Contradicting pathways were still activated though, with the increase in activity of the NFκB pathway. Overall, it is the balance of effects of these pathways that leads to the phenotype of the cell.

Lastly, we also employed a microarray analysis to study the possible direct targets of miR-181a. This differs from the previous methods because of its much higher throughput. However, one should note that, because miRNAs are generally known to affect gene expression at the translational level, the use of this array would only be useful for miRNA targeting via mRNA degradation. However, we also know that miRNAs exert their effect

not just through their direct targets but also indirectly on other genes-- not a surprise due to the interconnectedness of the components of a cell. Therefore, the microarray analysis was carried out as an overall gene expression analysis, instead of focusing on downregulation of target mRNAs. Among 84 genes probed, two particular genes garnered interest. A significant increase in BMPR2 mRNA expression was seen in HepG2 cells transfected with miR-181a. The gene product is a receptor that mediates the SMAD, MAPK and NFκB signalling pathways, which are important pathways in cancer. Incidentally, these pathways were seen to be activated when HepG2 cells were transfected with miR-181a (as shown in the previous microarray analysis on cancer-pathways). MAPK and NFκB are activated in most cancers, while the activation of SMAD pathway has an opposing tumour suppressing effect. The balance of these activated pathways may have led to an overall increase in cell viability of HepG2 cells when transfected with miR-181a. Inhibiting miR-181a, however, significantly increased the gene expression of GATA6. GATA6 is involved in aiding cellular differentiation, and the reduced expression of this gene encourages 'stemness', allowing cells to proliferate indefinitely. Inhibiting miR-181a has been shown to reduce cell viability, and one such mechanism may be due to the increase in GATA6, which decreases the chances of forming cancer stem cells in HCC.

In conclusion, we find that miR-181a has an overall oncogenetic effect in HepG2 cells. It increases HepG2 cell viability, possibly through the activation of a myriad of cancer-causing pathways (ie. MAPK/JNK). It also significantly increases gene expression of BMPR2 that mediates the activation of these pathways. Not only that, but it is found to bind to and downregulate CDKN1β and E2F7 mRNAs and proteins respectively, which both play a part in the negative regulation of the cell cycle. Inhibiting miR-181a, on the

other hand, reduces HepG2 cell viability, possibly by activating tumour suppressing networks (ie. SMAD) and deactivating tumour causing pathways (ie. HIF). It also causes a significant delay in cell cycle progression, perhaps by the slight reduction of activity of E2F proteins. It decreases the expression of Hsp-90β protein, reducing the inherent protection of HepG2 cells. The 20% decrease in viability measured may have been limited though, due to the simultaneous activation of tumour-causing pathways like NFκB. Direct targeting of this pathway using siRNAs, along with the inhibition of miR-181a, could potentially increase its therapeutic effect in HCC. A suggested role of miR-181a in HepG2 cells is illustrated in Figure 30.

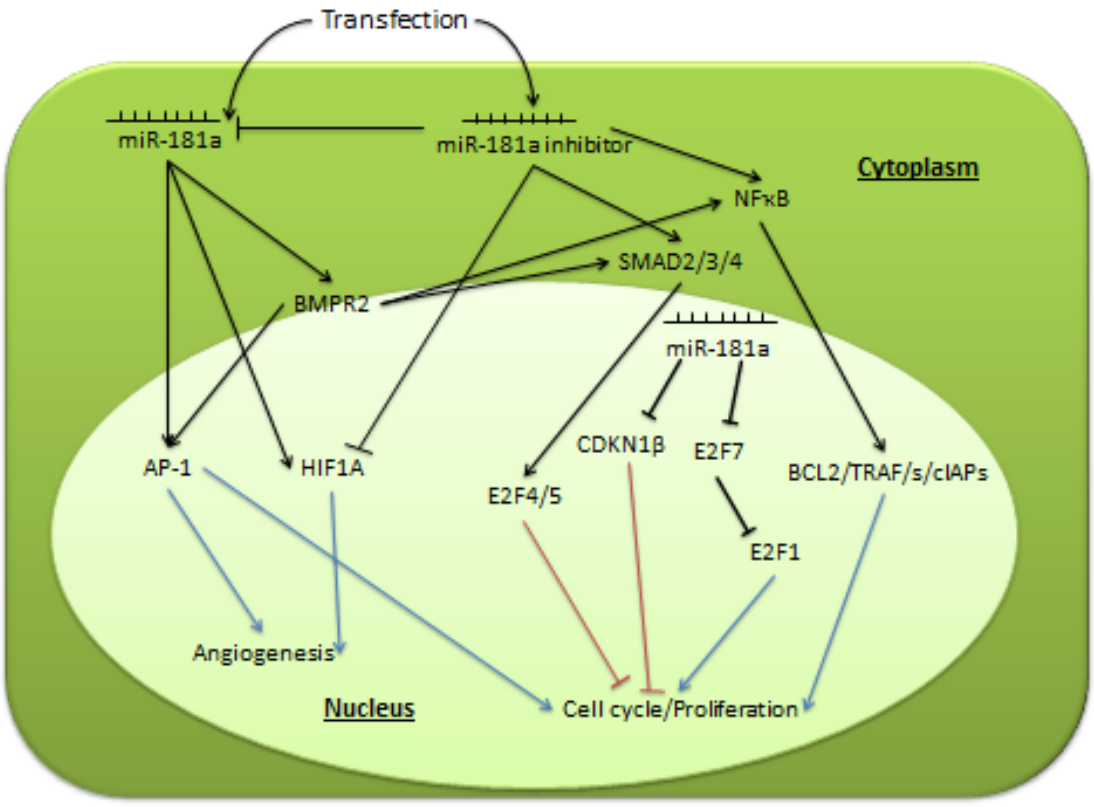

Figure 32. Illustration of suggested pathways affected by miR-181a in HepG2 cells. Overall, miR-181a activates many proteins and pathways involved in cell cycle/proliferation and angiogenesis, which are crucial pathways also activated in most cancers. Inhibiting this miRNA abolishes this and even may inhibit these cancer-promoting pathways from progression.

8. Future Work

Our data has shown that inhibiting miR-181a in HepG2 cells produces a therapeutic effect, albeit limited. We have also elucidated certain important proteins and pathways activated by inhibiting miR-181a, mostly tumour suppressing but a few other contradicting oncogenetic pathways. Because we are interested in HCC therapy, the use of miR-181a inhibitor with siRNAs may be a viable method in causing a further decrease in cancer cell viability. The problem with cancers is that many proteins and pathways tend to be dysregulated simultaneously, such that the use of siRNAs alone that target specific pathways does not cause total eradication of the cancer. MiRNAs, therefore, serve as a good vehicle for targeting multiple pathways at the same time. However, its main setback is the non-specificity of its targeting, as seen in our project, such that it is able to cause activation in both tumour cell growth and apoptosis pathways. A balance of both the use of miRNAs and siRNAs, could therefore aid in targeting multiple pathways yet prevent the activation of unwanted, tumour-promoting pathways. A co-transfection of miR-181a inhibitor with NFκB siRNA into HepG2 cells may be one area of study that could potentially lead to a further decrease of cancer viability.

As in the case of siRNAs that causes a knock down in gene expression, small activating RNAs (saRNAs) cause an increase in gene transcription. This may be used along with miR-181a inhibitor in now activating genes that are tumour suppressing. Genes like p53, which are slightly upregulated due to miR-181a inhibition, may be further upregulated when co-transfected with the saRNA for p53.

Other than the use of miRNAs with siRNAs or saRNAs, many different combinations of therapy could be used to further improve on the results. MiRNAs with drugs, as shown in our study, may cause an additive decrease in cancer cell viability, proving that miRNAs may be used in tandem with chemotherapy to produce an enhanced therapeutic effect. This may mean that the dosage of drugs used in treatment need not be as high as before, therefore minimizing unwanted harmful side effects in patients. Of course, the side effects caused by miRNAs would have to be investigated upon prior to that. MiRNAs are endogenous molecules by nature, therefore their use in patient therapies are likely to be better received than the use of chemicals or radiotherapy.

Other miRNAs may also be used in HCC therapy, or used alongside miR-181a inhibitor. However, because a single miRNA alone is able to cause a massive change in cellular profile, the combination of miRNAs may complicate the cellular network such that there are too many variables changing at the same time. That saying, a combination of miRNAs in therapy may theoretically work; however the study of underlying mechanisms may not be as simple as the other methods proposed earlier.

Apart from the use of miR-181a inhibitor on HepG2 cells, it may also be used to study other liver cancer cell lines like Hep3B, HuH7 or even HepG2.215. Because HCC is a cancer of heterogeneous background, the use of miR-181a inhibitor in HepG2 cells may cause a different effect in other cell lines and/or *in vivo* in human patients. Hence, a more thorough investigation is required to obtain a broader picture of the function of miR-181a inhibitor in HCC.

In these potential studies, the use of the LC-MS/MS may be very useful in investigating the proteins profile due to treatment. Not only can this technology be used in miRNA studies, it may also be used in studying cancer cells treated with drugs, radiation, siRNAs, or a combination of these. Through the use of the LC-MS/MS, we are able to gain an understanding of important proteins perturbed by these treatments. Further improvements can then be made upon the investigations once the molecular mechanisms are elucidated, and this cycle of testing and understanding is repeated until an optimal treatment method is developed.

9. References

[1] D.M. Parkin, F. Bray, J. Ferlay, P. Pisani, Estimating the world cancer burden: GLOBOCAN 2000, Int. J. Cancer, 94 (2001) 153-156.

[2] M.B. Thomas, A.X. Zhu, Hepatocellular Carcinoma: The Need for Progress, J Clin Oncol, 23 (2005) 2892-2899.

[3] A.X. Zhu, Systemic Therapy of Advanced Hepatocellular Carcinoma: How Hopeful Should We Be?, Oncologist, 11 (2006) 790-800.

[4] A. Kato, M. Miyazaki, S. Ambiru, H. Yoshitomi, H. Ito, K. Nakagawa, H. Shimizu, O. Yokosuka, N. Nakajima, Multidrug resistance gene (MDR-1) expression as a useful prognostic factor in patients with human hepatocellular carcinoma after surgical resection, Journal of Surgical Oncology, 78 (2001) 110-115.

[5] G. Egger, L. Gangning, A. Aparicio, P.A. Jones, Epigenetics in human disease and prospects for epigenetic therapy, Nature, 429 (2004) 457.

[6] C.M. Croce, Oncogenes and Cancer, N Engl J Med, 358 (2008) 502-511.

[7] F. Bonvicini, C. Filippone, E. Manaresi, M. Zerbini, M. Musiani, G. Gallinella, HepG2 hepatocellular carcinoma cells are a non-permissive system for B19 virus infection, Journal of General Virology, 89 (2008) 3034-3038.

[8] J. Campbell, S. Hughes, D. Gilbertson, T. Palmer, M. Holdren, A. Haran, M. Odell, R. Bauer, H.-P. Ren, H. Haugen, M. Yeh, N. Fausto, Platelet-derived growth factor C induces liver fibrosis, steatosis, and hepatocellular carcinoma, Proceedings of the National Academy of Sciences of the United States of America, 102 (2005) 3389.

[9] S. Singh, M. Bhadra, H. Girschick, U. Bhadra, MicroRNAs--micro in size but macro in function, The FEBS journal, 275 (2008) 4929-4944.

[10] A. Rodriguez, S. Griffiths-Jones, J. Ashurst, A. Bradley, Identification of mammalian microRNA host genes and transcription units, Genome research, 14 (2004) 1902-1910.

[11] H. Robins, Y. Li, R. Padgett, Incorporating structure to predict microRNA targets, Proceedings of the National Academy of Sciences of the United States of America, 102 (2005) 4006-4009.

[12] X. Cai, C. Hagedorn, B. Cullen, Human microRNAs are processed from capped, polyadenylated transcripts that can also function as mRNAs, RNA, 10 (2004) 1957-1966.

[13] A. Köhler, E. Hurt, Exporting RNA from the nucleus to the cytoplasm, Nature Reviews. Molecular Cell Biology, 8 (2007) 761-773.

[14] J. Cummins, Y. He, R. Leary, R. Pagliarini, L. Diaz, T. Sjoblom, O. Barad, Z. Bentwich, A. Szafranska, E. Labourier, C. Raymond, B. Roberts, H. Juhl, K. Kinzler, B. Vogelstein, V. Velculescu,

The colorectal microRNAome, Proceedings of the National Academy of Sciences of the United States of America, 103 (2006) 3687-3692.

[15] A. Denli, B.B.J. Tops, R.H.A. Plasterk, R. Ketting, G. Hannon, Processing of primary microRNAs by the Microprocessor complex, Nature, 432 (2004) 231-235.

[16] E. Allen, Z. Xie, A. Gustafson, G.-H. Sung, J. Spatafora, J. Carrington, Evolution of microRNA genes by inverted duplication of target gene sequences in Arabidopsis thaliana, Nature Genetics, 36 (2004) 1282-1290.

[17] Y. Lee, C. Ahn, J. Han, H. Choi, J. Kim, J. Yim, J. Lee, P. Provost, O. Rådmark, S. Kim, V.N. Kim, The nuclear RNase III Drosha initiates microRNA processing, Nature, 425 (2003) 415-419.

[18] Z. Yan, Sequence requirements for micro RNA processing and function in human cells, RNA, background.

[19] H. Seitz, P. Zamore, Rethinking the microprocessor, Cell, 125 (2006) 827-829.

[20] E. Lund, S. Güttinger, A. Calado, J. Dahlberg, U. Kutay, Nuclear export of microRNA precursors, Science, 303 (2004) 95-98.

[21] M. Bohnsack, K. Czaplinski, D. Gorlich, Exportin 5 is a RanGTP-dependent dsRNA-binding protein that mediates nuclear export of pre-miRNAs, RNA, 10 (2004) 185-191.

[22] E. Wienholds, W. Kloosterman, E. Miska, E. Alvarez-Saavedra, E. Berezikov, E. de Bruijn, H.R. Horvitz, S. Kauppinen, R.H.A. Plasterk, MicroRNA expression in zebrafish embryonic development, Science, 309 (2005) 310-311.

[23] C. Gwizdek, B. Ossareh-Nazari, A. Brownawell, A. Doglio, E. Bertrand, I. Macara, C. Dargemont, Exportin-5 mediates nuclear export of minihelix-containing RNAs, The Journal of biological chemistry, 278 (2003) 5505-5508.

[24] B. Cullen, Derivation and function of small interfering RNAs and microRNAs, Virus research, 102 (2004) 3-9.

[25] G. Tang, siRNA and miRNA: an insight into RISCs, Trends in biochemical sciences, 30 (2005) 106-114.

[26] D. Schwarz, G. Hutvágner, T. Du, Z. Xu, N. Aronin, P. Zamore, Asymmetry in the assembly of the RNAi enzyme complex, Cell, 115 (2003) 199-208.

[27] T. Sasaki, A. Shiohama, S. Minoshima, N. Shimizu, Identification of eight members of the Argonaute family in the human genome small star, filled, Genomics, 82 (2003) 323-330.

[28] L. Jidong, A.C. Michelle, V.R. Fabiola, G.M. Carolyn, M. Thomson, S. Ji-Joon, M.H. Scott, J.-T. Leemor, Argonaute2 Is the Catalytic Engine of Mammalian RNAi, Science, 305 (2004) 1437-1441.

[29] G. Meister, M. Landthaler, A. Patkaniowska, Y. Dorsett, G. Teng, T. Tuschl, Human Argonaute2 mediates RNA cleavage targeted by miRNAs and siRNAs, Molecular cell, 15 (2004) 185-197.

[30] S. Yekta, I.H. Shih, D. Bartel, MicroRNA-directed cleavage of HOXB8 mRNA, Science, 304 (2004) 594-596.

[31] W. Filipowicz, S. Bhattacharyya, N. Sonenberg, Mechanisms of post-transcriptional regulation by microRNAs: are the answers in sight?, Nature Reviews. Genetics, 9 (2008) 102-114.

[32] M. Kiriakidou, G. Tan, S. Lamprinaki, M. De Planell-Saguer, P. Nelson, Z. Mourelatos, An mRNA m7G cap binding-like motif within human Ago2 represses translation, Cell, 129 (2007) 1141-1151.

[33] R. Pillai, S. Bhattacharyya, C. Artus, T. Zoller, N. Cougot, E. Basyuk, E. Bertrand, W. Filipowicz, Inhibition of translational initiation by Let-7 MicroRNA in human cells, Science, 309 (2005) 1573-1576.

[34] R. Pillai, S. Bhattacharyya, W. Filipowicz, Repression of protein synthesis by miRNAs: how many mechanisms?, Trends in cell biology, 17 (2007) 118-126.

[35] C. Petersen, M.-E. Bordeleau, J. Pelletier, P. Sharp, Short RNAs repress translation after initiation in mammalian cells, Molecular cell, 21 (2006) 533-542.

[36] D. Humphreys, B. Westman, D.I.K. Martin, T. Preiss, MicroRNAs control translation initiation by inhibiting eukaryotic initiation factor 4E/cap and poly(A) tail function, Proceedings of the National Academy of Sciences of the United States of America, 102 (2005) 16961-16966.

[37] L. Wu, J. Fan, J. Belasco, MicroRNAs direct rapid deadenylation of mRNA, Proceedings of the National Academy of Sciences of the United States of America, 103 (2006) 4034-4039.

[38] D. Teixeira, U. Sheth, M. Valencia-Sanchez, M. Brengues, R. Parker, Processing bodies require RNA for assembly and contain nontranslating mRNAs, RNA, 11 (2005) 371-382.

[39] D. Ingelfinger, D. Arndt-Jovin, R. Lührmann, T. Achsel, The human LSm1-7 proteins colocalize with the mRNA-degrading enzymes Dcp1/2 and Xrnl in distinct cytoplasmic foci, RNA, 8 (2002) 1489-1501.

[40] M. Kshirsagar, R. Parker, Identification of Edc3p as an enhancer of mRNA decapping in Saccharomyces cerevisiae, Genetics, 166 (2004) 729-739.

[41] N. Cougot, S. Babajko, B. Séraphin, Cytoplasmic foci are sites of mRNA decay in human cells, The journal of cell biology, 165 (2004) 31-40.

[42] C.J. Decker, R. Parker, A turnover pathway for both stable and unstable mRNAs in yeast: evidence for a requirement for deadenylation, Genes & development, 7 (1993) 1632-1643.

[43] D. Muhlrad, R. Parker, Premature translational termination triggers mRNA decapping, Nature, 370 (1994) 578-581.

[44] J. Liu, M. Valencia-Sanchez, G. Hannon, R. Parker, MicroRNA-dependent localization of targeted mRNAs to mammalian P-bodies, Nature Cell Biology, 7 (2005) 719-723.

[45] R.W. Carthew, E.J. Sontheimer, Origins and Mechanisms of miRNAs and siRNAs, Cell, 136 (2009) 642-655.

[46] D.P. Bartel, MicroRNAs: Genomics, Biogenesis, Mechanism, and Function, Cell, 116 (2004) 281-297.

[47] S. Griffiths-Jones, H.K. Saini, S. van Dongen, A.J. Enright, miRBase: tools for microRNA genomics, Nucl. Acids Res., 36 (2008) D154-158.

[48] P. Zamore, B. Haley, Ribo-gnome: the big world of small RNAs, Science, 309 (2005) 1519-1524.

[49] R. Backofen, S. Bernhart, C. Flamm, C. Fried, G. Fritzsch, J. Hackermüller, J. Hertel, I. Hofacker, K. Missal, A. Mosig, S. Prohaska, D. Rose, P. Stadler, A. Tanzer, S. Washietl, S. Will, RNAs everywhere: genome-wide annotation of structured RNAs, Journal of experimental zoology. part B, molecular and developmental evolution, 308 (2007) 1-25.

[50] W. Leor, C.C. Cristel, S.O. Karen, J. and, A database analysis method identifies an endogenous trans-acting short-interfering RNA that targets the Arabidopsis ARF2, ARF3, and ARF4 genes, Proceedings of the National Academy of Sciences of the United States of America, 102 (2005) 9703-9708.

[51] M. Kato, F. Slack, microRNAs: small molecules with big roles - C. elegans to human cancer, Biology of the cell, 100 (2008) 71-81.

[52] K. Ruan, X. Fang, G. Ouyang, MicroRNAs: novel regulators in the hallmarks of human cancer, Cancer Letters, 285 (2009) 116-126.

[53] V. Wang, W. Wu, MicroRNA-based therapeutics for cancer, BioDrugs, 23 (2009) 15-23.

[54] X. He, L. He, G. Hannon, The guardian's little helper: microRNAs in the p53 tumor suppressor network, Cancer research, 67 (2007) 11099-11101.

[55] G. Calin, C. Croce, MicroRNA signatures in human cancers, Nature Reviews. Cancer, 6 (2006) 857-866.

[56] C. Caldas, J. Brenton, Sizing up miRNAs as cancer genes, Nature Medicine, 11 (2005) 712-714.

[57] H.W. Hwang, J.T. Mendell, MicroRNAs in cell proliferation, cell death, and tumorigenesis, The British Journal of Cancer, 94 (2006) 776-780.

[58] J. Lu, G. Getz, E. Miska, E. Alvarez-Saavedra, J. Lamb, D. Peck, A. Sweet-Cordero, B. Ebert, R. Mak, A. Ferrando, J. Downing, T. Jacks, H.R. Horvitz, T. Golub, MicroRNA expression profiles classify human cancers, Nature, 435 (2005) 834-838.

[59] Y. Murakami, T. Yasuda, K. Saigo, T. Urashima, H. Toyoda, T. Okanoue, K. Shimotohno, Comprehensive analysis of microRNA expression patterns in hepatocellular carcinoma and non-tumorous tissues, Oncogene, 25 (2006) 2537-2545.

[60] S. Roessler, A. Budhu, X. Wang, Future of molecular profiling of human hepatocellular carcinoma, Future Oncology, 3 (2007) 429-439.

[61] J. Takamizawa, H. Konishi, K. Yanagisawa, S. Tomida, H. Osada, H. Endoh, T. Harano, Y. Yatabe, M. Nagino, Y. Nimura, T. Mitsudomi, T. Takahashi, Reduced expression of the let-7 microRNAs in human lung cancers in association with shortened postoperative survival, Cancer research, 64 (2004) 3753.

[62] J. Weidhaas, I. Babar, S. Nallur, P. Trang, S. Roush, M. Boehm, E. Gillespie, F. Slack, MicroRNAs as potential agents to alter resistance to cytotoxic anticancer therapy, Cancer research, 67 (2007) 11111.

[63] C. Johnson, A. Esquela-Kerscher, G. Stefani, M. Byrom, K. Kelnar, D. Ovcharenko, M. Wilson, X. Wang, J. Shelton, J. Shingara, L. Chin, D. Brown, F. Slack, The let-7 microRNA represses cell proliferation pathways in human cells, Cancer research, 67 (2007) 7713.

[64] J.H. Hoofnagle, E. Doo, T.J. Liang, R. Fleischer, A.S. Lok, Management of hepatitis B: summary of a clinical research workshop, Hepatology, 45 (2007) 1056-1075.

[65] S. Hammond, MicroRNA therapeutics: a new niche for antisense nucleic acids, Trends in molecular medicine, 12 (2006) 99.

[66] C. Wahlestedt, P. Salmi, L. Good, J. Kela, T. Johnsson, T. Hökfelt, C. Broberger, F. Porreca, J. Lai, K. Ren, M. Ossipov, A. Koshkin, N. Jakobsen, J. Skouv, H. Oerum, M.H. Jacobsen, J. Wengel, Potent and nontoxic antisense oligonucleotides containing locked nucleic acids, Proceedings of the National Academy of Sciences of the United States of America, 97 (2000) 5633.

[67] J. Chan, A. Krichevsky, K. Kosik, MicroRNA-21 is an antiapoptotic factor in human glioblastoma cells, Cancer research, 65 (2005) 6029.

[68] M.L. Si, S. Zhu, H. Wu, Z. Lu, F. Wu, Y.Y. Mo, miR-21-mediated tumor growth, Oncogene, 26 (2007) 2799.

[69] S. Zhu, H. Wu, F. Wu, D. Nie, S. Sheng, Y.-Y. Mo, MicroRNA-21 targets tumor suppressor genes in invasion and metastasis, Cell research, 18 (2008) 350.

[70] I.A. Asangani, S.A.K. Rasheed, D.A. Nikolova, J.H. Leupold, N.H. Colburn, S. Post, H. Allgayer, MicroRNA-21 (miR-21) post-transcriptionally downregulates tumor suppressor Pdcd4 and stimulates invasion, intravasation and metastasis in colorectal cancer, Oncogene, 27 (2008) 2128.

[71] G. Gabriely, T. Wurdinger, S. Kesari, C. Esau, J. Burchard, P. Linsley, A. Krichevsky, MicroRNA 21 promotes glioma invasion by targeting matrix metalloproteinase regulators, Molecular and cellular biology, 28 (2008) 5369.

[72] S. Thorgeirsson, J. Grisham, Molecular pathogenesis of human hepatocellular carcinoma, Nature Genetics, 31 (2002) 339.

[73] J. Jiang, Y. Gusev, I. Aderca, T. Mettler, D. Nagorney, D. Brackett, L. Roberts, T. Schmittgen, Association of MicroRNA expression in hepatocellular carcinomas with hepatitis infection, cirrhosis, and patient survival, Clinical cancer research, 14 (2008) 419.

[74] H. Varnholt, U. Drebber, F. Schulze, I. Wedemeyer, P. Schirmacher, H.-P. Dienes, M. Odenthal, MicroRNA gene expression profile of hepatitis C virus-associated hepatocellular carcinoma, Hepatology, 47 (2008) 1223.

[75] M. Michael, S. O'Connor, N.G. van Holst Pellekaan, G. Young, R. James, Reduced accumulation of specific microRNAs in colorectal neoplasia, Molecular cancer research, 1 (2003) 882.

[76] H. He, K. Jazdzewski, W. Li, S. Liyanarachchi, R. Nagy, S. Volinia, G. Calin, C.-G. Liu, K. Franssila, S. Suster, R. Kloos, C. Croce, A. de la Chapelle, The role of microRNA genes in papillary thyroid carcinoma, Proceedings of the National Academy of Sciences of the United States of America, 102 (2005) 19075.

[77] H. Varnholt, The role of microRNAs in primary liver cancer, Annals of hepatology, 7 104-113.

[78] J. Ji, T. Yamashita, A. Budhu, M. Forgues, H.-L. Jia, C. Li, C. Deng, E. Wauthier, L.M. Reid, Q.-H. Ye, L.-X. Qin, W. Yang, H.-Y. Wang, Z.-Y. Tang, C.M. Croce, X.W. Wang, Identification of microRNA-181 by genome-wide screening as a critical player in EpCAM–positive hepatic cancer stem cells, Hepatology, 50 (2009) 472-480.

[79] P. Polakis, Wnt signaling and cancer, Genes & development, 14 (2000) 1837-1851.

[80] J. Fei, Y. Li, X. Zhu, X. Luo, miR-181a Post-Transcriptionally Downregulates Oncogenic RalA and Contributes to Growth Inhibition and Apoptosis in Chronic Myelogenous Leukemia (CML), PloS one, 7 (2012) e32834.

[81] J.J. Pitt, Principles and applications of liquid chromatography-mass spectrometry in clinical biochemistry, The Clinical biochemist. Reviews / Australian Association of Clinical Biochemists, 30 (2009) 19-34.

[82] I.V. Chernushevich, A.V. Loboda, B.A. Thomson, An introduction to quadrupole–time-of-flight mass spectrometry, Journal of Mass Spectrometry, 36 (2001) 849-865.

[83] D. Chang, S.J. Kolis, K.H. Linderholm, T.F. Julian, R. Nachi, A.M. Dzerk, P.P. Lin, J.W. Lee, S.K. Bansal, Bioanalytical method development and validation for a large peptide HIV fusion inhibitor (Enfuvirtide, T-20) and its metabolite in human plasma using LC-MS/MS, J Pharm Biomed Anal, 38 (2005) 487-496.

[84] C.C. Lin, J.Y. Lau, Specific, sensitive and accurate LC-MS/MS method for the measurement of levovirin in rat and monkey plasma, J Pharm Biomed Anal, 30 (2002) 239-246.

[85] H. Feng, X. Li, D. Niu, W.N. Chen, Protein profile in HBx transfected cells: A comparative iTRAQ-coupled 2D LC-MS/MS analysis, Journal of Proteomics, In Press, Corrected Proof.

[86] H. Feng, M. Wang, W. Chen, iTRAQ-Coupled 2D LC–MS/MS Analysis of Secreted Proteome of HBV-Replicating HepG2 Cells: Potential in Biomarkers for Prognosis of HCC, Current Microbiology.

[87] J. Zhang, D. Niu, J. Sui, C. Ching, W. Chen, Protein profile in hepatitis B virus replicating rat primary hepatocytes and HepG2 cells by iTRAQ-coupled 2-D LC-MS/MS analysis: Insights on liver angiogenesis, Proteomics, 9 (2009) 2836.

[88] F. Sadeghian-Nodoushan, P. Eftekhari-Yazdi, A. Dalman, H. Eimani, H. Sepehri, Mimosine As Well As Serum Starvation Can Be Used for Cell Cycle Synchronization of Sheep Granulosa Cells, Chinese Journal of Biology, 2014 (2014) 7.

[89] Serum starvation: caveat emptor, 2011.

[90] X. Feng, J. Zhang, W.N. Chen, C.B. Ching, Proteome profiling of Epstein–Barr virus infected nasopharyngeal carcinoma cell line: Identification of potential biomarkers by comparative iTRAQ-coupled 2D LC/MS-MS analysis, Journal of Proteomics, 74 (2011) 567-576.

[91] I.M.A. Abdulhalim, Surface Plasmon Resonance for Biosensing: A Mini-Review, Electromagnetics, 28 (2008) 214-242.

[92] M.A. Cooper, Optical biosensors in drug discovery, Nature reviews. Drug discovery, 1 (2002) 515-528.

[93] D.G. Myszka, Improving biosensor analysis, Journal of Molecular Recognition, 12 (1999) 279-284.

[94] Y. Lin Jane Tan, N. A. Habib, W. Ning Chen, A Quantitative Proteomics Approach in the Study of MicroRNA 181a in HepG2 Cells, Current Proteomics, 9 (2012) 262-271.

[95] M. Chen, J. Huang, X. Yang, B. Liu, W. Zhang, L. Huang, F. Deng, J. Ma, Y. Bai, R. Lu, B. Huang, Q. Gao, Y. Zhuo, J. Ge, Serum starvation induced cell cycle synchronization facilitates human somatic cells reprogramming, PloS one, 7 (2012) e28203.

[96] J.C. Ghosh, T. Dohi, B.H. Kang, D.C. Altieri, Hsp60 Regulation of Tumor Cell Apoptosis, Journal of Biological Chemistry, 283 (2008) 5188-5194.

[97] P. Moseley, Stress proteins and the immune response, Immunopharmacology, 48 (2000) 299-302.

[98] D.R. Ciocca, S.K. Calderwood, Heat shock proteins in cancer: diagnostic, prognostic, predictive, and treatment implications, Cell stress & chaperones, 10 (2005) 86-103.

[99] L. Neckers, Heat shock protein 90: the cancer chaperone, J Biosci, 32 (2007) 517-530.

[100] Y. Liu, F. Zhang, X.F. Zhang, L.S. Qi, L. Yang, H. Guo, N. Zhang, Expression of nucleophosmin/NPM1 correlates with migration and invasiveness of colon cancer cells, Journal of biomedical science, 19 (2012) 53.

[101] J.P. Yun, J. Miao, G.G. Chen, Q.H. Tian, C.Q. Zhang, J. Xiang, J. Fu, P.B.S. Lai, Increased expression of nucleophosmin//B23 in hepatocellular carcinoma and correlation with clinicopathological parameters, Br J Cancer, 96 (2007) 477-484.

[102] H. Yang, Y. Zhang, R. Zhao, Y.Y. Wen, K. Fournier, H.B. Wu, H.Y. Yang, J. Diaz, C. Laronga, M.H. Lee, Negative cell cycle regulator 14-3-3[sigma] stabilizes p27 Kip1 by inhibiting the activity of PKB//Akt, Oncogene, 25 (2006) 4585-4594.

[103] H.-Y. Yang, Y.-Y. Wen, C.-H. Chen, G. Lozano, M.-H. Lee, 14-3-3σ Positively Regulates p53 and Suppresses Tumor Growth, Molecular and cellular biology, 23 (2003) 7096-7107.

[104] a. Norikazu Iwata1, Hiroyuki Yamamoto1,a, Shigeru Sasaki1, Fumio Itoh1, Hiromu Suzuki1, Takefumi Kikuchi1, Hiroyuki Kaneto1, Shouhei Iku1, Itaru Ozeki1, Yoshiyasu Karino2, Toshihiro Satoh3, Joji Toyota2, Masaaki Satoh4, Takao Endo1 and Kohzoh Imai1, Frequent hypermethylation of CpG islands and loss of expression of the 14-3-3 gene in human hepatocellular carcinoma, Oncogene, 19 (2000) 5298-5302.

[105] C. Laronga, H.-Y. Yang, C. Neal, M.-H. Lee, Association of the Cyclin-dependent Kinases and 14-3-3 Sigma Negatively Regulates Cell Cycle Progression, Journal of Biological Chemistry, 275 (2000) 23106-23112.

[106] Z.H. Siddik, Cisplatin: mode of cytotoxic action and molecular basis of resistance, Oncogene, 22 (0000) 7265-7279.

[107] M. Zuker, Mfold web server for nucleic acid folding and hybridization prediction, Nucleic Acids Research, 31 (2003) 3406-3415.

[108] L.A. Macfarlane, P.R. Murphy, MicroRNA: Biogenesis, Function and Role in Cancer, Current genomics, 11 (2010) 537-561.

[109] O. Coqueret, New roles for p21 and p27 cell-cycle inhibitors: a function for each cell compartment?, Trends in cell biology, 13 (2003) 65-70.

[110] A. de Bruin, B. Maiti, L. Jakoi, C. Timmers, R. Buerki, G. Leone, Identification and Characterization of E2F7, a Novel Mammalian E2F Family Member Capable of Blocking Cellular Proliferation, Journal of Biological Chemistry, 278 (2003) 42041-42049.

[111] M. Karin, Z. Liu, E. Zandi, AP-1 function and regulation, Current opinion in cell biology, 9 (1997) 240-246.

[112] M.P. de Caestecker, E. Piek, A.B. Roberts, Role of Transforming Growth Factor-β Signaling in Cancer, Journal of the National Cancer Institute, 92 (2000) 1388-1402.

[113] C. Lobry, P. Oh, I. Aifantis, Oncogenic and tumor suppressor functions of Notch in cancer: it's NOTCH what you think, The Journal of Experimental Medicine, 208 (2011) 1931-1935.

[114] Q. Ke, M. Costa, Hypoxia-Inducible Factor-1 (HIF-1), Molecular Pharmacology, 70 (2006) 1469-1480.

[115] M. Karin, Y. Cao, F.R. Greten, Z.W. Li, NF-kappaB in cancer: from innocent bystander to major culprit, Nature reviews. Cancer, 2 (2002) 301-310.

[116] J. West, Cross talk between Smad, MAPK, and actin in the etiology of pulmonary arterial hypertension, Advances in experimental medicine and biology, 661 (2010) 265-278.

[117] K.G. Leong, X. Hu, L. Li, M. Noseda, B. Larrivee, C. Hull, L. Hood, F. Wong, A. Karsan, Activated Notch4 inhibits angiogenesis: role of beta 1-integrin activation, Molecular and cellular biology, 22 (2002) 2830-2841.

[118] L. Gramantieri, C. Giovannini, A. Lanzi, P. Chieco, M. Ravaioli, A. Venturi, G.L. Grazi, L. Bolondi, Aberrant Notch3 and Notch4 expression in human hepatocellular carcinoma, Liver international : official journal of the International Association for the Study of the Liver, 27 (2007) 997-1007.

[119] S. Huang, S. Wu, J. Ding, J. Lin, L. Wei, J. Gu, X. He, MicroRNA-181a modulates gene expression of zinc finger family members by directly targeting their coding regions, Nucleic Acids Res, 38 (2010) 7211-7218.

10. Appendix

Gene Table for miR-181a Target Array Analysis

Gene Table					
Position	Unigene	GeneBank	Symbol	Description	Gene Name
A01	Hs.470174	NM_001616	ACVR2A	Activin A receptor, type IIA	ACTRII, ACVR2
A02	Hs.474018	NM_001112	ADARB1	Adenosine deaminase, RNA-specific, B1	ADAR2, DRABA2, DRADA2, RED1
A03	Hs.192215	NM_021116	ADCY1	Adenylate cyclase 1 (brain)	AC1
A04	Hs.149342	NM_020661	AICDA	Activation-induced cytidine deaminase	AID, ARP2, CDA2, HIGM2
A05	Hs.486063	NM_004849	ATG5	ATG5 autophagy related 5 homolog (S. cerevisiae)	APG5, APG5-LIKE, APG5L, ASP, hAPG5
A06	Hs.367437	NM_000051	ATM	Ataxia telangiectasia mutated	AT1, ATA, ATC, ATD, ATDC, ATE, DKFZp781A0353, MGC74674, TEL1, TELO1
A07	Hs.150749	NM_000633	BCL2	B-cell CLL/lymphoma 2	Bcl-2
A08	Hs.469658	NM_006538	BCL2L11	BCL2-like 11 (apoptosis facilitator)	BAM, BIM, BIM-alpha6, BIM-beta6, BIM-beta7, BOD, BimEL, BimL
A09	Hs.502182	NM_001709	BDNF	Brain-derived neurotrophic factor	MGC34632
A10	Hs.471119	NM_001204	BMPR2	Bone morphogenetic protein receptor, type II (serine/threonine kinase)	BMPR-II, BMPR3, BMR2, BRK-3, FLJ41585, FLJ76945, PPH1, T-ALK
A11	Hs.406551	NM_001001436	C16orf87	Chromosome 16 open reading frame 87	MGC62018
A12	Hs.519930	NM_030939	C6orf62	Chromosome 6 open reading frame 62	DKFZp564G182, FLJ12619, Nbla00237, XTP12, dJ30M3.2
B01	Hs.234355	NM_023925	CAPRIN2	Caprin family member 2	C1QDC1, EEG-1, EEG1, FLJ11391, FLJ22569, KIAA1873, MGC102894, MGC134847, MGC134848, RNG140
B02	Hs.141125	NM_004346	CASP3	Caspase 3, apoptosis-related cysteine peptidase	CPP32, CPP32B, SCA-1
B03	Hs.430589	NM_170662	CBLB	Cas-Br-M (murine) ecotropic retroviral transforming sequence b	Cbl-b, DKFZp686J10223, DKFZp779A0729, DKFZp779F1443, FLJ36865, FLJ41152, RNF56
B04	Hs.356416	NM_175709	CBX7	Chromobox homolog 7	-
B05	Hs.208854	NM_001781	CD69	CD69 molecule	CLEC2C
B06	Hs.238990	NM_004064	CDKN1B	Cyclin-dependent kinase inhibitor 1B (p27, Kip1)	CDKN4, KIP1, MEN1B, MEN4, P27KIP1
B07	Hs.174249	NM_001265	CDX2	Caudal type homeobox 2	CDX-3, CDX3
B08	Hs.369614	NM_004236	COPS2	COP9 constitutive photomorphogenic homolog subunit 2 (Arabidopsis)	ALIEN, CSN2, SGN2, TRIP15
B09	Hs.198252	NM_001504	CXCR3	Chemokine (C-X-C motif) receptor 3	CD182, CD183, CKR-L2, CMKAR3, GPR9, IP10-R, Mig-R, MigR
B10	Hs.578973	NM_015247	CYLD	Cylindromatosis (turban tumor syndrome)	CDMT, CYLD1, CYLDI, EAC, FLJ20180, FLJ31664, FLJ78684, KIAA0849, MFT, MFT1, SBS, TEM, USPL2
B11	Hs.523012	NM_019058	DDIT4	DNA-damage-inducible transcript 4	Dig2, FLJ20500, REDD-1, REDD1, RP11-442H21.1, RTP801
B12	Hs.13318	NM_018662	DISC1	Disrupted in schizophrenia 1	C1orf136, FLJ13381, FLJ21640, FLJ25311, FLJ41105, KIAA0457, SCZD9
C01	Hs.654652	NM_014705	DOCK4	Dedicator of cytokinesis 4	FLJ34238, KIAA0716, MGC134911, MGC134912
C02	Hs.2128	NM_004419	DUSP5	Dual specificity phosphatase 5	DUSP, HVH3
C03	Hs.298654	NM_001946	DUSP6	Dual specificity phosphatase 6	MKP3, PYST1
C04	Hs.599481	NM_001967	EIF4A2	Eukaryotic translation initiation factor 4A2	BM-010, DDX2B, EIF4A, EIF4F, eIF-4A-II, eIF4A-II
C05	Hs.534486	NM_145010	ENKUR	Enkurin, TRPC channel interacting protein	C10orf63, DKFZp781F21103, MGC26778, enkurin
C06	Hs.504765	NM_001987	ETV6	Ets variant 6	TEL, TEL, ABL
C07	Hs.508284	NM_012158	FBXL3	F-box and leucine-rich repeat protein 3	FBL3, FBL3A, FBXL3A
C08	Hs.471933	NM_000801	FKBP1A	FK506 binding protein 1A, 12kDa	FKBP-12, FKBP1, FKBP12, PKC12,

					PKCI2, PPIASE
C09	Hs.728789	NM_005252	FOS	FBJ murine osteosarcoma viral oncogene homolog	AP-1, C-FOS
C10	Hs.175934	NM_000806	GABRA1	Gamma-aminobutyric acid (GABA) A receptor, alpha 1	ECA4, EJM, EJM5
C11	Hs.514746	NM_005257	GATA6	GATA binding protein 6	-
C12	Hs.116448	NM_014905	GLS	Glutaminase	AAD20, DKFZp686O15119, FLJ10358, GLS1, KIAA0838
D01	Hs.519693	NM_000827	GRIA1	Glutamate receptor, ionotropic, AMPA 1	GLUH1, GLUR1, GLURA, GluA1, HBGR1, MGC133252
D02	Hs.32763	NM_000826	GRIA2	Glutamate receptor, ionotropic, AMPA 2	GLUR2, GLURB, GluA2, GluR-K2, HBGR2
D03	Hs.706747	NM_000830	GRIK1	Glutamate receptor, ionotropic, kainate 1	EAA3, EEA3, GLR5, GLUR5
D04	Hs.729705	NM_022740	HIPK2	Homeodomain interacting protein kinase 2	DKFZp686K02111, FLJ23711, PRO0593
D05	Hs.406266	NM_000189	HK2	Hexokinase 2	DKFZp686M1669, HKII, HXK2
D06	Hs.434953	NM_002129	HMGB2	High mobility group box 2	HMG2
D07	Hs.643120	NM_000875	IGF1R	Insulin-like growth factor 1 receptor	CD221, IGFIR, IGFR, JTK13, MGC142170, MGC142172, MGC18216
D08	Hs.1722	NM_000575	IL1A	Interleukin 1, alpha	IL-1A, IL1, IL1-ALPHA, IL1F1
D09	Hs.306764	NM_153186	KANK1	KN motif and ankyrin repeat domains 1	ANKRD15, DKFZp451G231, KANK, KIAA0172, MGC43128
D10	Hs.533055	NM_003884	KAT2B	K(lysine) acetyltransferase 2B	CAF, P, P, CAF, PCAF
D11	Hs.592002	NM_002233	KCNA4	Potassium voltage-gated channel, shaker-related subfamily, member 4	HBK4, HK1, HPCN2, HUKII, KCNA4L, KCNA8, KV1.4, PCN2
D12	Hs.514474	NM_014738	KIAA0195	KIAA0195	DKFZp781M1056, FLJ37545, TMEM94
E01	Hs.388668	NM_007246	KLHL2	Kelch-like 2, Mayven (Drosophila)	ABP-KELCH, MAV, MAYVEN
E02	Hs.505033	NM_004985	KRAS	V-Ki-ras2 Kirsten rat sarcoma viral oncogene homolog	C-K-RAS, K-RAS2A, K-RAS2B, K-RAS4A, K-RAS4B, KI-RAS, KRAS1, KRAS2, NS, NS3, RASK2
E03	Hs.480938	NM_006726	LRBA	LPS-responsive vesicle trafficking, beach and anchor containing	BGL, CDC4L, DKFZp686A09128, DKFZp686K03100, DKFZp686P2258, FLJ16600, FLJ25686, LAB300, LBA, MGC72098
E04	Hs.335079	NM_005909	MAP1B	Microtubule-associated protein 1B	DKFZp686E1099, DKFZp686F1345, FLJ38954, FUTSCH, MAP5
E05	Hs.466743	NM_002446	MAP3K10	Mitogen-activated protein kinase kinase kinase 10	MEKK10, MLK2, MST
E06	Hs.501522	NM_002412	MGMT	O-6-methylguanine-DNA methyltransferase	-
E07	Hs.256526	NM_012336	NARF	Nuclear prelamin A recognition factor	DKFZp434G0420, FLJ10067, IOP2
E08	Hs.208759	NM_016231	NLK	Nemo-like kinase	DKFZp761G1211, FLJ21033
E09	Hs.60339	NM_004808	NMT2	N-myristoyltransferase 2	-
E10	Hs.436100	NM_004557	NOTCH4	Notch 4	FLJ16302, INT3, MGC74442, NOTCH3
E11	Hs.443837	NM_006310	NPEPPS	Aminopeptidase puromycin sensitive	AAP-S, MP100, PSA
E12	Hs.14968	NM_002655	PLAG1	Pleiomorphic adenoma gene 1	PSA, SGPA, ZNF912
F01	Hs.77274	NM_002658	PLAU	Plasminogen activator, urokinase	ATF, UPA, URK, u-PA
F02	Hs.202010	NM_015184	PLCL2	Phospholipase C-like 2	FLJ13484, KIAA1092, PLCE2
F03	Hs.155342	NM_006254	PRKCD	Protein kinase C, delta	MAY1, MGC49908, PKCD, nPKC-delta
F04	Hs.585369	NM_002763	PROX1	Prospero homeobox 1	-
F05	Hs.506852	NM_002834	PTPN11	Protein tyrosine phosphatase, non-receptor type 11	BPTP3, CFC, MGC14433, NS1, PTP-1D, PTP2C, SH-PTP2, SH-PTP3, SHP2
F06	Hs.535276	NM_012411	PTPN22	Protein tyrosine phosphatase, non-receptor type 22 (lymphoid)	LYP, LYP1, LYP2, PEP, PTPN8
F07	Hs.6906	NM_005402	RALA	V-ral simian leukemia viral oncogene homolog A (ras related)	MGC48949, RAL
F08	Hs.205627	NM_012421	RLF	Rearranged L-myc fusion	MGC142226, ZN-15L, ZNF292L
F09	Hs.591490	NM_007212	RNF2	Ring finger protein 2	BAP-1, BAP1, DING, HIPI3, RING1B, RING2
F10	Hs.369779	NM_012238	SIRT1	Sirtuin 1	SIR2L1

F11	Hs.473721	NM_006516	SLC2A1	Solute carrier family 2 (facilitated glucose transporter), member 1	DYT17, DYT18, GLUT, GLUT1, GLUT1DS, MGC141895, MGC141896, PED
F12	Hs.642990	NM_007315	STAT1	Signal transducer and activator of transcription 1, 91kDa	DKFZp686B04100, ISGF-3, STAT91
G01	Hs.410889	NM_025185	TANC2	Tetratricopeptide repeat, ankyrin repeat and coiled-coil containing 2	DKFZp564D166, FLJ10215, FLJ11824, KIAA1148, KIAA1636, ROLSA, rols
G02	Hs.486507	NM_004865	TBPL1	TBP-like 1	MGC:8389, MGC:9620, STUD, TLF, TLP, TRF2
G03	Hs.443465	NM_006706	TCERG1	Transcription elongation regulator 1	CA150, MGC133200, TAF2S, Urn1
G04	Hs.2484	NM_021966	TCL1A	T-cell leukemia/lymphoma 1A	TCL1
G05	Hs.469376	NM_015348	TMEM131	Transmembrane protein 131	CC28, KIAA0257, PRO1048, RW1, YR-23
G06	Hs.444212	NM_003385	VSNL1	Visinin-like 1	HLP3, HPCAL3, HUVISL1, VILIP, VILIP-1
G07	Hs.175955	NM_133370	YTHDC1	YTH domain containing 1	KIAA1966, YT521, YT521-B
G08	Hs.85155	NM_004926	ZFP36L1	Zinc finger protein 36, C3H type-like 1	BRF1, Berg36, ERF-1, ERF1, RNF162B, TIS11B, cMG1
G09	Hs.503093	NM_006887	ZFP36L2	Zinc finger protein 36, C3H type-like 2	BRF2, ERF-2, ERF2, RNF162C, TIS11D
G10	Hs.22305	NM_013256	ZNF180	Zinc finger protein 180	HHZ168
G11	Hs.292575	NM_001007094	ZNF37A	Zinc finger protein 37A	FLJ3472, KOX21, ZNF37
G12	Hs.467210	NM_018300	ZNF83	Zinc finger protein 83	FLJ11015, FLJ14876, FLJ30097, FLJ90585, HPF1, MGC33853, ZNF816B
H01	Hs.520640	NM_001101	ACTB	Actin, beta	PS1TP5BP1
H02	Hs.534255	NM_004048	B2M	Beta-2-microglobulin	-
H03	Hs.592355	NM_002046	GAPDH	Glyceraldehyde-3-phosphate dehydrogenase	G3PD, GAPD, MGC88685
H04	Hs.412707	NM_000194	HPRT1	Hypoxanthine phosphoribosyltransferase 1	HGPRT, HPRT
H05	Hs.546285	NM_001002	RPLP0	Ribosomal protein, large, P0	L10E, LP0, MGC111226, MGC88175, P0, PRLP0, RPP0
H06	N/A	SA_00105	HGDC	Human Genomic DNA Contamination	HIGX1A
H07	N/A	SA_00104	RTC	Reverse Transcription Control	RTC
H08	N/A	SA_00104	RTC	Reverse Transcription Control	RTC
H09	N/A	SA_00104	RTC	Reverse Transcription Control	RTC
H10	N/A	SA_00103	PPC	Positive PCR Control	PPC
H11	N/A	SA_00103	PPC	Positive PCR Control	PPC
H12	N/A	SA_00103	PPC	Positive PCR Control	PPC

Additional Data for miR-181a in Target Array Analysis

3D Profile plot values

3D Profile	A	B	C	D	E	F	G	H
1	1.19	1.26	1.57	0.10	1.09	2.94	1.23	0.71
2	1.37	0.35	1.73	0.15	1.20	0.52	0.93	1.17
3	0.71	1.59	0.53	1.93	1.26	2.29	0.69	1.28
4	5.87	1.37	1.06	0.90	1.21	0.29	0.53	0.73
5	1.23	2.85	0.99	1.18	1.62	1.04	1.26	1.28
6	1.47	1.17	1.49	1.17	2.34	0.08	28.34	
7	1.32	0.10	0.33	0.66	0.81	1.12	1.11	
8	0.91	1.03	0.77	1.20	1.21	1.13	0.67	
9	1.27	2.69	1.13	0.59	0.69	1.26	0.73	
10	1.64	1.06	3.05	0.97	1.38	1.18	1.23	
11	0.93	0.69	1.46	0.89	1.06	1.09	1.65	
12	1.27	2.14	1.27	1.36	0.41	3.75	1.09	

Scatter Plot

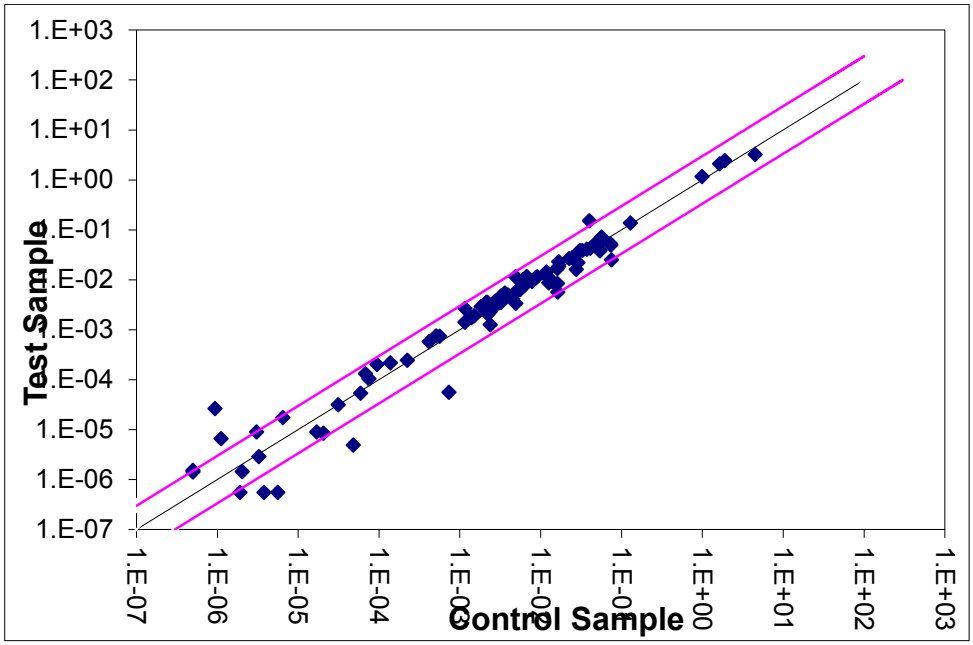

Volcano Plot

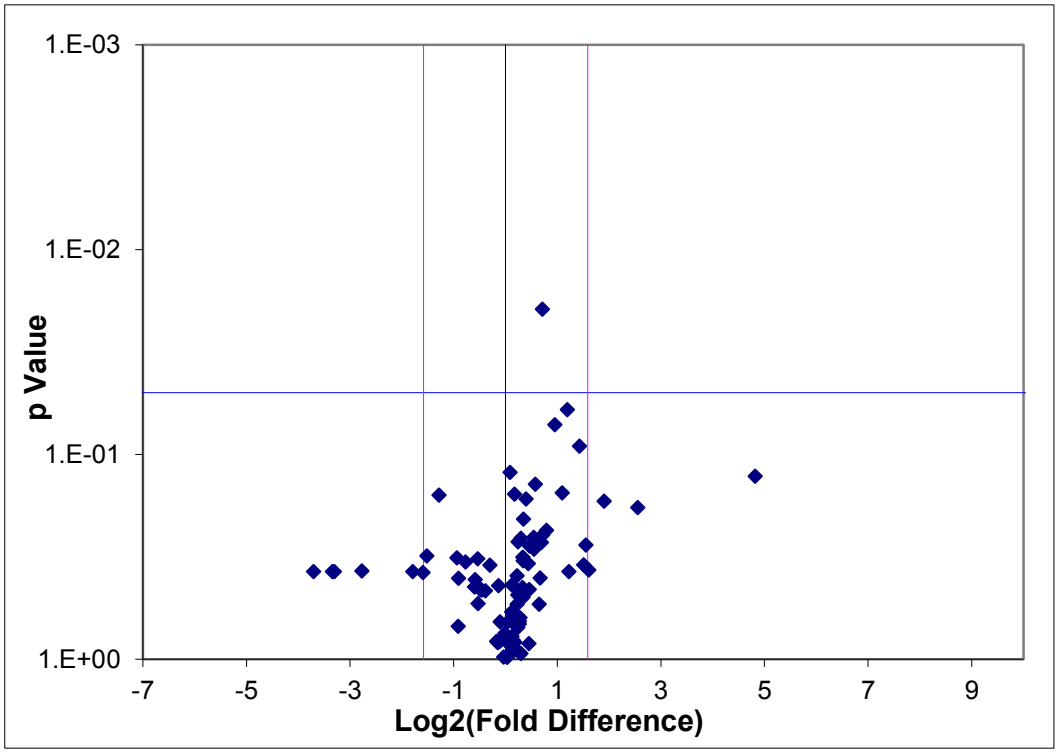

Additional Data for miR-181a inhibitor in Target Array Analysis

3D Profile plot values

3D Profile	A	B	C	D	E	F	G	H
1	1.33	1.05	1.08	0.25	1.15	3.97	1.19	0.77
2	1.22	0.30	1.47	1.43	0.98	0.71	1.27	1.16
3	0.85	1.47	0.44	1.31	1.13	2.11	1.18	1.24
4	1.60	2.35	0.62	1.20	1.21	0.35	0.17	0.78
5	1.09	2.91	1.42	1.25	1.67	0.81	1.09	1.16
6	1.34	0.81	1.26	1.10	1.07	0.03	6.45	
7	1.25	0.05	0.47	0.58	0.93	1.28	1.13	
8	1.00	0.90	0.84	0.59	1.36	1.26	0.66	
9	0.98	1.04	0.88	0.63	0.69	1.39	0.92	
10	1.66	1.04	3.26	1.13	1.30	1.16	1.53	
11	0.77	0.54	1.89	1.05	1.16	1.03	1.98	
12	1.00	1.53	1.49	1.49	0.25	2.64	0.64	

Scatter Plot

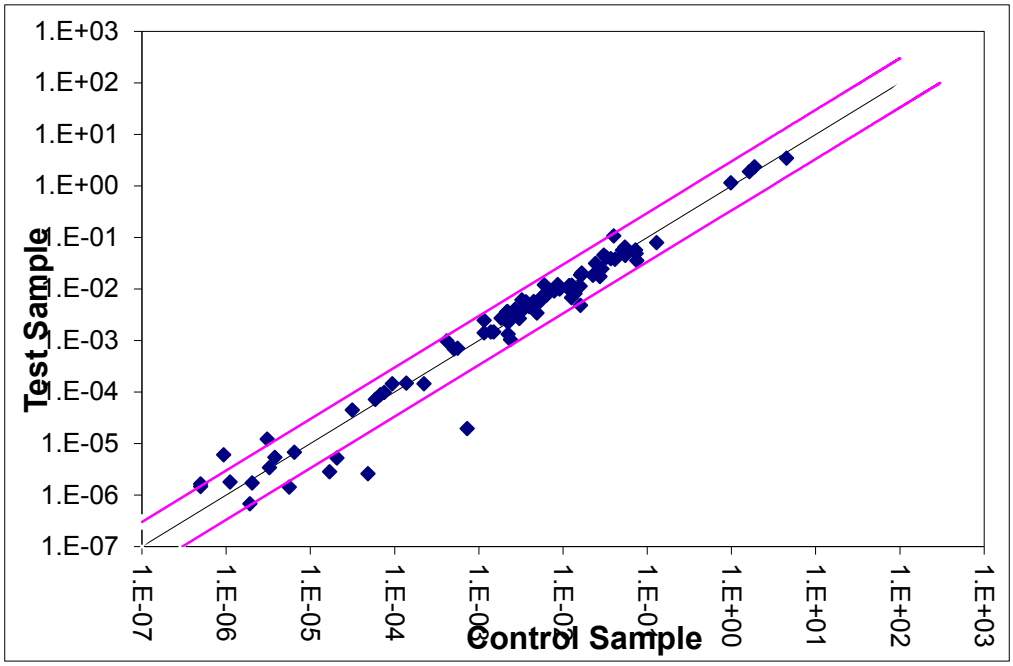

Volcano Plot